Field Guide

Madygen Expedition

August 2026

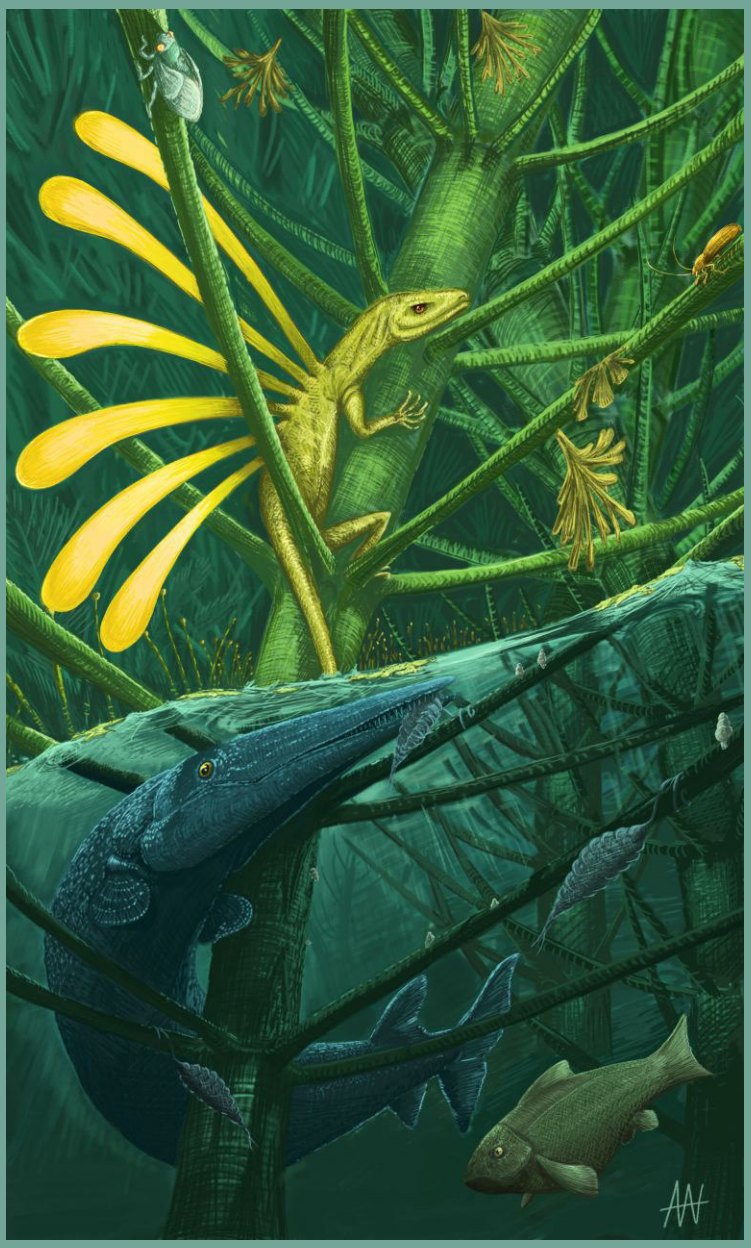

Artwork: „Inside the Madygen Lake“ by Alina Winkler

GEOPARK

MADYGEN

Andreas Brosig

Ilja Kogan

Alina Winkler

Philippe Moisan

Contents

1 Geography, Flora and Fauna 2

2 Kyrgyz History and Culture 5

3 Research History 6

4 Regional Geology of the Geopark 8

4.1 Paleozoic 8

4.2 Mesozoic 13

4.3 Paleogene 13

4.4 Neogene – Quaternary 14

5 Key sections 16

5.1 Madygen Formation 16

5.2 Kylötok Formation 18

5.3 Kamysh-Bashi-Formation 19

5.4 Sogul and Samarkandyk Formations 21

5.5 Cretaceous 22

5.6 Paleogene sections 23

5.7 Paleosoil profiles – A Mesozoic climate archive 25

6 Paleontology – Introduction to the main fossil groups 29

6.1 Cambrian 29

6.2 Triassic - Jurassic 31

6.2.1 Flora 31

6.2.2 Plant-Insect interactions 35

6.2.3 Roots 36

6.2.4 Insects 39

6.2.5 Chondrichthyes 43

6.2.6 Osteichthyes 46

6.2.7 Tetrapods 50

6.2.8 Trace fossils 54

6.3 Cretaceous 57

6.4 Paleogene 58

7 Mineralization 62

7.1 Pb-Zn-Ag 62

7.2 Uranium 64

8 Selected References 66

1 Geography, Flora and Fauna



Fig. 1: Geography of the Fergana Basin and the West Tien Shan. From UNDP, 2005

The Madygen Geopark is situated on the southern margins of the Fergana Valley basin and the northern slopes of the Alay and Turkestan mountain ranges. This geographic area is divided among Kyrgyzstan, Uzbekistan, and Tajikistan, featuring complex borders established during the Soviet delimitation process. The physical terrain drops from alpine ridges exceeding 5,000 meters down to flat alluvial plains situated at elevations between 400 and 800 meters above sea level.

The northernmost zone consists of flat basin plains formed by thick layers of fluvial sediment. This area is highly modified by human activity, featuring dense irrigation canal networks and agricultural land. Towards the south, the flat plains transition into *adyrs*—long, parallel chains of clay and loess foothills that rise between 100 and 400 meters above the valley floor. These foothills are highly prone to erosion, mudflows, and landslides during seasonal rains.

Behind the foothills, the terrain rises abruptly into the rugged mountain systems of the South Tien Shan. The primary chains are the Turkestan Range to the west and the Alay Range to the east. These mountains act as a massive geographic barrier, blocking hot air from the south and trapping moisture coming from the north and west. The lower mountain slopes contain deep V-shaped valleys and narrow limestone gorges carved by fast-flowing rivers. Higher up, above 3,000 meters, the landscape is defined by glaciated peaks, scree slopes, and high-altitude alpine meadows.

The hydrology of South Fergana depends entirely on mountain snowmelt and glacier runoff. Major rivers include the Isfara, Shakhimardan, Sokh, and Ak-Bura. These rivers originate in the high glaciers of the Alay and Turkestan ranges and flow northward toward the central Fergana Valley. In the arid climate, the rivers lose water rapidly due to evaporation and heavy agricultural irrigation as

soon as they reach the foothill zone. Most of these rivers terminate in irrigation networks or alluvial fans before they can reach the Syr Darya River, the central drainage artery of the broader valley basin.

The vertical topography creates distinct geographic belts. The lowest elevations feature desert and semi-desert conditions with sparse vegetation. The middle elevations, particularly between 1,200 and 2,500 meters, contain fertile river oases, pockets of wild walnut forests on northern-facing slopes, and juniper woodlands. Above the tree line, the geography changes to subalpine and alpine zones, which serve as seasonal grazing pastures. The highest elevations consist of permanent permafrost, bare rock, and glaciers.

The climate of South Fergana is extremely continental, warm, and arid, defined by prolonged, hot summers, short, moderate winters, and highly irregular precipitation. The lowlands are heavily shielded from freezing northern air masses by the North Tien Shan Mountains, resulting in a much warmer, more stable macroclimate than the surrounding alpine regions of Kyrgyzstan.

Summers last from May through September. During this period, the region experiences intense, clear-sky solar radiation and low atmospheric humidity. August temperatures routinely average between 27°C and 35°C (81°F to 95°F), with maximum spikes frequently exceeding 40°C (104°F) on the valley floor. This extreme summer heat accelerates evaporation rates, driving a severe mid-summer deficit in soil moisture. Conversely, winters are relatively brief and mild compared to northern Central Asia. January temperatures hover between -1°C and -4°C (25°F to 30°F) in the foothills, though periodic incursions of Siberian air can still plunge temperatures down to -20°C (-4°F) for short spans. Snow cover on the low plains is light, highly inconsistent, and rarely persists for long.

Precipitation is scarce and unevenly distributed, averaging 250 mm (10 inches) annually in the lowlands. The region experiences a distinct Mediterranean-style precipitation curve, with the vast majority of moisture falling as rain in early spring (March and April) and late autumn (October and November). The five months of mid-to-late summer see virtually zero precipitation.

Today, this climatic balance is facing substantial pressure from global warming. Rapidly rising average temperatures are accelerating the melting of regional glaciers, which alters the seasonal timing of river runoff. This shift threatens both the sustainability of the downstream agricultural oases and the natural water retention capacity of the surrounding mountain ecosystems.

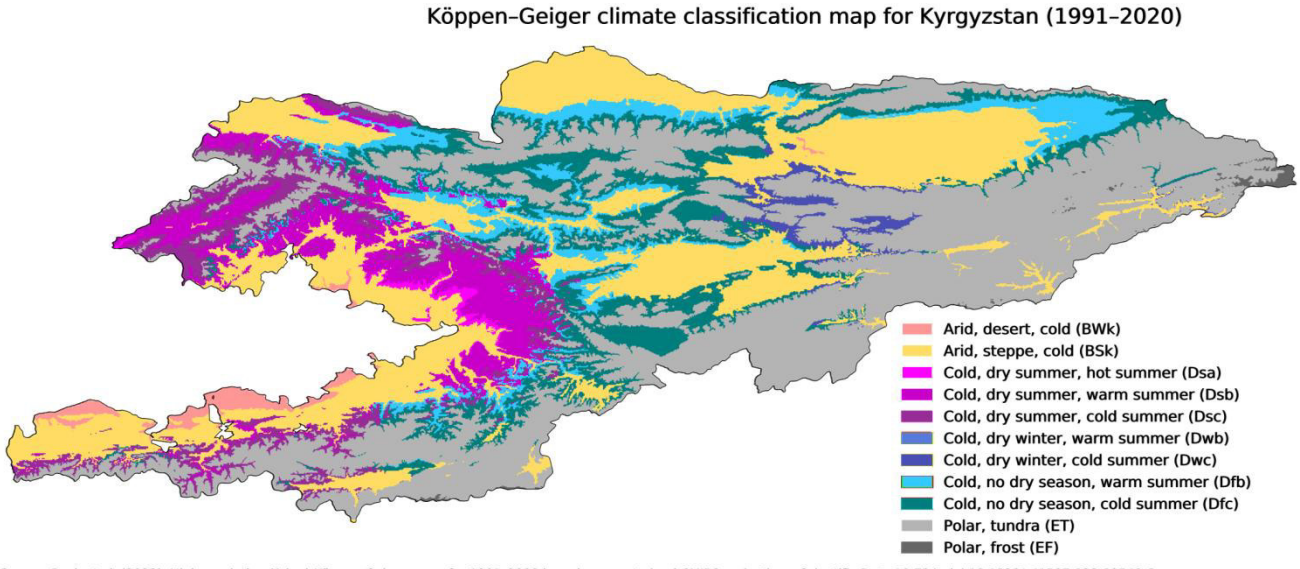

Fig. 2: Climate zones of Kyrgyzstan

The lowland plains and *adyr* (foothill) zones feature a desert and semi-desert floral profile. Vegetation is sparse and dominated by xerophytic, drought-resistant shrubs such as wormwood, saltwort, camel thorn, and various species of *Astragalus*. In early spring, a brief window of moisture triggers the growth of ephemeral plants, including wild poppies, irises, and ancestral tulip species like *Tulipa greigii*. Fauna in this lower belt consists of species adapted to high summer temperatures and low water availability. Reptiles are highly prevalent, including the steppe tortoise, the desert lidless skink, and various geckos. Mammals are represented by rodents such as gerbils, jerboas, and the long-eared hedgehog.

Between 1,200 and 2,500 meters, increased orographic precipitation sustains a more diverse mid-altitude ecosystem. Northern-facing slopes and river valleys support stands of wild walnut-fruit forests dominated by *Juglans regia*. These forests include an understory of wild ancestors of domestic fruits, such as *Malus sieversii* (wild apple), wild pears, cherry plums, pistachios, and almonds. Drier slopes in this belt are occupied by open juniper woodlands. The fauna of this forest and woodland zone includes mammalian species such as the Eurasian wild boar, roe deer, badger, Indian porcupine, and the Eurasian red squirrel. Avian diversity is high, featuring the common nightingale, various warblers, and the hoopoe.

Above 2,500 meters, the landscape transitions into subalpine and alpine meadows. The flora consists of dense mats of low-growing perennial grasses, sedges, wild onions, and specialized alpine flowers such as gentian, primrose, and edelweiss. These high-altitude pastures serve as seasonal feeding grounds for large wild herbivores, primarily the Siberian ibex and, in more remote ridges, the Marco Polo sheep. These ungulates form the primary prey base for top-tier alpine predators. The apex predator of this zone is the endangered snow leopard, which coexists with the Eurasian lynx, grey wolf, and Central Asian brown bear. The avian population at high elevations is dominated by large raptors and scavengers, including the golden eagle, bearded vulture, and Himalayan griffon.

2 Kyrgyz History and Culture

The origins of the Kyrgyz people trace back to the Yenisei River region in Siberia. By the 9th century, they established the Yenisei Kyrgyz Khaganate, defeating the Uyghurs in 840 AD. Subsequent Mongol expansions in the 13th century forced groups southward and westward into the Tien Shan region. By the 15th and 16th centuries, the distinct Kyrgyz ethnicity formed in modern Kyrgyzstan, subdivided into many clans.

Throughout the 17th and 18th centuries, the Kyrgyz faced military pressure from the Oirats (Jungars). By the early 19th century, the region fell under the administrative control of the Kokand Khanate. In the late 19th century, the Russian Empire annexed the territory following the suppression of local uprisings. Under Russian and later Soviet rule, the traditional nomadic lifestyle underwent forced collectivization in the 1920s and 1930s, transitioning the population to sedentary agricultural and industrial labour. The territory was reorganized as the Kyrgyz Soviet Socialist Republic in 1936 and achieved independence as the Kyrgyz Republic in 1991.

Kyrgyz traditional culture centres on seasonal nomadism (transhumance). Livestock, specifically horses, sheep, and goats, formed the basis of the historical economy. The primary dwelling was the yurt, a portable, felt-covered wooden lattice structure designed for rapid assembly during seasonal migration to high-altitude pastures. Horse riding remains central to social customs, preserved through traditional equestrian sports such as Kok-Boru (a team game involving a goat carcass), Er Enish (horseback wrestling), and At-Chabysh (long-distance racing).
The oral tradition served as the primary mechanism for preserving historical data and cultural values. The central cultural artefact is the Epic of Manas, a continuous narrative poem consisting of over 500,000 lines. It documents the unification of the Kyrgyz tribes against external adversaries and is transmitted orally by specialized bards known as manaschis.

Traditional craftsmanship includes the production of shyrdaks and ala-kiyiz—patterned felt carpets made from sheep's wool using inlay and mosaic techniques. The national instrument is the komuz, a three-stringed, fretless plucked lute carved from a single piece of wood, used for both solo instrumental pieces and vocal accompaniment. Traditional attire includes the kalpak, a white felt hat worn by men, which indicates social status and age through its specific embroidery patterns and shape.




Fig. 3: The yurt is the traditional housing of Kyrgyz and other Central Asian nomads. The central part of the roof structure, the tündük, is represented as the central symbol of the national flag, surrounded by 40 sun rays representing the traditional tribes or clans.

3 Research History

The stratotype area of the Madygen Formation in the northern foothills of the Turkestan Range in southwest Kyrgyzstan is one of the world's richest assemblages of Triassic non-marine fossils, now commonly referred to as the Madygen Lagerstätte. Formation and site are named after a small livestock herders' settlement near the centre of the remote outcrop area. Exploration of the Madygen Formation and its fossil content commenced in the 1930s, when the territories of the Soviet Union (to which Kyrgyzstan belonged) were systematically surveyed for natural resources. In 1945, after the end of World War II, the West Uzbek Geological Expedition and the Tashkent State University started systematic work in the Madygen area as part of the 1:200,000 geological mapping programme of Soviet Central Asia. Uzbek research in Kyrgyzstan lasted for more than two decades and resulted in numerous publications on the macroflora, stratigraphy, and depositional environment of the Madygen Formation.

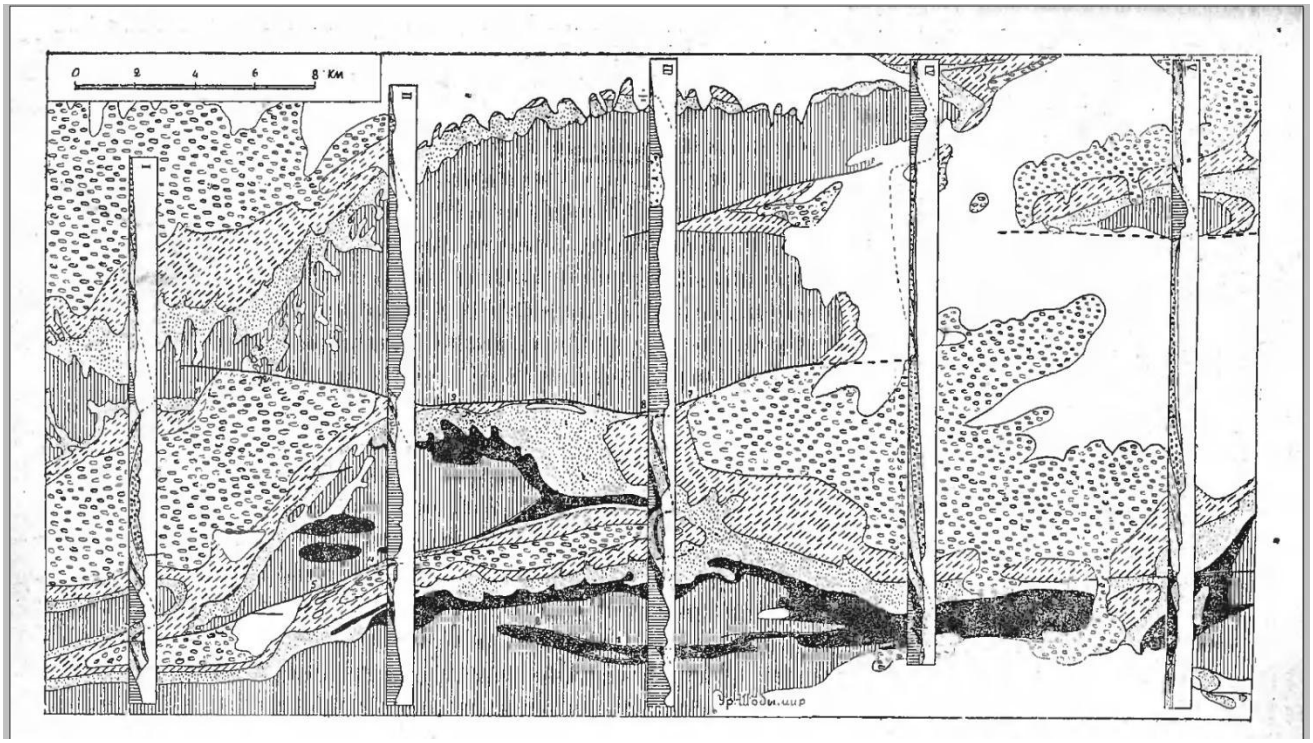

Fig. 4: The first geologic map of the wider Madygen area, drawn by Veber in 1934

The Palaeontological Institute of the Soviet (now Russian) Academy of Sciences in Moscow became involved in the Madygen research through the analysis of fossil insects. Between 1957 and 1971, field parties joined by Elena E. Becker-Migdisova, Inna A. Dobruskina, Alla V. and Maxim G. Minikh, Nestor I. Novojilov, Evgeny N. Kurochkin, Alexander G. Ponomarenko, Alexander P. Rasnitsyn, Alexander G. Sharov, Emilia I. Vorobyeva and many other well-known Russian palaeontologists gathered more than 20,000 fossils from the Madygen Formation. These finds included plants, crustaceans, insects, fishes, and, most spectacular, unique small reptiles with skin impressions that established the scientific importance of this Lagerstätte. Fossil collecting at Madygen peaked in 1962-1967 during five field parties headed by A. G. Sharov. The untimely death of this outstanding entomologist in 1973 may have led to essential stagnation of palaeontological work in the area during the 1970s and 1980s. In autumn 1987, a Madygen field conference was organized by I. A. Dobruskina and M. G. Minikh in order to coordinate future research on the deposits. Implementation of projects, however, failed due to the break-up of the Soviet Union and the independence of Kyrgyzstan in 1991.

In 1993-1998, Madygen and adjoining areas were remapped at a scale of 1:50,000 by the South Kyrgyz Geological Expedition for mineral exploration purposes. In spring 2005, almost 40 years after the main activities of A. G. Sharov and colleagues, a German expedition, initiated by Hartmut Haubold (Martin-Luther-Universität Halle-Wittenberg), rediscovered Madygen as a fossil site of global interest. Following up, a research team based at TU Bergakademie Freiberg executed a multi-year research project. During four field seasons in 2006-2009, the first detailed geological mapping at a scale of 1:5,000 of the Madygen area was undertaken, 1200 m of strati-graphic sections measured at the centimetre scale, five systematic fossil excavations conducted, and more than 3000 specimens of fossil plants, molluscs, crustaceans, insects, fishes, tetrapods, and trace fossils recovered from both previously known and many new sites. After a joint Russian—German expedition in the autumn of 2005 and a joint German—Russian expedition in 2006, Madygen fossil collecting has also been continued independently by the Palaeontological Institute of the Russian Academy of Sciences with field parties in 2007 and 2009.

Starting in 2021 research by members of the former TU Bergakademie Freiberg team was restarted in connection with the planned establishment of the Madygen Geopark. Extensive geologic mapping and field reconnaissance has revealed the paleontological potential of the younger strata (Jurassic to Paleogene), which so far had been little studied in the Madygen area. The current research objectives are to establish the fossil record of these formations, understanding of depositional environments, paleogeography and finally, an integrated paleoecological and paleoclimatic understanding of the region from the Triassic into the Cenozoic.

4 Regional Geology of the Geopark

Central Asia is composed of numerous terranes and islands arcs accreted mostly in the Neoproterozoic and Palaeozoic. In South Asia accretion continued into the Cenozoic, and the India-Asia collision has reactivated faults throughout the area. The West Tien Shan sits at the southern margin of the Palaeozoic accretion belt. It is separated from the Central Tien Shan by the Talasso-Fergana Fault. To the South lie the Pamir terranes, and the Tarim Block is adjoined in the SE. In the North the (Atbashi-)South Fergana Fault marks the suture of the Palaeozoic Turkestan Ocean.

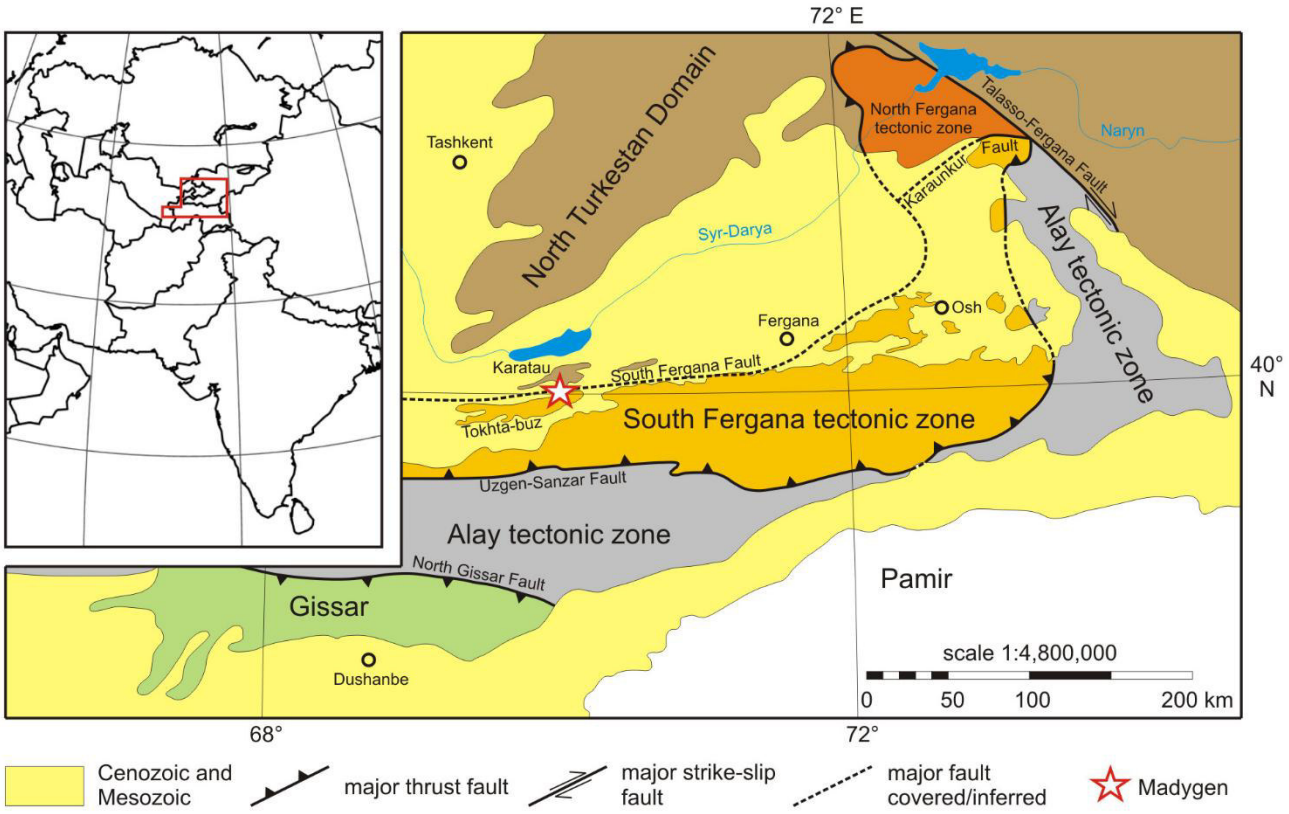

Fig. 5: Simplified tectonic map of the West Tien Shan. The North Turkestan domain is the deformed southern margin of the Kazakhstan microcontinent. The south Fergana Fault is the suture of the Turkestan Ocean. To the south of the suture a stack of nappes derived from accretionary wedge sediments and marginal deposits of the Alay terrane comprises the South Fergana tectonic zone. The basement of the Alay terrane and parts of its Palaeozoic sedimentary cover form the Alay tectonic zone. The Gissar Domain and Pamir are some of the terranes accreted in the Late Permian to Early Cretaceous, a process collectively known as Cimmerian orogenies. Redrawn from BURTMAN (2008).

4.1 Paleozoic

The landmass that is now North Eurasia contains several accretion centres that were joined in the Carboniferous – Permian by the closure of several branches of the Palaeoasian Ocean. The southern accretion centre was the Kazakhstan microcontinent comprising several Peri- Gondwanan terranes, island arcs and suture zones with accretionary wedges. It was largely consolidated by the Late Silurian and continued to drift northwards with respect to the recent orientation.

To the south, the Turkestan Ocean opened at least since the Late Ordovician and its oceanic crust was subducted beneath the southern margin of Kazakhstan since the Lower Devonian, creating an Andean-Type magmatic arc. An alternative view has a continuous subduction zone (Kipchak Arc) on the northern Palaeotethys margin with numerous accreted Cambrian – Ordovician island arcs forming the Kazakhstan “orocline” as a consequence of oblique subduction.

Independent of the precise scenario, the southern margin of the Turkestan Ocean was delineated by the Tarim microcontinent and the Alay-Zeravshan terranes. In the Early Carboniferous Tarim docked with Kazakhstan; and the Talasso-Fergana Fault, a dextral strike-slip fault, developed between the Tarim microcontinent and the remaining Turkestan Ocean and Alay terrane. The terminal stage of closure of the western part of the Turkestan Ocean continued to the Early Permian. Beginning in the Serpukhovian overthrusting in the accretionary wedge created the Shankol-Kan and Taldyk nappes composed mostly of ocean floor basalt, pelagial and flysch-type sediments and olistostromes.

By the Moscovian the oceanic crust was wholly subducted and the pelagic to marly sediments and olistostromes of the Alay terrane continental slope were thrust under the accretionary wedge. In the Early Permian marginal continental crust of the Alay terrane was subducted, resulting in the shearing off of pelagic sediments which are thrust over dominantly carbonaceous shelf sediments as Taldyk nappe. In the final stage of convergence, the shelf sediments were partially sheared off as Isfayram nappe and the nappe stack was folded in E-W trending. Finally, a secondary thrust fault (the Uzgen-Sanzar thrust fault) decoupled the Alay and South Fergana tectonic domains, which together with the Alay terrane basement form the western segment of the South Tien Shan.

However, significant subduction of continental crust in the SW Tien Shan appears unlikely, because the observed shoshonitic post-collisional magmatism and contemporary S- and I-Type granites are more consistent with mantle-derived melts modified to various degrees by the partial melting of delaminated lithosphere.

The continuing oblique subduction along the Palaeotethys margin appears to have created a sinistral shear zone along the Central Asian accretion belt that may have set the extension regime for the late orogenic (Permian) alkaline magmatism in the West Tien Shan.

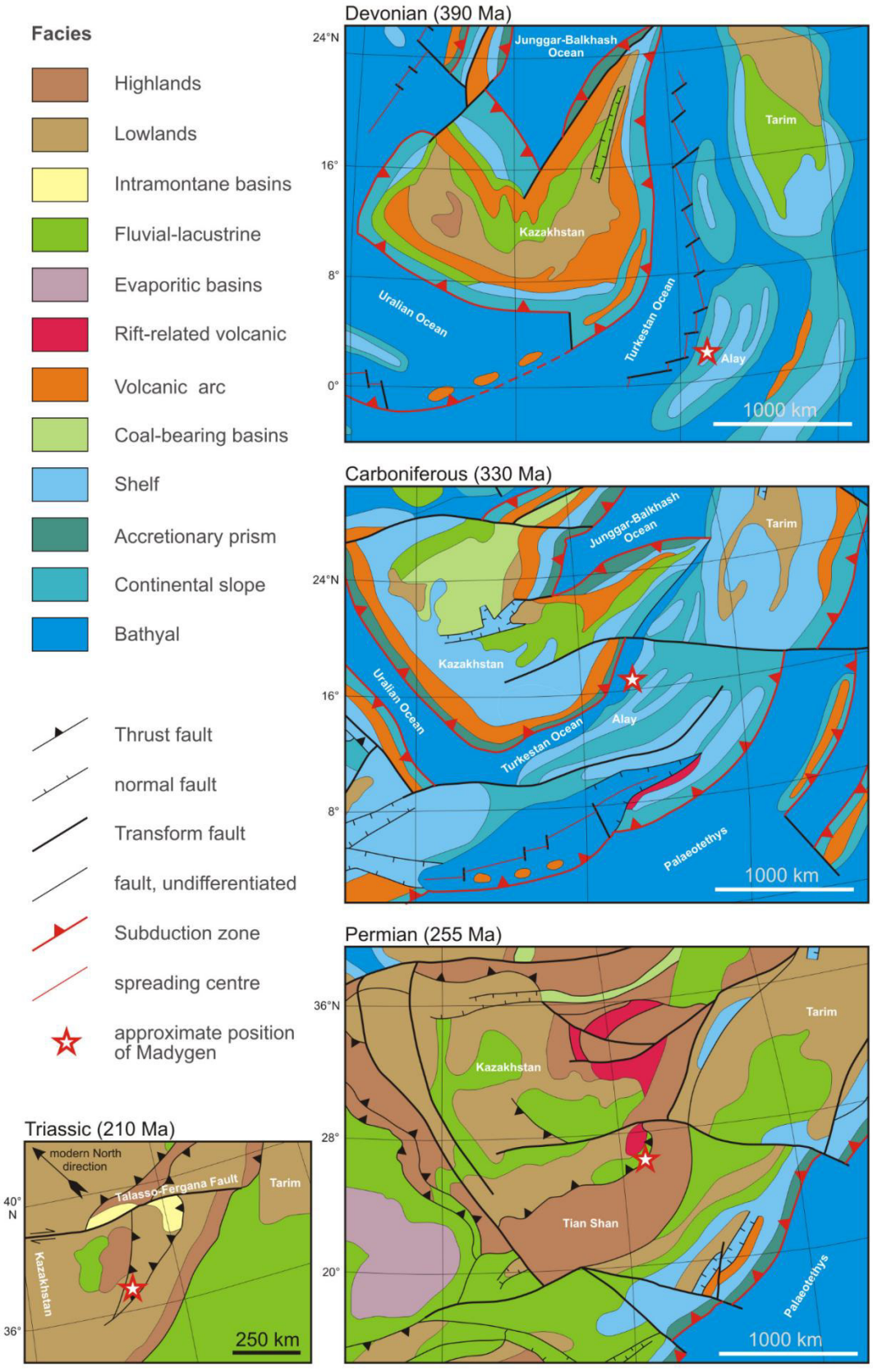

Fig. 6: Palinspastic reconstruction of the closure of the Turkestan Ocean during the Upper Palaeozoic. The accretionary wedge, as well as the shelf and continental slope sediments of the Alay terrane form a complex stack of nappes in the last phase of the closure. This stack forms the basement of the Mesozoic sediments in the study area. Note that, while the latitude of Madygen is almost identical with the recent latitude, although about 40° of counter-clockwise rotation have occurred since the Late Triassic. Redrawn from BYKADOROV (2003) and FEDORENKO & MILITENKO (2002).

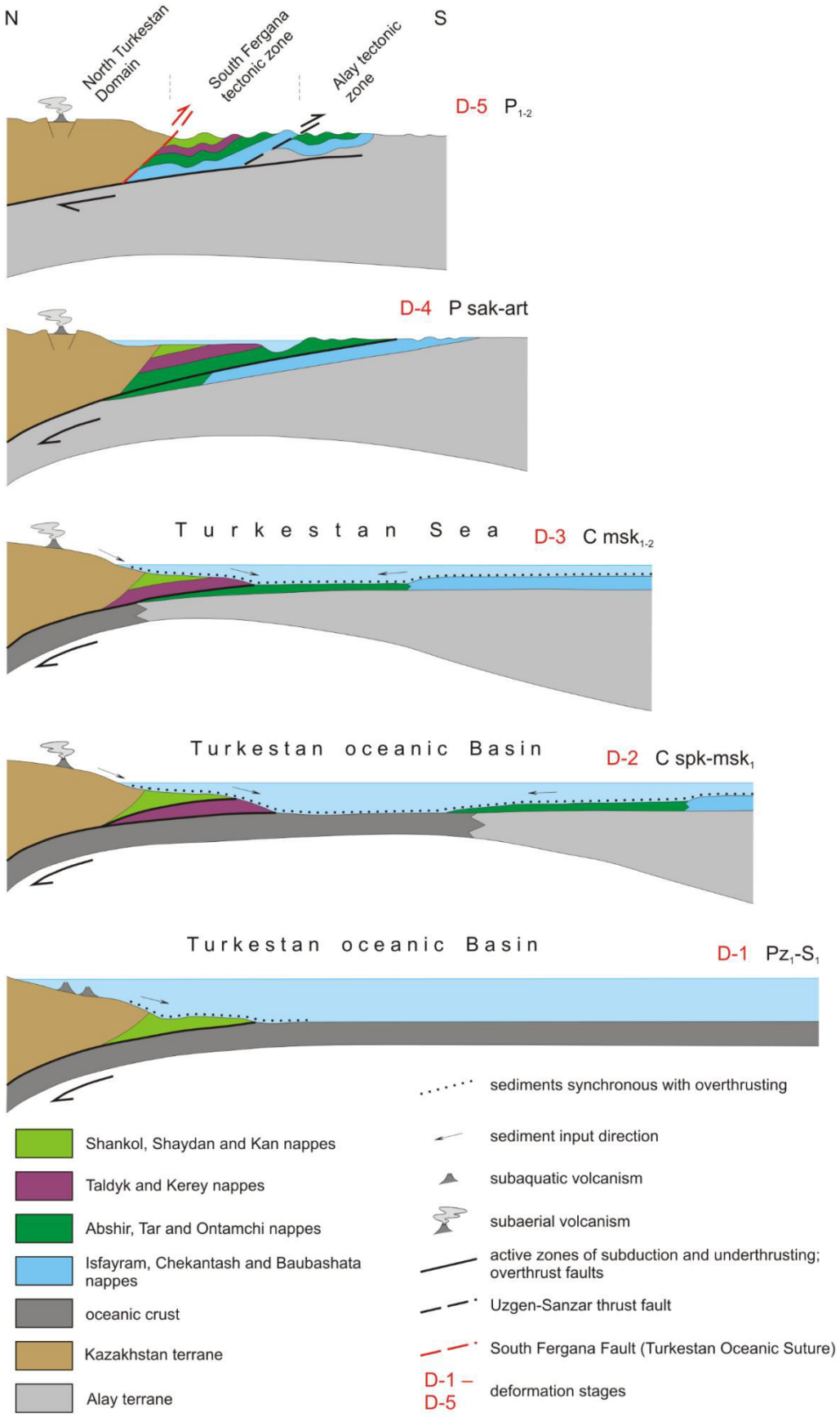

Fig. 7: Schematic north-south cross-sections illustrating the closure of the Turkestan Ocean and the emergence of the nappe stack. Redrawn from BURTMAN (2008).

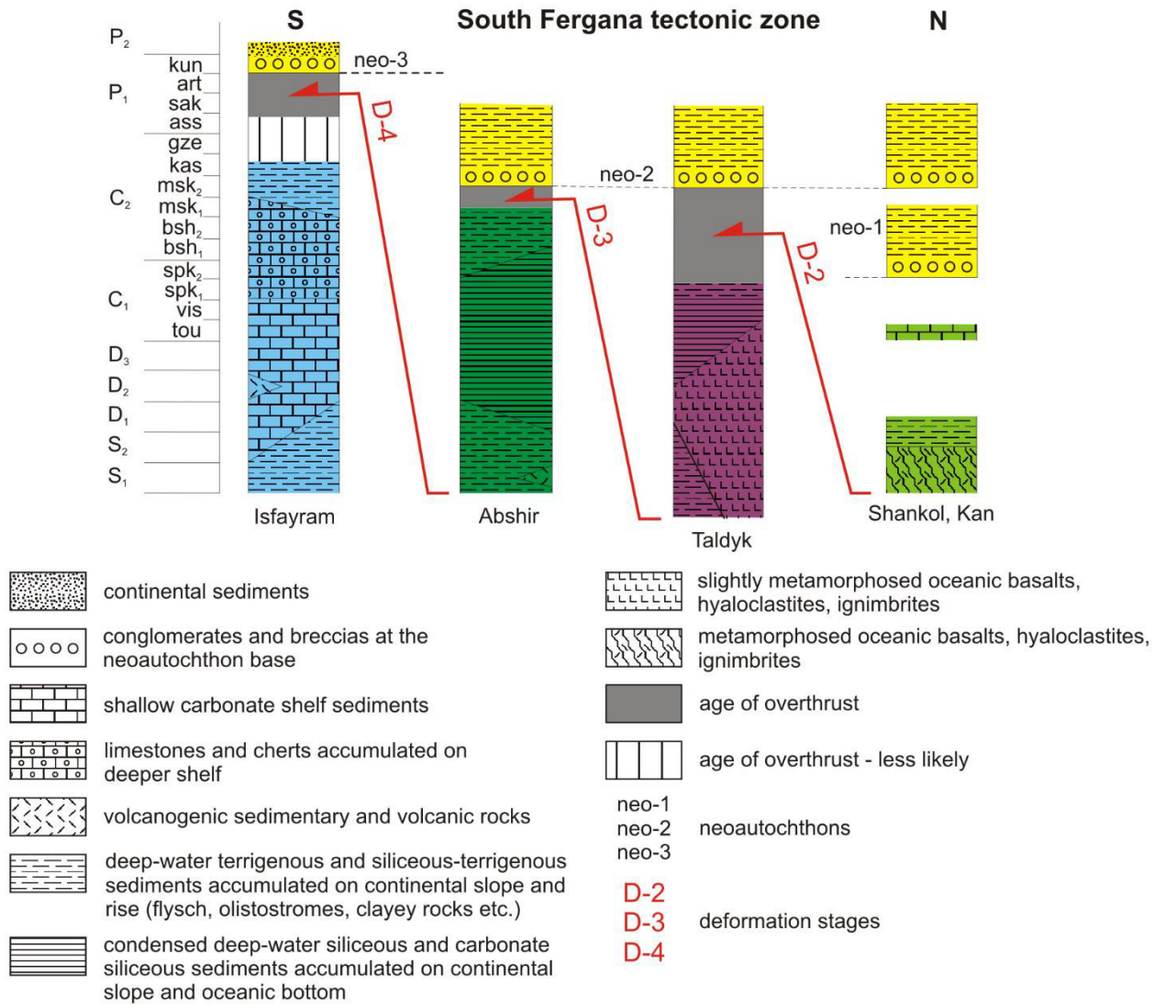

Fig. 8: Facies scheme of the nappes of the South Fergana tectonic zone and timing of the deformation stages. Redrawn from BURTMAN (2008).

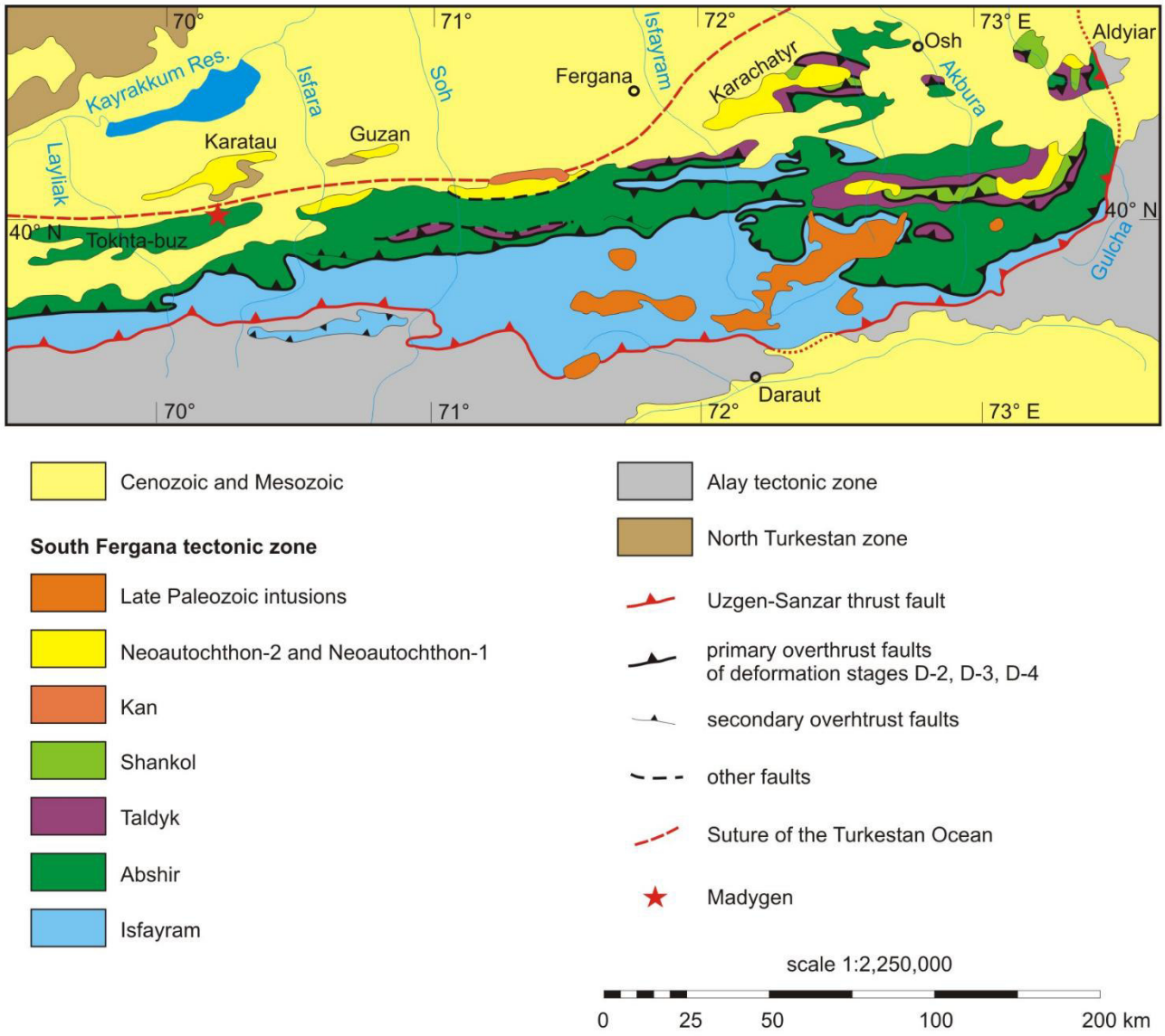

Fig. 9: Tectonic map of the South Fergana tectonic zone, showing the nappe architecture of the area. In the Madygen area only the Abshir and Isfayram nappes are exposed. Close to the suture, the former is strongly disrupted and partially covered by Mesozoic sediments including the Madygen Formation. The nappes of the Alay tectonic zone are not differentiated (compare Fig. 4). Redrawn from BURTMAN (2008).

4.2 Mesozoic

This regime persisted up to the Middle Triassic. Deformation was accommodated by sinistral rotation of minor crustal blocks which may have induced the formation of continental basins of transtensional and transpressive types. Additionally, dextral displacement along the Talasso-Fergana Fault continued into the Triassic and amounted to at least 180 km by that time. During the Jurassic, some terrestrial sediments were deposited in the Fergana depression and in two basins along the Talasso-Fergana Fault. Convergence resumed in the Middle Cretaceous in a last episode of the Cimmerian orogeny as a far-field effect of the collision of the Lhasa block with Eurasia.

4.3 Paleogene

The beginning of the Cenozoic saw the flooding of the Fergana depression from the south and later also from the west, and the onset of the India-Asia collision. Between the Pamir and the southern margin of the Tien Shan, this event is thought to have caused 300 to 400 km of Crustal shortening.

4.4 Neogene – Quaternary

However, the South Fergana tectonic domain has been significantly affected by the collision only since the Miocene, about 8 to 10 Ma before present. In essence, crustal shortening caused uplift on the order of several kilometres of Paleozoic tectonic blocks and younger sediments, widespread erosion of these mountain ranges and deposition of up to 5 km of terrestrial sediments in the Fergana depression. The combined thickness of the Late Permian to recent sediments in the centre of the depression is 12 km. Additionally, the Fergana basin and South Fergana tectonic zone have been – and are still – rotating since that time counter-clockwise along the Talasso-Fergana Fault.

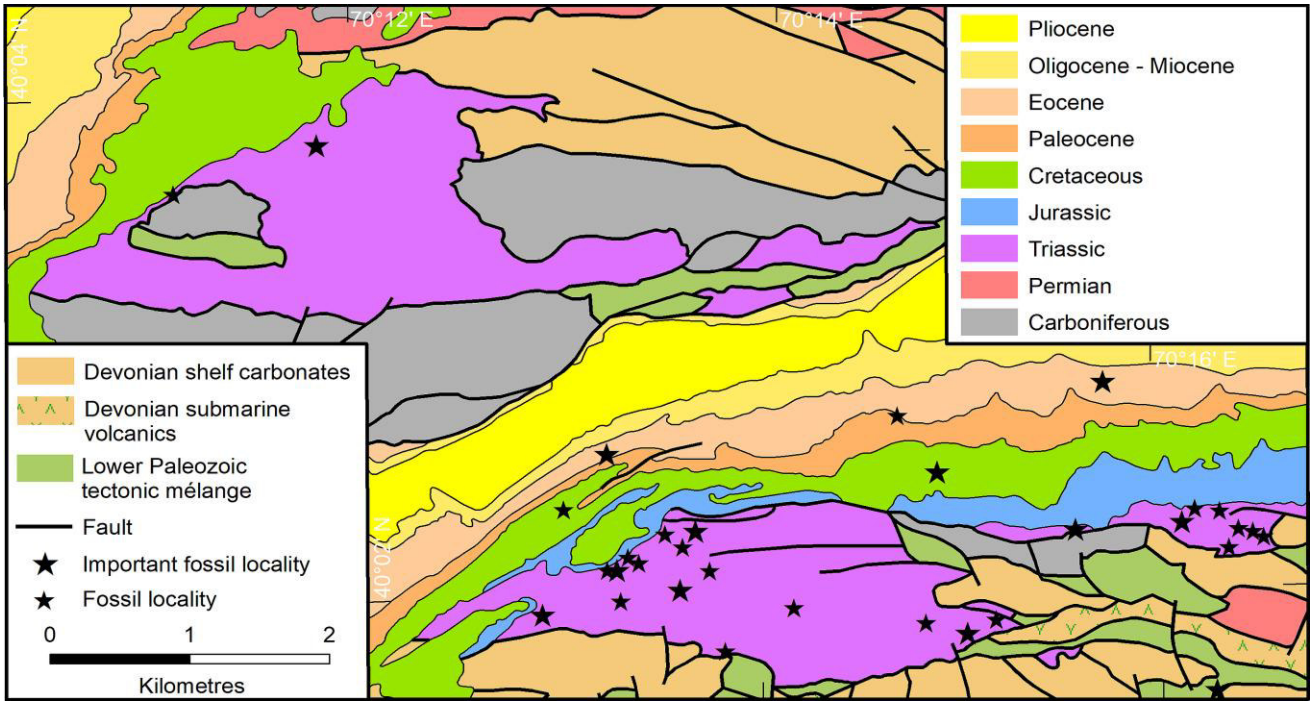

Fig. 9: Geologic map of the central part of the Madygen Geopark with the outcrops of the Madygen Formation and other fossil localities.

Fig. 10 (next page): Synoptic scheme of the geologic evolution of the South Fergana area, including the Madygen Geopark by Oleg Lopatko

Era	System	Section	Geodynamic setting	Rosks		Basic processes	Tectonics	Mineralization
CENOZOIC	Quaternary		Geodynamic complex of Alpine epiplatform orogeny	N_1-Q	Gray molasses: blocks, boulders, pebbles, crushed stone, gravel, sands, siltstones, clays; clay-sand cement	Orogeny (as a consequence of collision), denudation of mountains and sedimentation on mountain slopes and in intermountain depressions	Alpine tectonic stage. A significant tectonic structure complication of the region as a whole and deposits in particular	Erosion of indigenous ore deposits and formation of placers
	Neogene	Pliocene						
		Miocene		P_3-N_1	Red-colored molasses: conglobreccias and conglomerates massive and coarse-layered with layers of gravelites and gravel sandstones; sand-clay cement	Intra-platform dislocations with the formation of shallow seas and partial erosion of gentle uplifts		
	Paleogene	Oligocene						
		Eocene	Geodynamic complexes of passive continental margin	P_1-3	Formation of intraplate sediments: gypsum, dolomites, oyster limestones, red-colored conglomerates, gravelites, sandstones, clays, trap magmatism in some places	Landform peneplanization, erosion of ochreous weathering crusts, accumulation of sediments in shallow continental seas	Relative tectonic stabilization	Fragmentary erosion of indigenous ore deposits
		Paleocene						
MESOZOIC	Cretaceous			K	Sedimentation in gentle intermountain depressions: red-colored massive conglomerates and gravelites of dry and watered riverbeds and sandstones, clays and marls of shallow reservoirs	Minor intra-platform dislocations, formation of weakly hilly terrain	Weak tectonic activation under the influence of peripheral collision	
	Jurassic			T-J	Formation of sedimentary complexes at the passive tectonic margin: variegated clays and marls, rarely sandstones and siltstones, with interlayers and horizons of coal	Accumulation of rich by organic residues continental sediments in swampy lowlands at a warm humid climate	Calm tectonic regime	Formation of coal deposits, where in places there are industrially significant concentrations of uranium in the form of organometallic compounds formed due to biosorption - the concentration of metal dissolved in surface waters on particles of biogenic origin
	Triassic							
PALEOZOIC	Permian		Geodynamic complex of Late Paleozoic collision	C_3-P	Collisional magmatism: formation of intrusions from medium acid to alkaline composition - granodiorites, granites, less often monzonites and syenites	Melting of continental plates fragments and crowded oceanic crust at great depths with the formation of batholiths and small bodies; metasomatism in the apical parts of intrusions	Active collision tectonics: occurrence of shifts, thrusts and tectonic "windows" of stretching	Metals from the crowded oceanic crust are concentrated in the apical parts of magmatic foci and are transported upwards as part of pneumatolite solutions with excessive pressures and temperatures, forming ore deposits near intrusive contacts and inside fault shear zones
	Carboniferous	Upper	Geodynamic complex of inland sea at the epoch of end Tethys Paleocean closing	C_2-3	Terrigenous sediments of shallow seas (flysch): rhythmic alternation of polymictic sandstones and siltstones with subordinate interlayers of sanded mudstones, sometimes facially replaced by lenses of gravelites and conglomerates of underwater channel flows	Weak sagging of continental margin	Low tectonic activity	Contents of metals are insignificant in the flysch strata
		Middle						
		Lower	Geodynamic complex of marginal sea at the epoch of start Tethys Paleocean closing	D-C_2	Carbonate sedimentary strata of bathyal zone: mostly chemogenic limestones and dolomites in the lower part of section, mostly organogenic limestones in the upper part	The displacement of subduction zone towards the rift and Gondwana continent and formation of the marginal and then the inland sea, where mostly carbonate marine sediments formed at depths from 3000 to 130 m	Relative tectonic stability of the back arc basin	Contents of metals are insignificant in the carbonate strata
	Devonian	Upper						
		Middle						
		Lower						
	Silurian	Upper	Geodynamic complex of Tethys Paleocean formation and development	Є-S_2	Ophiolite association of rocks of ancient oceanic crust: hyperbasites, carbonaceous sherts (phthanites), carbonaceous-siliceous-clay and calcareous-siliceous schists, sometimes sills and dikes of basaltoids	Build-up of oceanic crust in the rift zone due to new portions of ultrabasic magma coming from the bowels of the planet; formation of oceanic sediments in a calm hydrodynamic environment on the ocean abyssal plains (depths of more than 3000 m), introduction of basaltoids from second order oceanic volcanoes; crowding of oceanic crust in the subduction zone and its melting at depth at appropriate pressures and temperatures with the formation of island - arc volcanites	Shear and axial displacements by formation of mid-oceanic ridges in the zone of rifting; relative tectonic stability of oceanic plates against the background of their gradual movement to the continents in zone of abyssal plains; tectonic crowding of ophiolite crusts in the subduction zone with the formation of intensely tectonized accretion prisms	Supply of useful metals to ocean basin through rift channels, their accumulation in bottom sediments due to biosorption - concentration of elements dissolved in ocean waters (Au, Ag, Co, Zn, Ni, Cu, etc.) on particles of biogenic origin in the form of organometallic compounds. Concentrations of useful components in sediments are increased (above Clark), but do not reach industrially significant. Remobilization of metal-enriched organic matter occurs in the deep-water trough during washing by currents
	Ordovician	Upper						
		Middle						
		Lower						
	Cambrian	Upper						
		Middle						
		Lower						

5 Key sections

5.1 Madygen Formation

The most complete section of the Madygen Formation is located in the Urochishche Madygen area and has a revised thickness of 560 m. A subdivision based on sediment genesis into four units (Madygen sequences 1–4, abbreviated MS1 to MS4) and 10 subunits (MS1–1 to MS1–4, MS2–1 to MS2–3, MS3–1 to MS3–2, MS4) is established.

The section begins with coarse-grained alluvial sediments (MS1–1), followed by thin fluvial deposits (MS1–2). These are overlain by an 80 m thick succession of fine-grained lacustrine-palustrine clastics with sub-bituminous coal at the base (MS1–3). Next are 110 m of lacustrine deposits characterized by increased input of coarse-grained terrigenous clastics (fan delta) (MS1–4).

Massive conglomerates (MS2–1) of a prograding fan delta initiate Madygen sequence 2, which is volumetrically dominated by alluvial-fluvial sediments (MS2–2) but transitions upwards into deltaic deposits and fine-grained lacustrine clastics (MS2–3).

Coarse alluvial conglomerates of Madygen sequence 3 (MS3–1) follow with an erosional base; they are overlain by a 60 m thick series of fluvial-palustrine sediments containing hydromorphic soils (MS3–2).

The final Madygen sequence 4 (MS4) begins with profundal lacustrine sediments and transitions upwards into increasingly coarse-grained clastic deposits of a prograding delta.

The Madygen Formation in the Urochishche Madygen area comprises three basal cycles (MS1–1 to MS1–3, MS2, MS3) and one distinct upper cycle (MS4). Sequence boundaries represent significant shifts in the mode of sedimentation, presumably triggered by tectonic pulses: at the MS1/MS2 boundary, the MS1–4 lake was infilled by a rapidly prograding fan delta (MS2–1); at the MS2/MS3 boundary, following a hiatus in sedimentation, coarse-grained alluvial fans (MS3–1) eroded down into the fine-grained lacustrine deposits of MS2–3; and at the MS3/MS4 boundary, a fluvial-palustrine basin depression (MS3–2) was transformed into a lake bottom (MS4) by abrupt flooding—an event possibly induced by seismic activity. The dynamic nature of the depositional environment is further underscored by evidence from paleocurrent indicators and the lateral thickness variations of individual facies belts, which reveal a shift in the dominant sediment dispersal direction from N–NE (MS1–1 to MS2–1) to S–SW (MS2–2 to MS4).

In the Sauk Tanga area, a highly disturbed succession contains equivalents of all lithostratigraphic subunits belonging to Madygen Sequence 1 (as defined at Urochishche Madygen). The only difference is that, at the NE margin of Sauk Tanga, the lacustrine deposits of MS1–4 begin with alluvial-fluvial sediments (MS1–4a, Fig. 1), a feature consistent with the dominant sediment dispersal direction observed in the lower part of the Madygen Formation.

Lacustrine-deltaic fine-grained clastics at the northwestern margin of Urochishche Dzhaylyaucho (including the Sharov fossil locality) likely correlate with MS2–3.

Fig. 11 (next page): Madygen Formation reference section (Voigt et al., 2017)

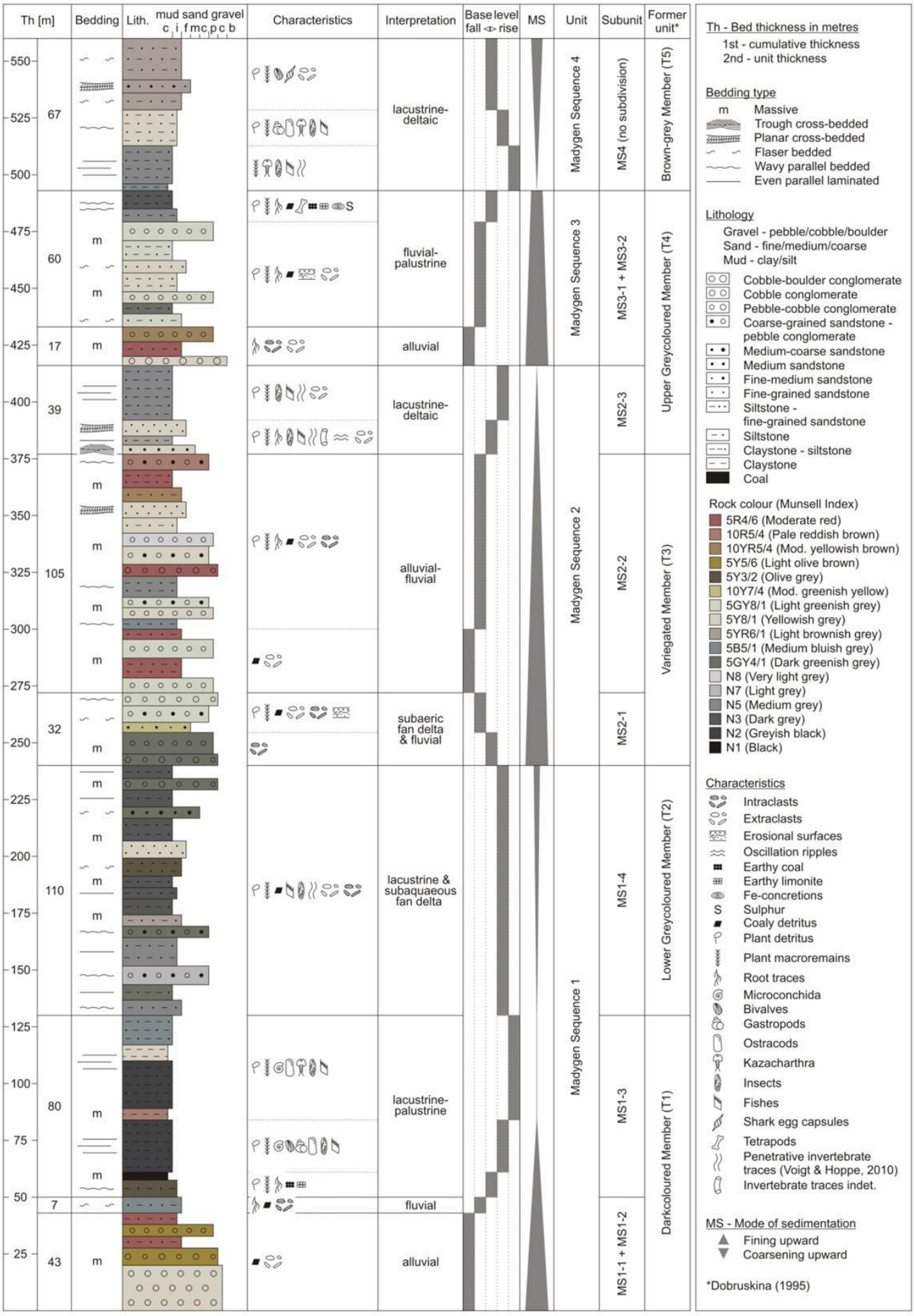
Th [m]
Bedding
Lith.
mud sand gravel
c i f m c p c b
Characteristics
Interpretation
Base level fall ◁▷ rise
MS
Unit
Subunit
Former unit*
550
525
500
475
450
425
400
375
350
325
300
275
250
225
200
175
150
125
100
75
50
25
67
60
17
39
105
32
110
80
7
43
m
lacustrine-deltaic
fluvial-palustrine
alluvial
lacustrine-deltaic
alluvial-fluvial
subaeric fan delta & fluvial
lacustrine & subaquaeous fan delta
lacustrine-palustrine
fluvial
alluvial
Madygen Sequence 4
Madygen Sequence 3
Madygen Sequence 2
Madygen Sequence 1
MS4 (no subdivision)
MS3-1 + MS3-2
MS2-3
MS2-2
MS2-1
MS1-4
MS1-3
MS1-1 + MS1-2
Brown-grey Member (T5)
Upper Greycoloured Member (T4)
Variegated Member (T3)
Lower Greycoloured Member (T2)
Darkcoloured Member (T1)
Th - Bed thickness in metres
1st - cumulative thickness
2nd - unit thickness
Bedding type
m Massive
Trough cross-bedded
Planar cross-bedded
Flaser bedded
Wavy parallel bedded
Even parallel laminated
Lithology
Gravel - pebble/cobble/boulder
Sand - fine/medium/coarse
Mud - clay/silt
Cobble-boulder conglomerate
Cobble conglomerate
Pebble-cobble conglomerate
Coarse-grained sandstone - pebble conglomerate
Medium-coarse sandstone
Medium sandstone
Fine-medium sandstone
Fine-grained sandstone
Siltstone - fine-grained sandstone
Siltstone
Claystone - siltstone
Claystone
Coal
Rock colour (Munsell Index)
5R4/6 (Moderate red)
10R5/4 (Pale reddish brown)
10YR5/4 (Mod. yellowish brown)
5Y5/6 (Light olive brown)
5Y3/2 (Olive grey)
10Y7/4 (Mod. greenish yellow)
5GY8/1 (Light greenish grey)
5Y8/1 (Yellowish grey)
5YR6/1 (Light brownish grey)
5B5/1 (Medium bluish grey)
5GY4/1 (Dark greenish grey)
N8 (Very light grey)
N7 (Light grey)
N5 (Medium grey)
N3 (Dark grey)
N2 (Greyish black)
N1 (Black)
Characteristics
Intraclasts
Extraclasts
Erosional surfaces
Oscillation ripples
Earthy coal
Earthy limonite
Fe-concretions
S Sulphur
Coaly detritus
Plant detritus
Plant macroremains
Root traces
Microconchida
Bivalves
Gastropods
Ostracods
Kazacharthra
Insects
Fishes
Shark egg capsules
Tetrapods
Penetrative invertebrate traces (Voigt & Hoppe, 2010)
Invertebrate traces indet.
MS - Mode of sedimentation
Fining upward
Coarsening upward
*Dobruskina (1995)

5.2 Kylötok Formation

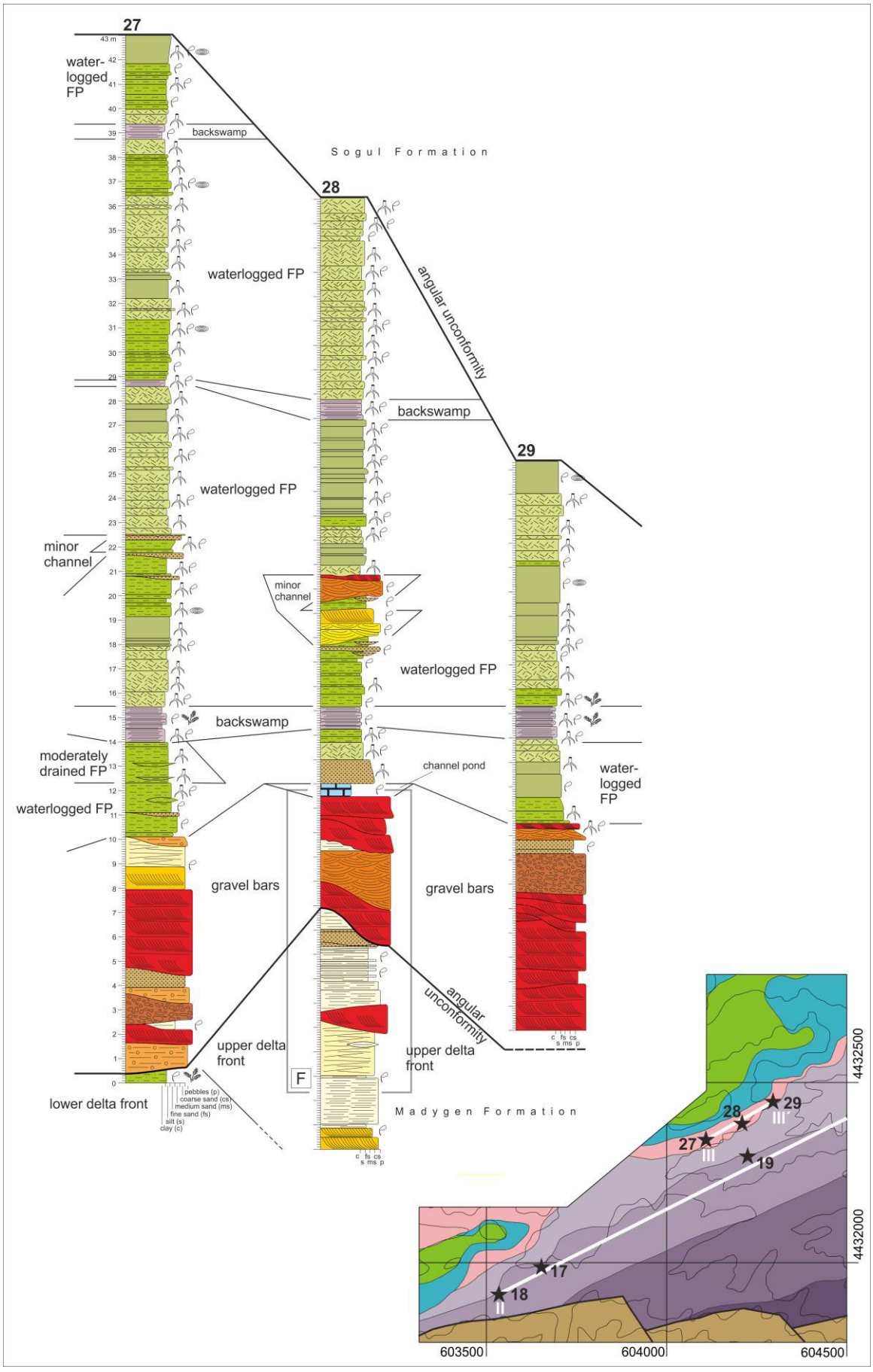

5.3 Kamysh-Bashi-Formation

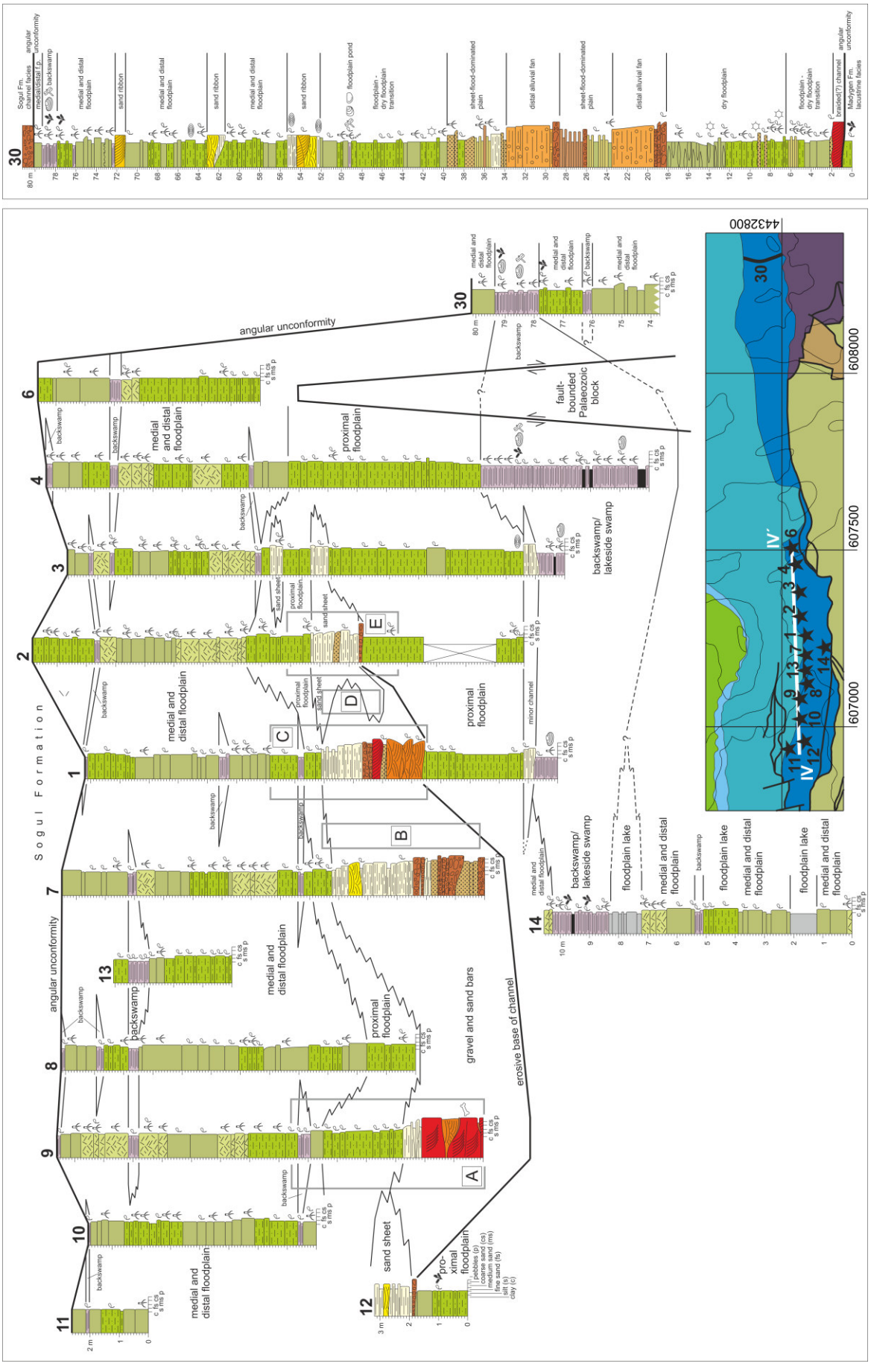

Symbol	Facies Type	Sedimentary Features	Interpretation	Madygen Fm.	Kylötok Fm.	Kamysh-Bashi Fm.
Gcm	Clast-supported massive conglomerate	Light grey to brown-grey, fine to coarse subangular to rounded pebbles with sandy matrix, dominantly quartz, flint, silica shale and minor green sandstone clasts, limestone clasts only in coarse gravelly fraction, also silty rounded mudclasts in the lower Kamysh-Bashi-Fm., erosive bases	Pseudoplastic debris flow, intermediate clast-water-ratio, matrix partially washed out. Fills broad shallow channels, may include some poorly stratified gravel bars	X	X	X
Gp	Conglomerate with planar cross-bedding	Light grey to brown-grey, subangular to rounded granules to medium pebbles, dominantly quartz, flint, silica shale and minor green sandstone clasts, sometimes interstratified with sandy layers, foresets up to 40 cm high, rare disarticulated bones, erosive bases	Transverse bedforms, downstream accretion of gravel bars	X	X	X
Gt	Conglomerate with trough cross-bedding	Light grey to brown-grey, subangular to rounded granules to medium pebbles, dominantly quartz, flint, silica shale and minor green sandstone clasts, sometimes interstratified with sandy layers, foresets up to 60 cm high, erosive bases	Minor channel fills, component of gravel bars and lateral accretion macroforms		X	X
Gh	Clast-supported crudely bedded conglomerate	Light grey to brown-grey, subangular to rounded granules to coarse pebbles, dominantly quartz, flint, silica shale and minor green sandstone clasts, limestone clasts only in coarse gravelly fraction, indistinct planar bedding (5 – 20 cm), erosive to slightly erosive bases	Longitudinal bedforms, gravel bars with dominant downstream accretion	X	X	X
GFh	Conglomerate interstratified with silty to fine sandy layers	Clast-supported, red to light grey granular to medium pebbly mudclast conglomerate layers (3 – 15 cm) with silty matrix, some layers with abundant redeposited limonite concretions, interstatified with red siltstone to medium sandstone, partially laminated	Medial alluvial deposits, including fine clastics from unconfined sheet-like flows, and episodic diluted distal debris flows			X
Sp	Sandstone, fine to very coarse and pebbly, with planar cross-bedding	Light grey to light brown, pale violet-grey, planar foresets up to 20 cm high, some granular to fine pebbly layers, nonerosive to slightly erosive bases	Transverse dunes of sandy bedforms and sand-gravel-bars	X	X	X
St	Sandstone, fine to very coarse and pebbly, with trough cross-bedding	Light grey to light brown, pale violet-grey, troughs up to 100 x 15 cm, rare granular to fine pebbly layers, nonerosive to slightly erosive bases	Sinuous and linguoid dunes of sandy bedforms and sand-gravel-bars		X	X
Sr	Sandstone, fine to medium, partially silty, ripple cross-bedding	Light grey to yellow- and brown-grey, single ripple-sets, transitional to laminated and flaser-bedded fine sandstone, abundant fine coaly detritus, some root traces, nonerosive to slightly erosive bases	Ripples, in proximal floodplain deposits, waning flood stages of sandsheets, and last filling phase of minor channels	X		
Sl	Sandstone, fine to coarse and pebbly, low-angle cross-bedding	Light grey to light brown, bedding less than 5° from horizontal, cm-thick granular layers, no roots, rare fine coaly detritus, nonerosive to slightly erosive bases	Scour fills or humpback dunes, transverse sandy bedforms		X	X

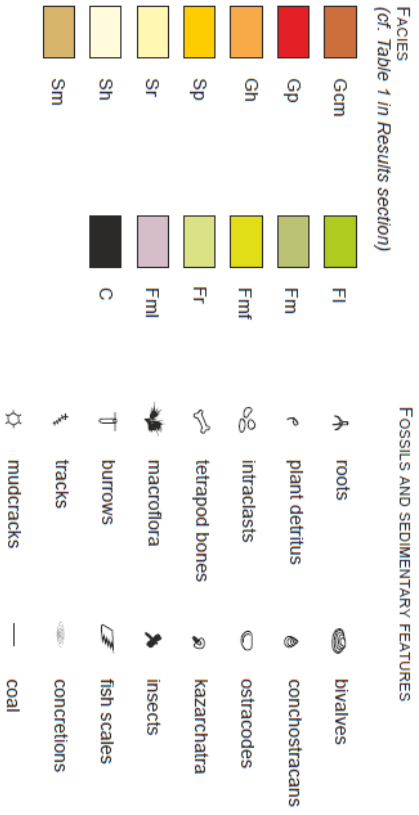

Symbol	Facies Type	Sedimentary Features	Interpretation	M	Ky	Kb
Sh	Sandstone, fine to coarse and pebbly, horizontal bedding	Light grey to brown, horizontal bedding to lamination (2 mm – 10 cm), sometimes large plant fragments, rare root traces, nonerosive to slightly erosive bases	Sandsheets and sandy bedforms deposited in upper flow regime	X	X	X
Sm	Sand, fine to coarse, unbedded	White-grey to brown, base sometimes erosive, may contain minor roots and plant detritus	Fills minor shallow channels, probably deposits from hyperconcentated flows, may include some bioturbated sands	X	X	X
SFh	Sandstone interstratified with silty to fine sandy layers	Fine clastics red-brown, 3 – 10 cm thick, sandstone light grey, 1 – 5 cm thick, mudcracks, soft sediment deformation, rarely contains fine roots, sandstone may contain some fine coaly detritus	Distal alluvial deposits, , including fine clastics from unconfined sheet-like flows, and episodic sheet-flood sands			X
Fl	Laminated fine sandstone, siltstone and claystone	Light to medium grey, yellow-grey and brown-grey, horizontal bedding to fine lamination (1 mm – several cm), fine sandstone typically with abundant fine coaly detritus, finer grain sizes with larger plant fragments, moderate amount of roots (typically type 1), rarely contains burrows, rare soft sediment deformation, sometimes mottled appearance	Overbank or waning flood deposits, dominantly in proximal to medial floodplain settings; distal alluvial deposits from unconfined flows and ephemeral ponds in the lower part of the Kamysh-Bashi-Fm.	X	X	X
Fm	massive fine sandstone, siltstone, and claystone	Light to medium grey, yellow-grey, brown-grey and drab colours, unbedded, moderate amounts of roots and detritus, rarely contains burrows, commonly mottled appearance	Proximal to distal floodplain deposits, lack of stratification may be due to bio- or pedoturbation	X	X	X
Fr	Strongly rooted fine sandstone, siltstone and claystone, horizontally bedded or massive	Light to medium grey, yellow-grey, brown-grey and drab colours, mostly massive to poorly stratified, probably due to intensive phytoturbation, abundant roots and some detritus, rarely contains burrows, commonly mottled appearance	Overbank and floodplain deposits, intensive phytoturbation obscures primary sedimentary features	X	X	X
Fmf	Massive siltstone to fine sandstone with mudclasts, inverse to normal grading	Medium to dark grey with lighter mudclasts, consisting of siltstone to fine sandstone, usually subangular to subrounded, different gradation patterns, may contain fine detritus and disarticulated bones	Mudflows with reworked floodplain sediments	X		
Fml	Laminated fossiliferous siltstone and claystone	Violet-grey with wide to fine lamination (< 1 – 4 mm), rich in plant fragments, sometimes abundant type 1 roots, bivalves and insects	Backswamp and short-lived floodplain ponds; and, if bivalves are present, litoral facies of floodplain lakes	X	X	X
Fcl	Laminated claystone	Dark grey to black with very fine lamination (< 1 mm), no macroscopic fossils, no bioturbation	Floodplain lakes with oxygen-depleted bottom water			X
C	Coal, coaly siltstone and claystone	Dark grey to black, Often indistinct lamination, may contain flasers of silty to fine sandy material, usually powdery sulphur concentrated near top	Peat and peat-enriched mud in backswamp deposits with associated lakes	X		X
Ca	Limestone	Light brown, completely recrystallised with fibrous texture and cone-in-cone structures, lenses 2 – 15 m wide and 2 – 6 cm thick in fine sandstone	Pond in abandoned channel		X	

5.4 Sogul and Samarkandyk Formations

The Sogul and Samarkandyk Formations (Lower to Middle Jurassic) are likely similar to the fluviopalustrine parts of the Kamysh-Bashi and Kylötok sections, however detailed profile logs are not completed yet.

5.5 Cretaceous

The Cretaceous is characterized by three marine transgressive cycles with widespread transgression conglomerates, followed by shallow to marginal marine red sediments and micritic limestone beds. Large clusters of crustacean burrows below the second transgression conglomerate indicate temporal marine recession. Detailed profile logs are not yet completed.

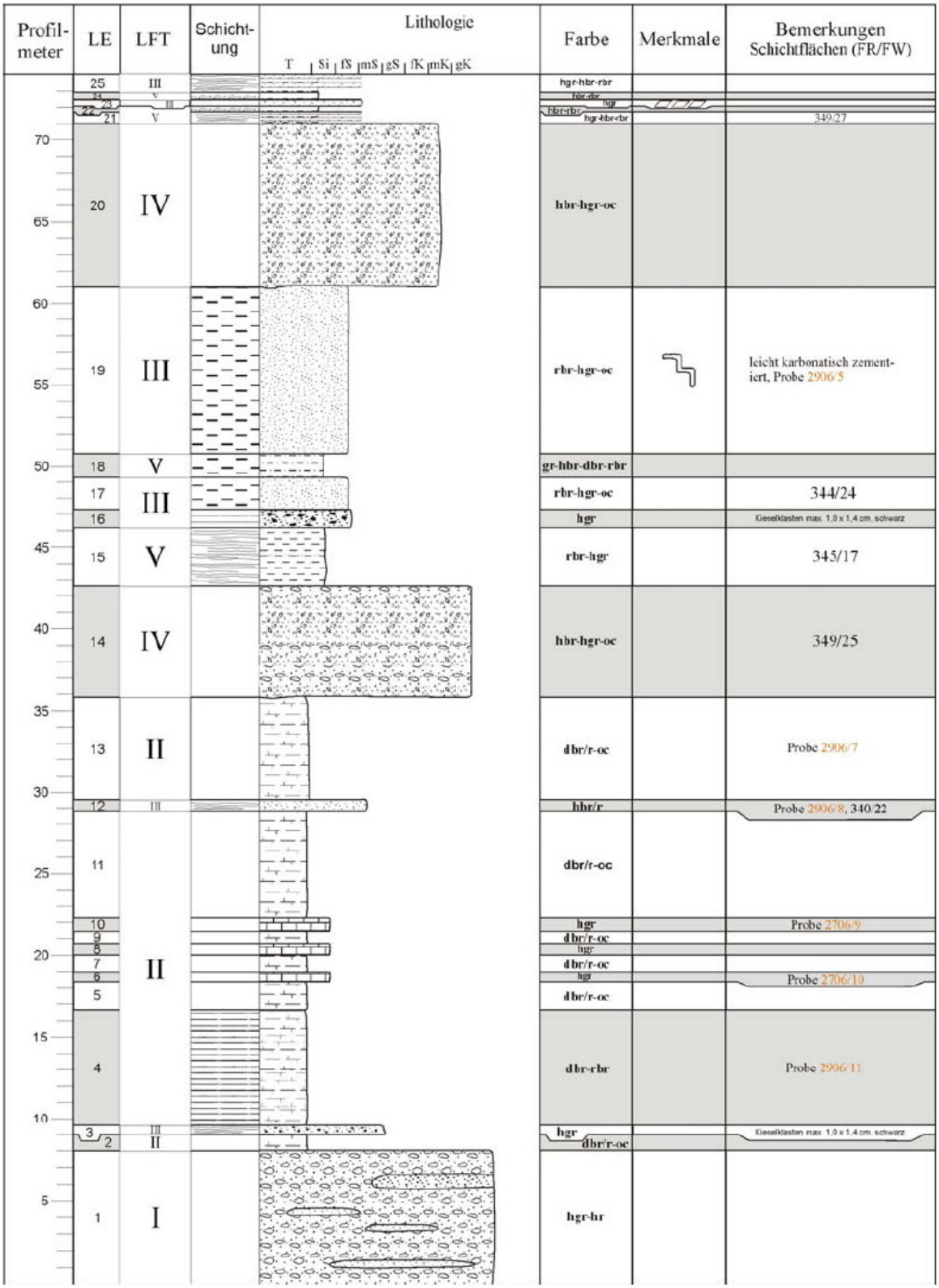

5.6 Paleogene sections

The Paleogene is represented by fossiliferous shallow marine sediments, of which only parts have been logged in detail so far. A complete detailed profile log is planned for 2026.

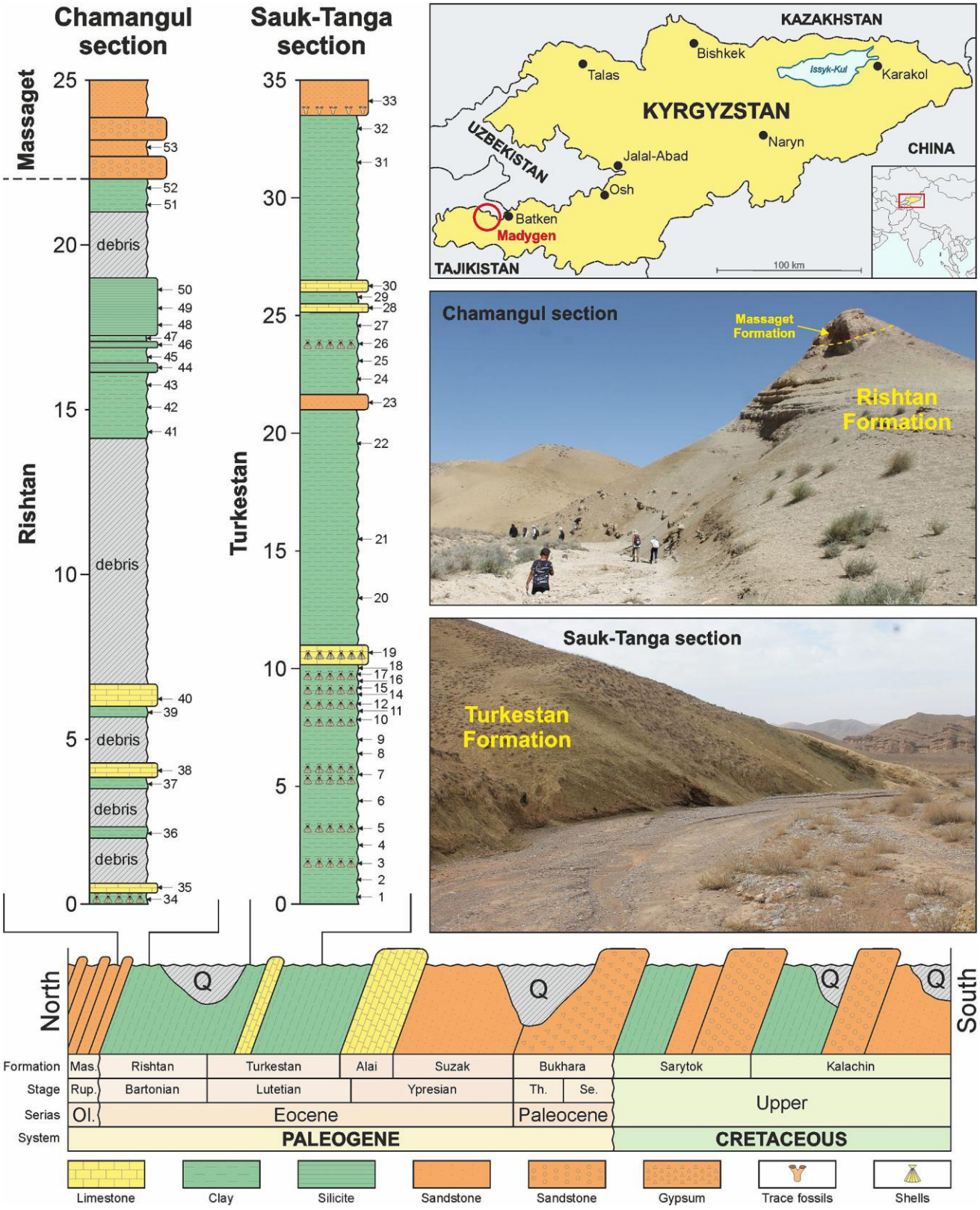

Isfara Paleogene Reference Section (c. 35 km NE of Madygen)

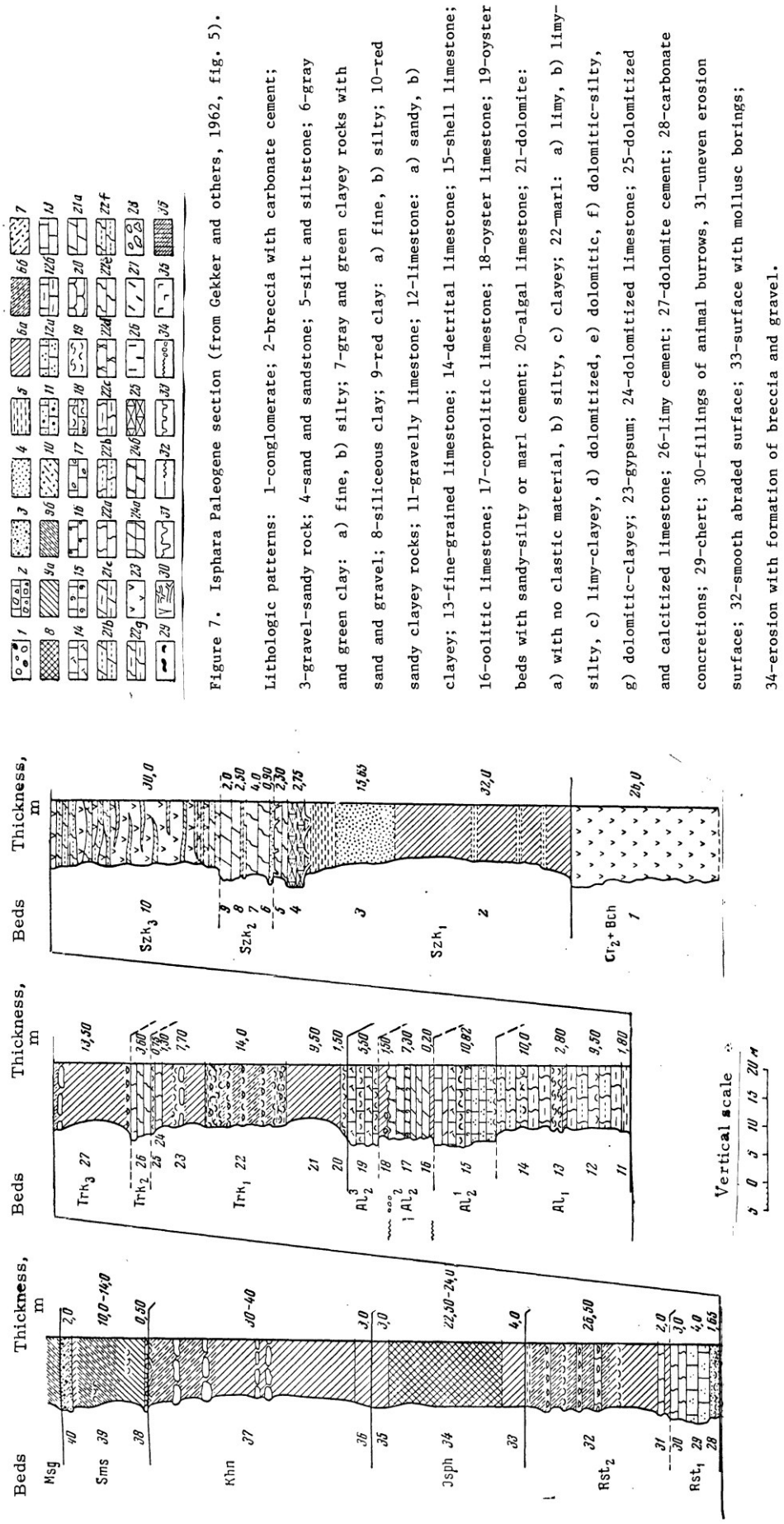

Figure 7. Isphara Paleogene section (from Gekker and others, 1962, fig. 5).

Lithologic patterns: 1-conglomerate; 2-breccia with carbonate cement; 3-gravel-sandy rock; 4-sand and sandstone; 5-silt and siltstone; 6-gray and green clay: a) fine, b) silty; 7-gray and green clayey rocks with sand and gravel; 8-siliceous clay; 9-red clay: a) fine, b) silty; 10-red sandy clayey rocks; 11-gravelly limestone; 12-limestone: a) sandy, b) clayey; 13-fine-grained limestone; 14-detrital limestone; 15-shell limestone; 16-oolitic limestone; 17-coprolitic limestone; 18-oyster limestone; 19-oyster beds with sandy-silty or marl cement; 20-algal limestone; 21-dolomite: a) with no clastic material, b) silty, c) clayey; 22-marl: a) limy, b) limy-silty, c) limy-clayey, d) dolomitized, e) dolomitic, f) dolomitic-silty, g) dolomitic-clayey; 23-gypsum; 24-dolomitized limestone; 25-dolomitized and calcitized limestone; 26-limy cement; 27-dolomite cement; 28-carbonate concretions; 29-chert; 30-fillings of animal burrows, 31-uneven erosion surface; 32-smooth abraded surface; 33-surface with mollusc borings; 34-erosion with formation of breccia and gravel.

5.7 Paleosoil profiles – A Mesozoic climate archive

Fossilized soil horizons preserve indications of the environmental conditions prevalent during soil formation and can be used both qualitative and quantitative paleoclimate reconstructions. The paleosoils in Middle Triassic to Lower Jurassic strata in the Madygen Geopark that can be described as fossil equivalents of modern Vertisols, Gleysols and Histosols. They document relatively high precipitation and groundwater levels throughout the Middle Triassic, with a trend to dryer conditions in the Upper Triassic and Lower Jurassic.

In general five soil types can be distinguished. Gleysols and Histosols are by far the most common types, but also have the most poorly defined profiles because their horizons are usually superimposed and blended in cumulative soils. Vertisols soils are restricted to the alluvial facies of the Kamysh-Bashi Formation.

Gleysol: This soil type has A-(Bw)-Bg-C profiles of about 0.8 to 1.5 m in thickness, if it is well developed. Usually, cumulative soils reaching 4 to 5 m in thickness with overlapping and overprinted horizons are found.

The A horizon is medium to dark grey or grey brown, with variable grain size and little structure, and often enriched in plant detritus and coaly material. The B horizon may have a bleached horizon of variable development and thickness, which is notably depleted in clay and thus of a lighter colour (white-grey to light grey with weak to moderate colour mottling) and coarser than the underlying Bg horizon. It is light to dark grey, usually with strong colour mottling in yellowish, pinkish or olive hues. Mottling is less well developed in the lower parts of many Bg horizons. C/f-related distribution patterns are mostly inherited from the primary sediment, but chitonic domains indicate a weak to moderate degree of clay illuviation (from Bw horizons), as do sparse argillans. Matrix clays are argillasepic or at most insepic, indicating high overall clay content, but little, if any, authigenic clay production from weathering. The C horizons are almost devoid of pedogenic features, but weak colour mottling and rare ferric nodules may be associated with pedogenic processes. However, mottling with diffuse boundaries is also known from lacustrine siltstones and therefore not sufficient to demonstrate soil formation.

Roots are generally abundant and all types are found, but types 1 and 3 clearly dominate. White-grey, pale turquoise and pink-grey haloes 1 – 3 mm wide and with slightly diffuse boundaries and carbonaceous root material are very frequent and indicate very poor drainage as expected in a waterlogged soil.

Histosol: This soil type has O-A-(Bss)-Bg-Cm profiles of up to 2.3 m in thickness. Cumulative soils with alternating O, A and B horizons are common in the backswamp deposits. Cm horizons, on the contrary, are only found below backswamp deposits.
The O horizon is the former peaty surface layer and preserved as crumbly to powdery subbituminous B coal rich in inertodetrinite and huminite, indicating a land plant origin. The A horizon is violet-grey to brown grey in colour and clayey to silty, with few millimetre thick discontinuous coal bands and finely disseminated coaly material. Bss horizons, if present, are 0.1 to 0.3 meters thick and differ in colour and material little from the A horizons. The horizon has a pervasive medium to coarse platy structure with subhorizontal slickensides, often with limonitic coatings. The Bg horizon is similar to that in gleysols, but tends to be thicker (0.8 to 1 m) and less mottled and structured. The lower boundary is sharp but very irregular, with embedded masses similar to the Cm horizon. The Cm horizon is characteristically white to light grey and more strongly cemented than any other soil

horizon. The C/f-related distribution pattern is porphyric and the B-fabric argillasepic, presumably representing original sediment conditions.
The moderately dense to very dense roots are mostly of type 1, but especially in the Kylötok Formation type 5 is frequent. Types 3 and 8 occur occasionally. Root halos are similar to those described for Gleysols. This is consistent with the very poor drainage for this soil type, in which the groundwater level is practically at, or even above the surface.

Vertisol: This soil type has A-Bss-C profiles of 0.5 to 0.9 m in thickness and is restricted to the alluvial facies of the lower Kamysh-Bashi Formation.
The A horizon is silty and red-brown and capped by a surface with mud cracks, which is sometimes not preserved due to subsequent erosion. Towards the base, the colour grades to light grey to greenish-grey hues, probably due to temporary saturation with vadose water that is ponded by the clayey Bss horizon. The Bss horizon is the defining horizon of this soil type and marked by abundant subhorizontal slickensides and a strongly developed platy soil structure. This is due to shrink-swell cycles of the accumulated clay minerals in an interpreted seasonal climate. The C/f-related distribution is mostly fine monic, but the intensive colour complicates the discrimination of matrix clays and illuviated clay, though both types are apparently present. Along slickensides, gefuric sandy crack fill is found near the base. This is incorporated material from the C horizon and might indicate temporary ascending water. The C horizon is barely altered sediment with some bleaching around plant detritus and along sandy layers, probably due to the percolation of vadose water or the presence of oxygenated groundwater. Along the contact with the Bss horizon, ferric nodules are common.

"Red1" paleosoil; This unique soil in the lower Kylötok Formation has an AB-Bc1-Bc2- Bg/Bct-2Bg profile, i.e. the Bg horizon of a gleysol was incompletely overprinted by the Bct horizon of this soil. The thickness is 1.35 m.
The reddened soil horizons have a chitonic C/f-related distribution pattern and skelsepic fabric, with vosepic domains around rare vesicles. This combination points to a certain degree of clay illuviation and strain in the matrix caused by shrink-swell cycles. Further illuviation manifests itself in crack-filling laminated argillans and ferri-argillans.
This soil would be classified as Argillasol, Alfisol or Ultisol, depending on the assumed original cation content. Independent of a particular scheme, it can be described as a moderately drained soil of moderate maturity developed on a Gleysol, due to a sinking groundwater level.

"Red2" paleosoil; This soil type has A-(Bk)-Bw-Bt (or Bc)-C profiles of 1.4 to 1.7 m in thickness. This soil type is generals similar to type Red1, but of higher maturity, with additional differentiation in the B horizon. As with the previous soil type, it could be classified as Argillasol
The A horizon is an unstructured dark brown-grey to grey silty fine sandstone with a moderate density of halo-less type 8 roots. A Bk horizon is moderately carbonatic, a rare feature in the studied paleosoils. The Bw horizon is white grey with dusty pink patches and fringes along poorly developed coarse blocky peds. The Bc or Bt horizons differ by the presence or absence of the nodules described above. Multiple crosscutting generations of ferriargillans create locally a breccia-like structure, but no brecciation is involved, as the cutans can be shown to fill one set of cracks before being cut by the next set. The insepic to mosepic clay fabric points to a limited clay production from localized weathering and a weak influence of shrink-swell cycles. Locally, a skelsepic or masepic fabric is observed in the generally insepic matrix, pointing to higher clay contents and considerable strain exerted by shrink-swell cycles. Intensive clay and sesquioxide illuviation is demonstrated by numerous and thick partially laminated ferri-argillans in crosscutting sets. The C horizon is made up of interbedded siltstones and fine sandstones, mostly light grey with some horizontal pinkish bands. The sharp and straight horizontal boundary with the B horizon suggests that this is the groundwater level, or the highest level in case of fluctuating groundwater conditions.

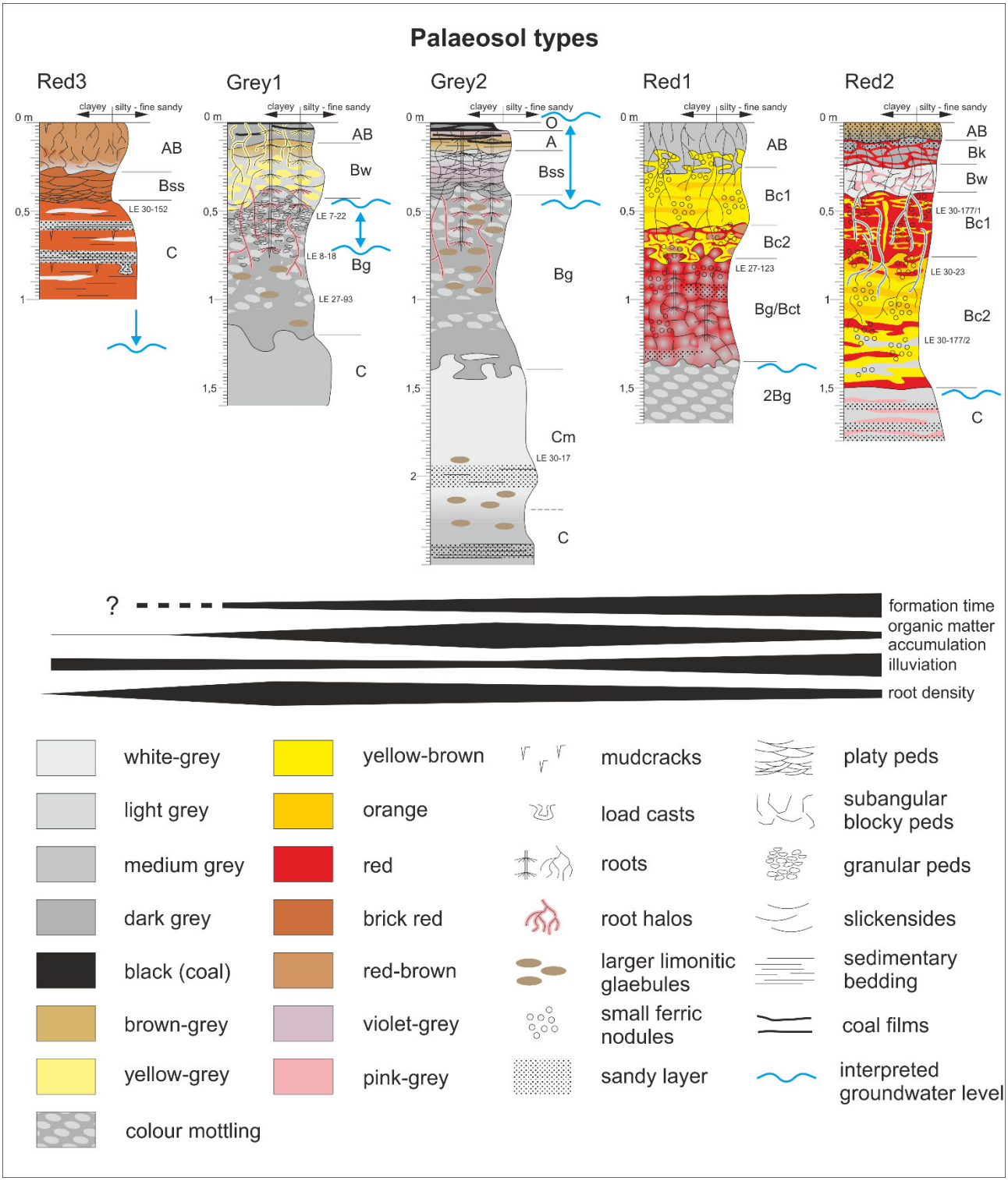

Fig. 1: Idealized diagrams of the paleosoil types (Red3 = Vertisol, Grey1 – Gleysol, Grey2 = Histosol, Red1&Red2 = possible Argillasol, Alfisol or Ultisol)

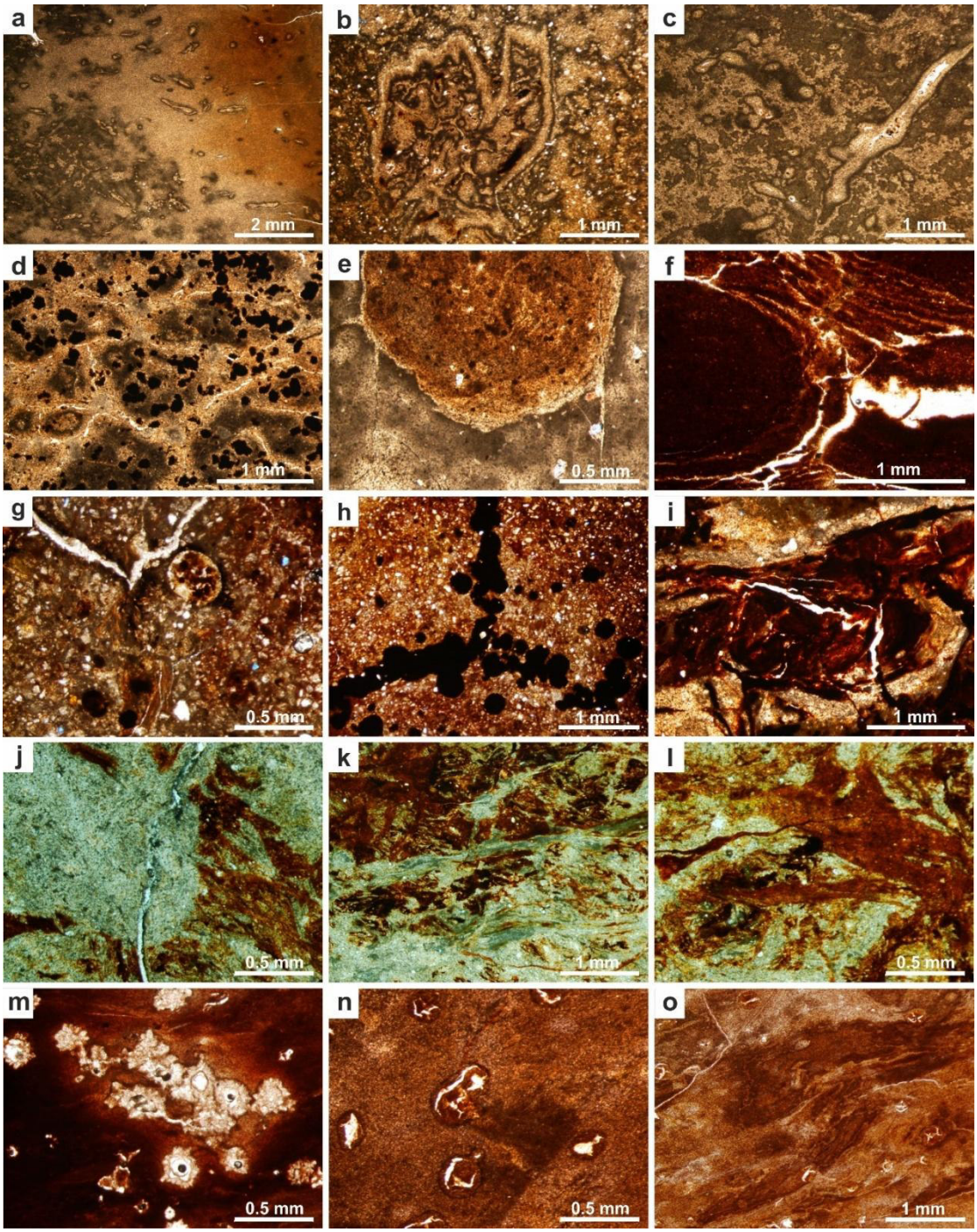

Fig. 2: Photographs of common micromorphological features in thin sections. (a) – (c): LE 7-22 (Bg Horizon of Grey1); (d) LE 8-18 (Bg Horizon of Grey1); (e): LE 30-17 (Cm Horizon of Grey2); (f): LE 30-152 (Bss Horizon of Red3); (g) – (h): LE 27-123 (Bg/Bct Horizon of Red1); (i): LE 30-177/1 (Bc1 Horizon of Red2); (j) – (l): LE 30-177/2 (Bc2 Horizon of Red2); (m) – (o): LE 30-23 (Bc2 Horizon of Red2).
(a) Root channels with two clayey filling layers, and clustering in the clayey matrix (b) Partly collapsed large root channel with complex filling of alternating clayey and silty layers that may reflect the subsequent decay of inner and outer root tissues (c) Root channels in a matrix with flecked clay distribution (d) Fine subangular to granular structure with clay-depleted margins and abundant hematitic nodules are preferably located away from the margins (e) Concretion with weakly developed concentric structure and enclosed skeletal grains. (f) Junction of two slickensides and concentric exfoliation of clayey layers. (g) A crack filled with laminated argillans joins an open crack. Illuviation is followed by formation of nodules with enclosed skeletal grains and finally deposition of ferric crusts on crack and nodule surfaces (h) Strings of subcircular ferric nodules, mostly free of skeletal grains (i) Root channel or other void filled with thick laminated ferri-argillans (j) Filled root channel (notably devoid of skeletal grains) cutting off ferri-argillans (k) Network of ferri-argillans and sequans crosscut by stress cutans arranged in shear bands. Shear bands are terminated by root channels, indicating they are also pedogenic (l) Iron-stained clayey nodule crosscut by a laminated ferri-argillan (m) spheroidal aggregates of gypsum (or other sulphate minerals), some with central cavity (n) pedodes with septarian cracks, often twinned (o) abundant thin ferri-argillans, some cross-cut by, others draped around pedodes

6 Paleontology – Introduction to the main fossil groups

6.1 Cambrian

Early Middle Cambrian bituminous coquinoid limestones from a tectonically isolated outcrop in southwestern Kyrgyzstan yield a remarkably diverse fauna, with stem-group cnidarians, trilobites, rhynchonelliformean brachiopods, and other shelly fossils. The fossil site is in the northern foothills of the Turkestan Range and thus forms part of the westernmost extension of the South Tien Shan. The fauna includes two fairly well known trilobite species, *Glabrella ventrosa* Lermontova (1940) and *Dorypyge richthofeniformis* Lermontova (1940) that provide confident support for an Amgan age of the rocks. New described taxa include the stem-group cnidarian *Cambroctoconus kyrgyzstanicus* Peel sp. nov., the trilobite *Olenoides sagittatus* Geyer sp. nov., and the helcionelloid *Manasoconus bifrons* Peel gen. et sp. nov. Additional fossils within the samples include the trilobites *Olenoides* sp. A, *Kootenia* sp., and *Pseudoeteraspis*? sp.; the rhynchonelliform brachiopods *Narynella* cf. *ferganensis* (Andreeva, 1962), *Narynella*? sp., *Austrohedra*? sp. nov., and two species of uncertain generic affinity; the tommotiid *Tesella* sp.; the hyolithelminth *Hyolithellus* sp.; and the palaeoscolecid *Hadimopanella oezgueli* Gedik, 1977. (Geyer et al., 2014)

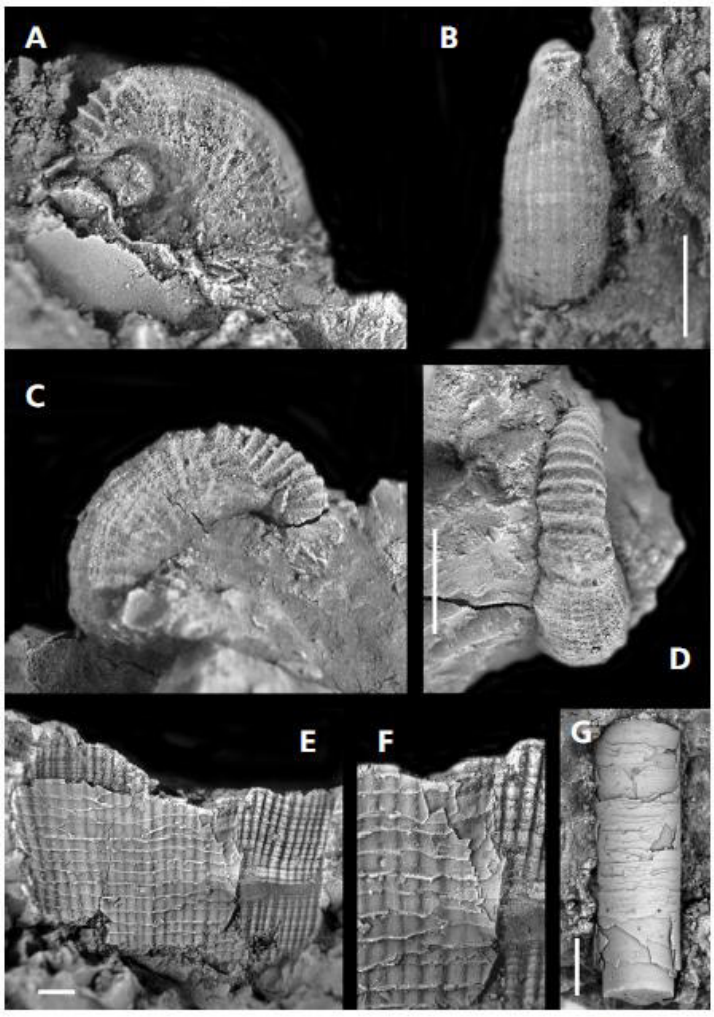

Figure 3. A–D – *Manasoconus bifrons* Peel gen. et sp. nov, Sauk Tanga locality; A, B – conch, internal mould, FG 596/XII/017b, lateral view and view of the abapical side of the whorl; C, D – conch, internal mould, holotype, FG 596/XII/029a, lateral view and view of the abapical side of the whorl. • E, F – *Tesella* sp., FG 596/XII/016b, entire specimen as preserved and detail. • G – *Hyolithellus* sp., FG 596/XII/004b, fragment of tube. All scale bars 1 mm.

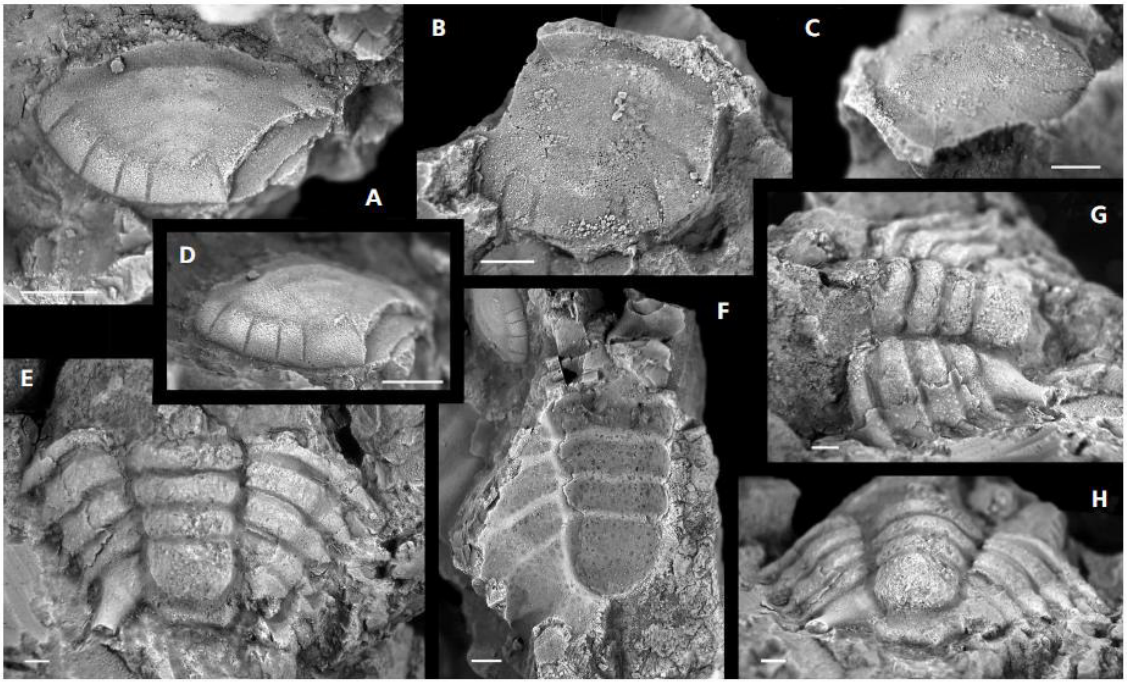

Figure 4. A–D – *Glabrella ventrosa* Lermontova, 1940, Sauk Tanga locality. • A, D – pygidium, internal mould, partly broken and exhibiting ventral doublure, FG 596/XII/018b; A – dorsal view; D – oblique posterior view. • B, C – incomplete pygidium, internal mould, FG 596/XII/014a; B – dorsal view; C – slightly oblique lateral view. Scale bar 1 mm. • E–H – *Dorypyge richthofeniformis* Lermontova, 1940, Sauk Tanga locality; E, G, H – pygidium, partly exfoliated, FG 596/XII/001a. E – dorsal view; G – left lateral view; H – posterior view. • F – incomplete pygidium, partly exfoliated, ventral view external mould, FG 596/XII/018a, together with pygidium of *Glabrella ventrosa* shown in Fig. 4A and 4D. Note infilling of a central canal in the coarse granules. Scale bar 1 mm.

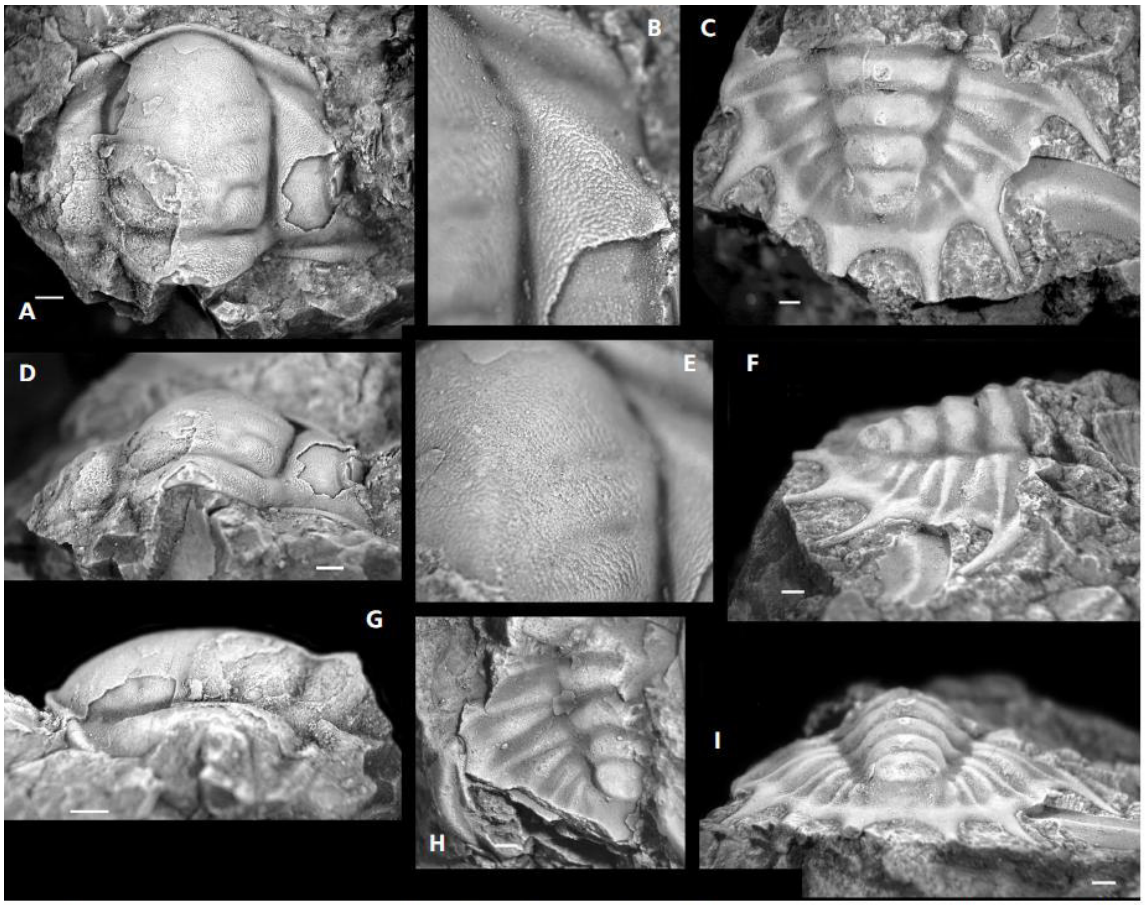

Figure 5. *Olenoides sagittatus* Geyer sp. nov., Sauk Tanga locality. • A, B, D, E, G – paratype, incomplete cranidium, partly exfoliated, FG 596/XII/011b. A – dorsal view; B – dorsal view, detail of fixigena and eye ridge showing pattern of terrace ridges; D – posterior view; E – dorsal view, detail of anterior part of glabella with pattern of terrace ridges; G – left lateral view. • C, F, I – holotype, incomplete pygidium, FG 596/XII/010a, internal mould, dorsal, lateral and posterior views. • H – paratype, fragment of pygidium, internal mould, FG 596/XII/016a.

6.2 Triassic - Jurassic

6.2.1 Flora

The plant fossils of the Madygen Formation constitute one of the richest and most diverse Triassic floras of Eurasia. This flora is dominated by pteridosperms, ginkgophytes, and sphenophytes; ferns, lycophytes, algae and mosses do also occur in lesser abundance. This unique fossil Lagerstätte shows a highly remarkable preservation of the fossil plants. Due to its very fine grain-size, the embedding sediment has often formed a natural cast of the epidermal cell pattern. In addition, are abundant. Many gymnosperm leaves show evidence for plant-insect interactions (e.g. margin feeding, oviposition, piercing, sucking). This coincides with one of the most important herbivore expansions seen in the fossil record. This phenomenon has been recognised in the Middle and Upper Triassic of the USA, Western Europe, and South Africa.



Division Lycophyta
Order Isoetales
Family Isoetaceae
Genus *Annalepis* Fliche, 1910 (Fig. 1) Ma Ky Kb

Sporophylls of 3-3.5 cm length. The sporangium is located in the proximal portion and is surrounded by wings. The distal portion ends with a small pointed tip. The ligular pit ca. 0.1 cm in diameter. Scale bar 1 cm.

Division Sphenophyta
Order Equisetales
Family Equisetaceae
Genus *Neocalamites*, Halle, 1908 (Figs. 2-3) Ma Ky Kb

Axes of these Triassic horsetails are characterized by distinct nodes, internodes, and longitudinal striae. The leaves or leaflets are linear, narrow and have a single vein. Scale bars 1 cm.

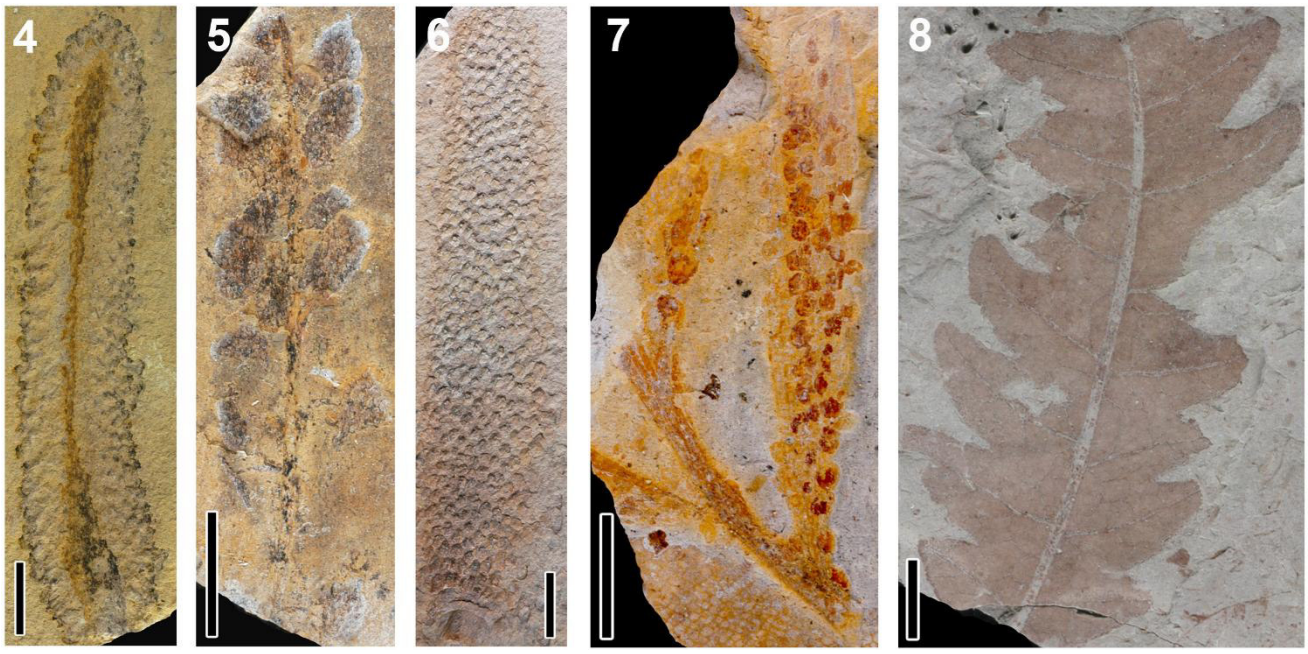

Division Sphenophyta
Order Equisetales
Family Equisetaceae
Genus *Neocalamostachys* Kon'no, 1962 (Figs. 4-7) Ma Ky Kb

These strobili are up to 7 cm long and 1-1.5 cm wide. They bear peltate sporangiophores with several sporangia, in which spores are produced. Scale 1 cm.

Division Pteridophyta
Order Filicales
Family Dipteridaceae
Genus *Dictyophyllum* (Lindley and Hutton, 1834) Webb, 1982 (Fig. 8) Ma Ky Kb

Pinnate fronds up to 6 cm long and 3 cm wide. Pinnules falcate. Venation reticulate, the veins arise at almost right angles to form polygonal vein meshes. Scale bar 1 cm.

Division Pteridophyta
Order Filicales
Family Osmundaceae
Genus *Cladophlebis* Brongniart, 1849 (Figs. 9-10) Ma Ky Kb

Sterile frond fragments. Pinnules mostly falcate to linear, margin entire to serrate. Pinnule base not contracted. Venation pecopterid with a midrib and secondary veins. Scale bars 1 cm.

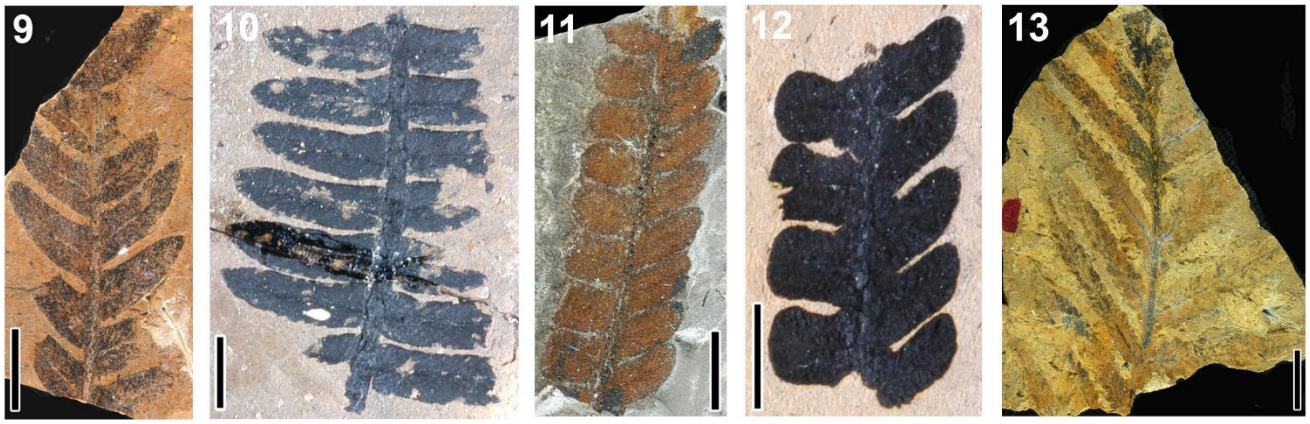

Division Pteridophyta
Order Marattiales
Family Pecopteridaceae
Genus *Pecopteris* Brongniart, 1822 (Figs. 11-12) Ma Ky Kb

Pinnate fronds with broadly having entire and parallel margins. Pinnules of 0.2-0.5 cm long and 0.2-0.3 cm wide. Venation with a single vein and lateral veins once or twice forked. Scale bars 0.5 cm.

Division Gymnospermophyta
Order Peltaspermales
Family Peltaspermaceae
Genus *Scytophyllum* Bornemann, 1856 (Fig. 13-14) Ma Ky Kb

Fronds imparipinnate (odd pinnate). Pinnules lanceolate, 3.5-4 cm long and 0.3-0.5 cm wide, are attached opposite to subopposite. Pinnule margins crenate to lobate. Venation is pinnate, with a strong midrib; secondary veins are rarely forked. Scale bar 1 cm.



Division Gymnospermophyta
Order Peltaspermales
Family Peltaspermaceae
Genus *Vittaephyllum* Dobruskina, 1975 (Figs. 15-16) Ma Ky Kb

Leaf lamina of 9-11cm long, divided twice into four parts, with entire or slightly lobed margin. Strong midrib with simple secondary veins; in some species they dichotomise. Scale bars 1 cm.

Genus *Lepidopteris* Schimper, 1869 (Fig.17) Ma Ky Kb

Fronds bipinnate. Pinnae up to 7 cm long and 0.6-1 cm wide, opposite to subopposite. Pinnules 0.3-0.5 cm long and 0.3-0.5 cm wide, obliquely inserted on the pinna rachis. Venation pinnate, secondary veins occasionally forked. A characteristic feature of this genus is the occurrence of intercalary pinnules attached to the main rachis (zwischerfiedern). Scale bar 1 cm.

Genus *Edyndella* Mogutcheva, 1973 (Fig. 18) Ma Ky Kb

Fronds pinnate 8 cm long and 2.5 cm wide. Pinnae elongated-linear 3 cm long and 0.3-0.4 cm wide. The top of the pinnae is obtuse or rounded. Parallel veins, occasionally dichotomizing. Scale bar 1 cm.

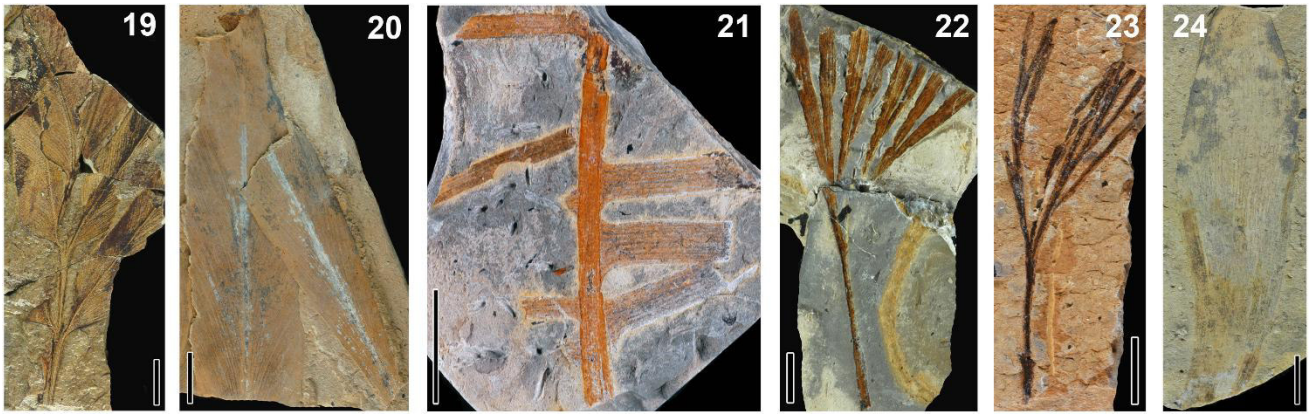

Division Gymnospermophyta
Order Peltaspermales
Family Peltaspermaceae
Genus *Uralophyllum* Kryshtofovich et Prynada, 1933 (Figs. 19-20) Ma Ky Kb

Pinnate fronds or isolated pinnae may be found. Pinnae of 4-10 cm long and 1.5-3 cm wide, are oblanceolate to ovate and with a clear petiole. Pinnae with a distinctive and strong midrib from which the veins arise with an acute angle. Scale bars 1 cm.

Division Gymnospermophyta
Order Bennettitales
Genus *Pterophyllum* Brongniart, 1825 (Fig. 21) Ma Ky Kb

Fronds once pinnate; pinna segments inserted laterally and with parallel margins. Pinna segments with parallel veins are attached broadly at the base, arising at right angles to the rachis. Rachis up to 0.5 cm wide, longitudinally striated. Scale bar 1 cm.

Division Gymnospermophyta
Order Ginkgoales
Genus *Baiera* Braun, 1843 (Figs. 22-23) Ma Ky Kb

Leaves are laciniate, triangular to semicircular in shape up to 9 cm long and 5 cm wide. The most important feature of this ginkgophyte leaf type is the presence a distinct petiole and deeply divided lamina in narrow segments (filiform segments or laciniae). The width of the laciniae is between 0.1-0.4 cm and the length is between 3-4 cm. Each lacinia contains no more than 4-6 veins. Scale bars 1 cm.

Genus *Eretmophyllum* Thomas, 1913 (Fig. 24) Ma Ky Kb

Oblanceolate undivided, petiolate leaves, 8 cm long with an entire margin. Leaves are gradually narrowing towards the petiole. Veins are parallel and often forked in the basal part of the leaf. Scale bar 1 cm.

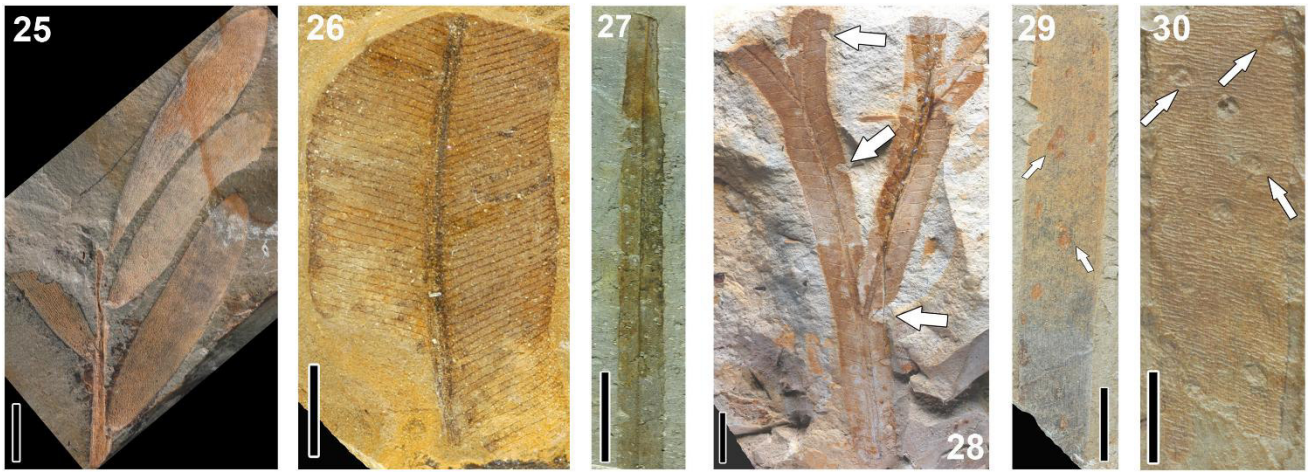

Division Gymnospermophyta
Order Coniferales
Family Voltziaceae
Genus *Podozamites* Braun, 1843 (Fig. 25) Ma Ky Kb

Planate shoot systems with leaves 4 cm long and 0.5-1 cm wide, mostly lanceolate to oblanceolate and with a short petiole. Parallel veins divided in the basal portion of the leaf and converge slightly near the leaf apex. Scale bar 1 cm.

Pteridophylla incertae sedis
Taeniopteris Brongniart, 1832 (Fig. 26) Ma Ky Kb

Simple isolated leaves. They are lanceolate, oblanceolate, obovate, oblong or linear in shape. Leaves with a prominent midrib that is extending through the entire leaf. Lateral veins arising at angles of approximately 80-90°, simple or forking at the base. Scale bar 0.5 cm.

Mesenteriophyllum Sixtel, 1962 (Fig. 27) Ma Ky Kb

Simple and linear to lanceolate leaves up to 5 cm long and 0.3-0.5 cm wide, with a strong midrib and spine-like protuberances along the margin. Scale bar 1 cm.

6.2.2 Plant-Insect interactions

Margin Feeding (Fig. 28)
semicircular, shallow to deep excision of leaf margin. Scale bar 1 cm.
Oviposition (Fig. 29)
Lenticular-ovoidal scars in cluster or isolated. Oriented longitudinally to the leaf. Scale bar 1 cm.
Piercing or sucking (Fig. 30)
Circular punctures of ca. 2 mm diameter with a central dome. Scale bar 1 cm.

6.2.3 Roots

Fossil root traces that can be classified into eight different morphological types have been documented in profile sections in the Middle Triassic to Lower Jurassic fluvial-palustrine sediments of the Madygen Geopark. From a morphological perspective the traces can be compared to several fossil root taxa described previously. From a paleoecological perspective the distribution and frequency of the various root types is useful to reconstruct patterns of vegetation distribution in the paleolandscape at higher spatial resolution than would be possible from typical finds of floral remains. Because of this, the utilization of root traces in the sedimentological interpretation of facies patterns and the architecture of fluvial-palustrine depositional systems is of great value.

Type 1 : Vertical tubes 3 to 11 mm in diameter, but mostly in the 5 to 7 mm range, usually preserved as silty to fine sandy casts. The root is structured by nodes spaced 2.5 to 6 cm apart with an irregular wavy to dented seam line. The internodes are covered by slightly curvilinear ribs spaced 1 to 1.5 mm apart, which, at least under good preservation conditions, are continuous from one node to the next. Rarely less than 1 cm long ribs branch off from the continuous ribs. Lateral roots grow radially from the nodes. This type of root can be related to horsetails, likely *Equisetites* sp. and *Neocalamites* sp., which are the most common flora.

Type 2: This root type is morphologically similar to type 1. Diagnostic differences are the smaller length of internodes (1 to 1.5 cm) and the fine reticular surface structure composed of 0.2 to 0.4 mm wide square cells. All samples are preserved as silty casts with irregular curvy ridges. This type of root can be related to horsetails, likely *Equisetites* sp. and *Neocalamites* sp., which are the most common flora.

Type 3: Main roots have dominantly vertical orientation and are preserved as 2 to 5 mm wide brown imprints, partially with dark brown limonite coatings and 1 to 3 mm wide diffuse limonite haloes. No casts are found. Individual roots can rarely be traced for more than 5 cm. Lateral roots are strongly branching, typically every 1 to 3 cm, and show no preferred orientation.

Type 4: Main roots are found exclusively in horizontal to subhorizontal orientation and are preserved as 3 to 9 mm wide brown imprints, partially with limonite crusts or reticular patterns with 0.5 to 2 mm wide divisions. Lateral roots branch off at right angles from the main roots in clusters, while other sections of main roots have no lateral roots at all. The distance between individual lateral roots is 3 to 6 mm. They are preserved as 1 to 2.5 mm wide brown imprints, but their length seldom exceeds 2 cm, Like the main roots, most lateral roots are oriented horizontally.

Type 5: The width varies from 10 mm to 25 cm, with most roots being in the 2 to 5 cm span. The two branches split off from the original direction enclosing variable angles up to 120°. Both branches are only marginally less wide than the root from which they branch. Lateral roots are rarely seen; they are preserved as 1 to 2 mm wide brown imprints without surface markings. Their orientation is also horizontal. The size and structure of this root type suggests that is part of a tree-like plant. The plant groups with such forms that are documented from the Madygen Formation are *Pteridospermatophyta*, *Ginkgophyta*, *Coniferophyta* and *Cycadophyta*, among other less frequent forms.

Type 6: This root type is characterised by vertical main roots which taper downwards. They are preserved as light to medium grey silty to fine sandy casts with elliptical cross-sections up to 24 x 17 mm. The filling has vague concentric less than 1 mm wide lighter and darker bands. Contacts of the cast and the surrounding sediments are overprinted by slickensides, obscuring any superficial

markings. Possible lateral roots are preserved as light grey silty to fine sandy casts 1 to 2 mm in diameter, with variable orientation and some dichotomous branching.

Type 7: This type groups tubular branched structures of variable orientation with root-like morphology, but without any root remains preserved. The tubes are 1 to 10 mm in diameter, with the larger ones having more diffuse boundaries. Generally, the tubes are brighter than the surrounding sediment, but colour varies from white-grey to pink-grey and pale turquoise.

Type 8: This root type includes various small roots which are mostly preserved as brown imprints. Typical examples are 0.5 – 2 mm wide and few centimetres long, with irregular orientation and branching patterns. This type is not attached to any larger roots, and in this respect different from the lateral roots of type 3.
This root type is quite frequent in all three formations.



Fig. 1: (a – c) Microphotographs of preserved cell structure on horsetail root casts in three-dimensional preservation

Fig. 2(next page): Diagrams of the eight root types known from the Triassic and Jurassic fluviopalustrine sediments at Madygen.

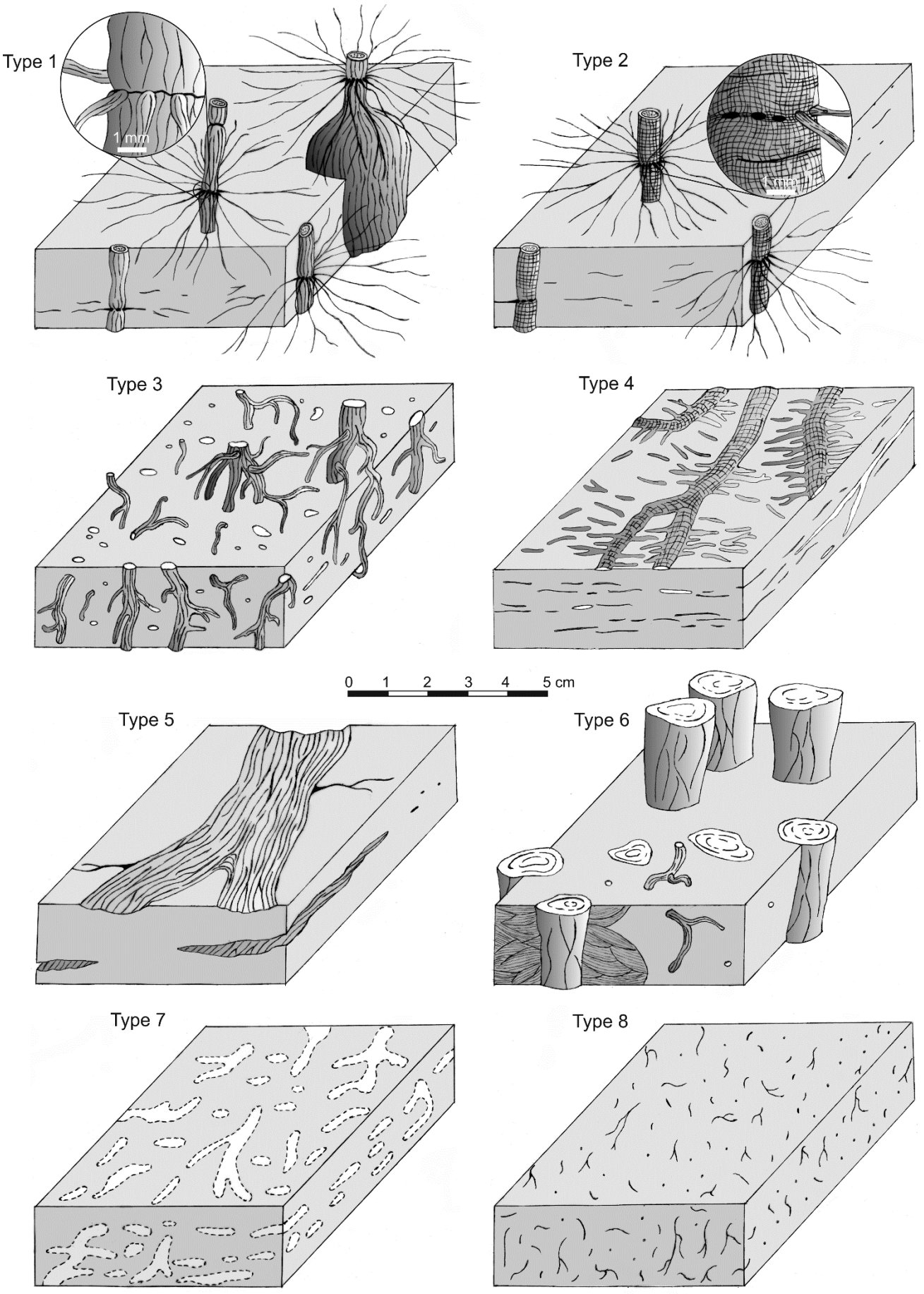
Type 1
1 mm
Type 2
Type 3
Type 4
0 1 2 3 4 5 cm
Type 5
Type 6
Type 7
Type 8

6.2.4 Insects

The most important feature for the taxonomic identification of insects is their wings. Fore wings are in general longer than hind wings and narrower. Hind wings are proximally broad. **Fig. 1** is a more simplified overview over main vein areas, often added with an A (anterior) or P (posterior).

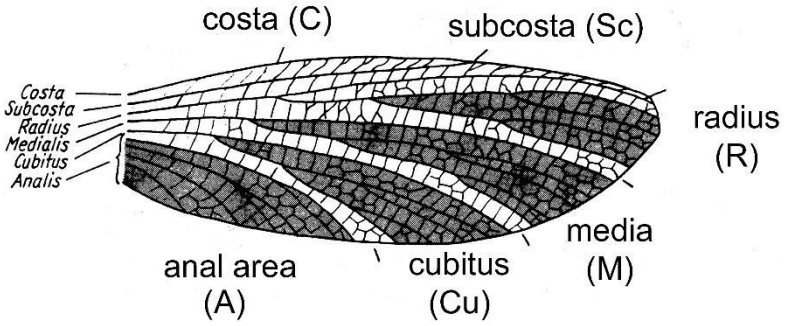

Fig. 1: Nomenclature for the main vein areas of a generalized insect wing. Modified from MÜLLER 1989.

The main veins are long and follow the direction of wing. Generally the major veins are alternately convex (+) or concave (-) relative to the surface plane of the wing, especially near the wing attachment. The space between the veins is mostly filled with cross veins, which may form a fine meshwork.

Here are the distinguishable orders. All other insect orders or insect remains are more difficult to identify in the field.

Ensifera (from Orthoptera)

- subcosta concave
- sigmoid main veins typical (male)
- fore wing thicker or leathery (tegma)

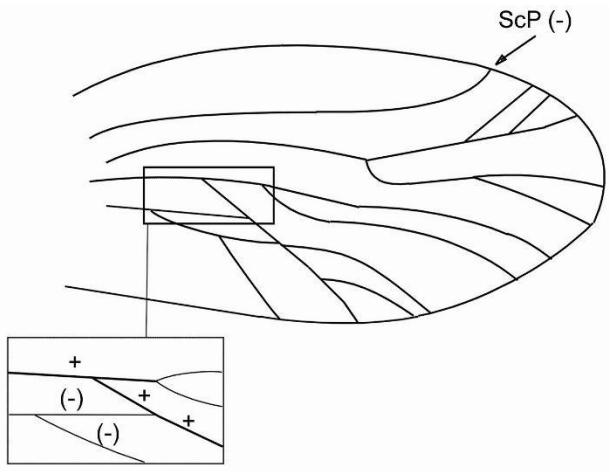

Caelifera (from Orthoptera)

- many cross veins
- fore wings longer than body and narrow
- fore wing thicker

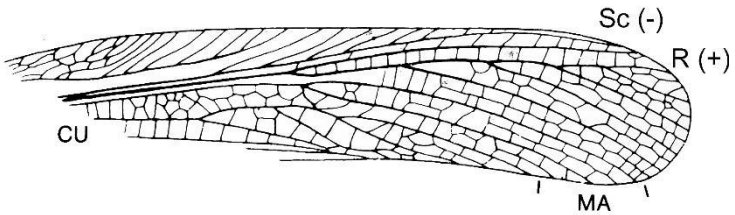

Mecoptera (scorpionflies, hangingflies)

- two pairs of similar wings
- M often with more than two branches (dichotomus)
- few cross veins
- many main veins

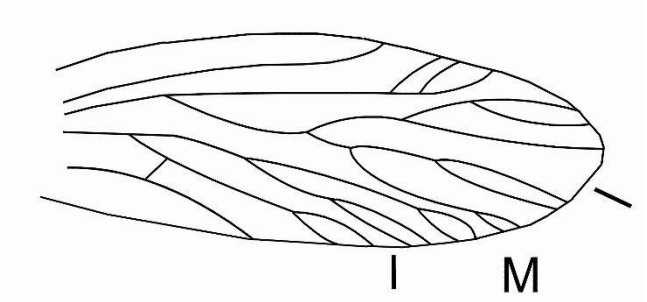

Blattodea (roaches)

- broad pronotum
- numerous veins
- homogeneous vein relief
- cross veins not well visible
- wings have not equal length
- one wing overlaps the other
- antennas sometimes visible

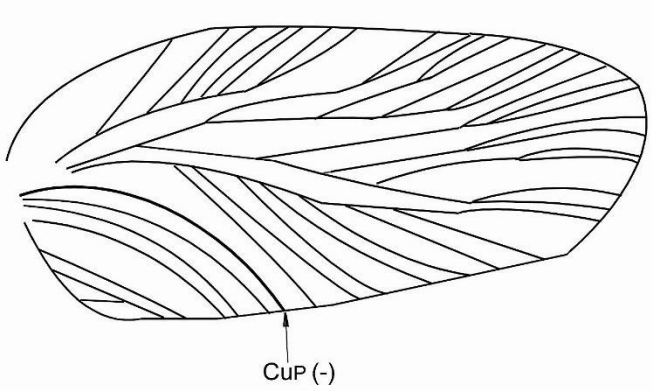

Titanopterida

- usually huge insects, several cm to 10 or 20 cm
- broad area in the middle of forewing
- usually big, venous cross veins, often alternating convex and concave
- sclerotic between cross veins

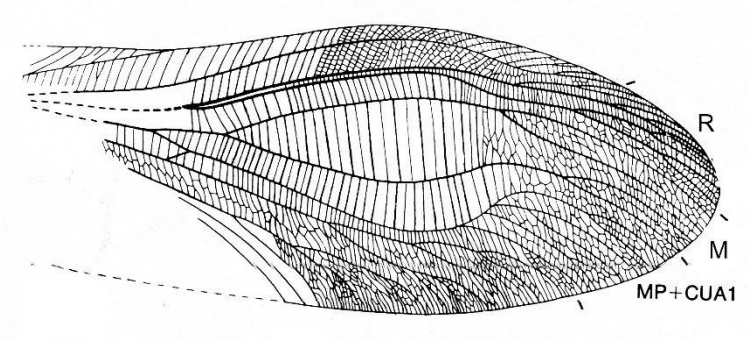

Coleoptera (beetles)

- forewings visible (elytra) punctuated
- no or few main veins and relatively parallel
- many cells (punctuation) with 5 or 6 edges

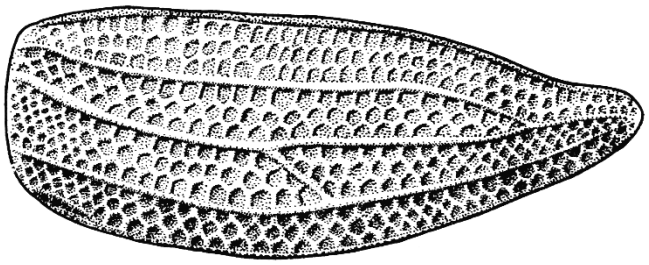

Hymenoptera

- forewing and hind wing are coupled
- main veins not straight
- relatively few main veins
- cells between main veins with 5 – 6 edges
- some species with v-shaped stigma

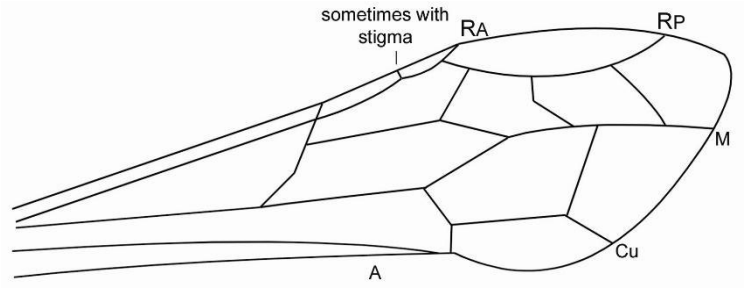

Heteroptera (Hemiptera)

- few cross veins
- wings flat
- sclerotic part on proximal wing part
- not sclerotic part on distal wing part, membranous
- wide costal area without main veins (“head area”)

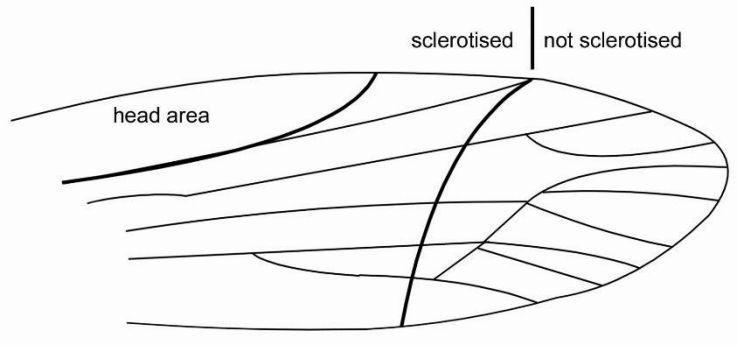

Ephemeroptera (mayflies)

- hind wings reduced and small
- costal brace proximal
- “double branching” in R and M areas (look at arrow)
- stray in convex / concave alternation
- many cross veins

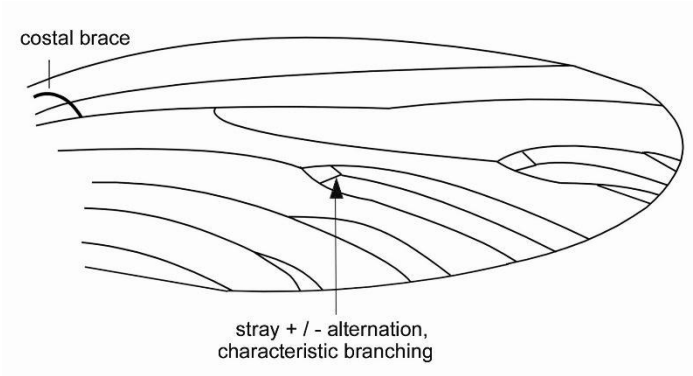

Odonata (dragonflies, damselflies)

- equal fore and hind wings ore hind wings wider
- large head with huge eyes
- nodus in costal area
- many cross veins
- proximal is wing narrow
- stray in convex / concave alternation

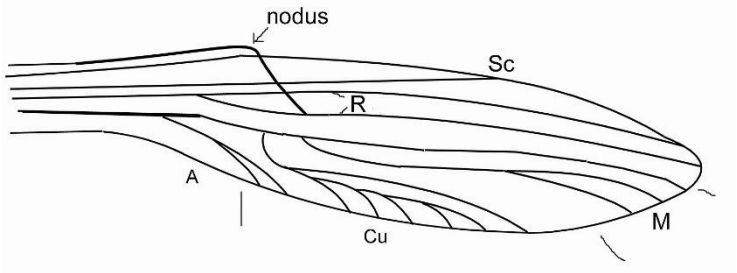

Grylloblattodea (rock crawlers or ice crawlers)

- CuA with a proximal branching (O)
- cubitus concave
- cross veins well visible
- many cross veins

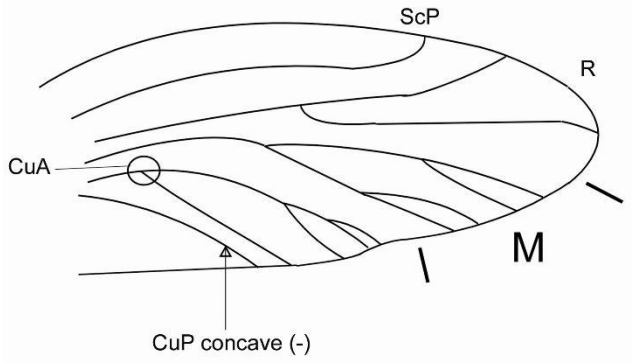

Glosselytrodea

- fore and hind wings subequal size
- many cross veins (similar to Coleoptera)
- straight line through the whole wing (M)
- fore wing with precostal area (many cross veins)
- Cu long and sometimes touches M

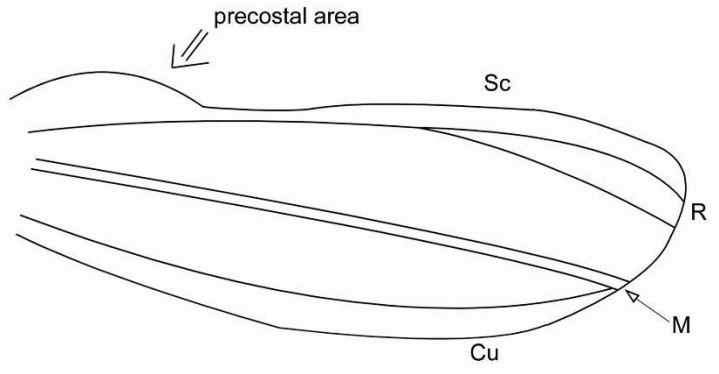

Plecoptera (stoneflies)

- fore and hind wings are subequal
- wings wrap abdomen
- few cross veins, proximal
- M with 2 branches
- cubitus area concave, posterior (it goes in the surface)

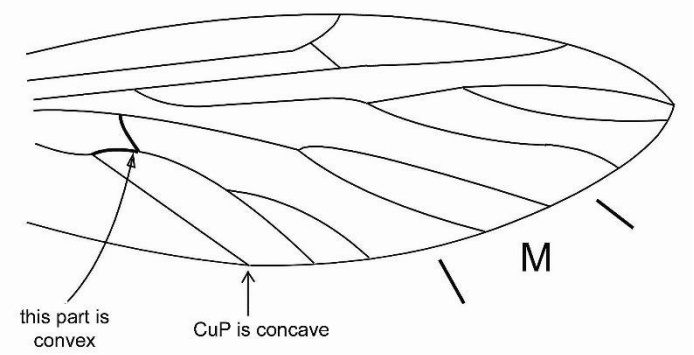

Phasmatodea (stick-insects)

- many cross veins, +
- R simple or only distally branched

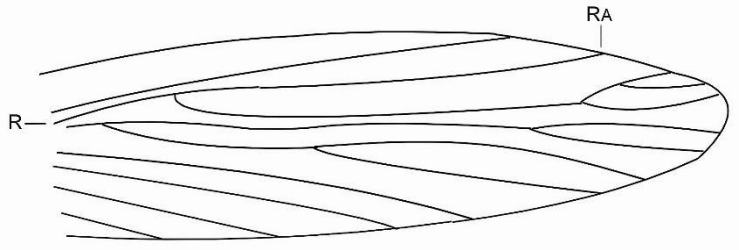

Miocoptera

- **no** cross veins (!)
- small size
- very few main veins

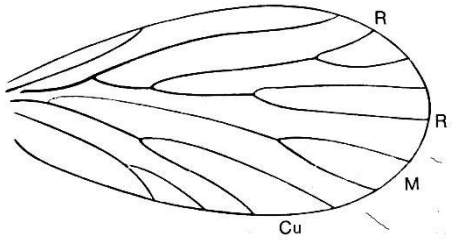

Panelcanida

- few cross veins
- R and M fused

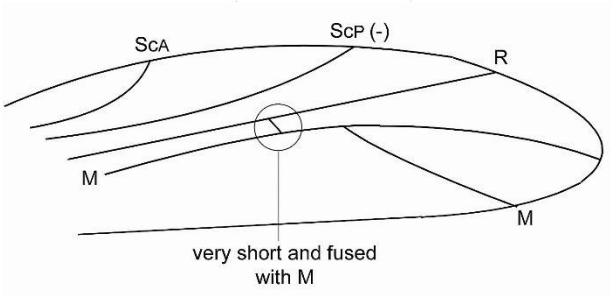

6.2.5 Chondrichthyes

The Madygen Formation has yielded two types of freshwater shark egg capsules and shark teeth referable to one of the capsule types.

Xenacanthiformes
Genus *Fayolia* Renault & Zeiller, 1884 (Figs. 1, 2)

Fayolia sharovi

Fayolia is preserved in uncompressed and compressed specimens. The body is cone-like, averaging 34 mm in length and 8 mm in width uncompressed and up to 18 mm compressed. A beak is not visible. A slender pedicle, twisted in spirals, with a length of at least 13 mm and a maximum width of 2 mm, is occasionally preserved. The body is sectioned by two spiral bands averaging 10 mm in width and bearing a broad flange (collarette). Compression of the spiral band produced a rhomboidal surface pattern in flattened specimens. A fine longitudinal striation of the two bands parallel to the intersecting collarettes is noticeable. One specimen shows two egg capsules attached by their pointed beaks (Fig. 2).

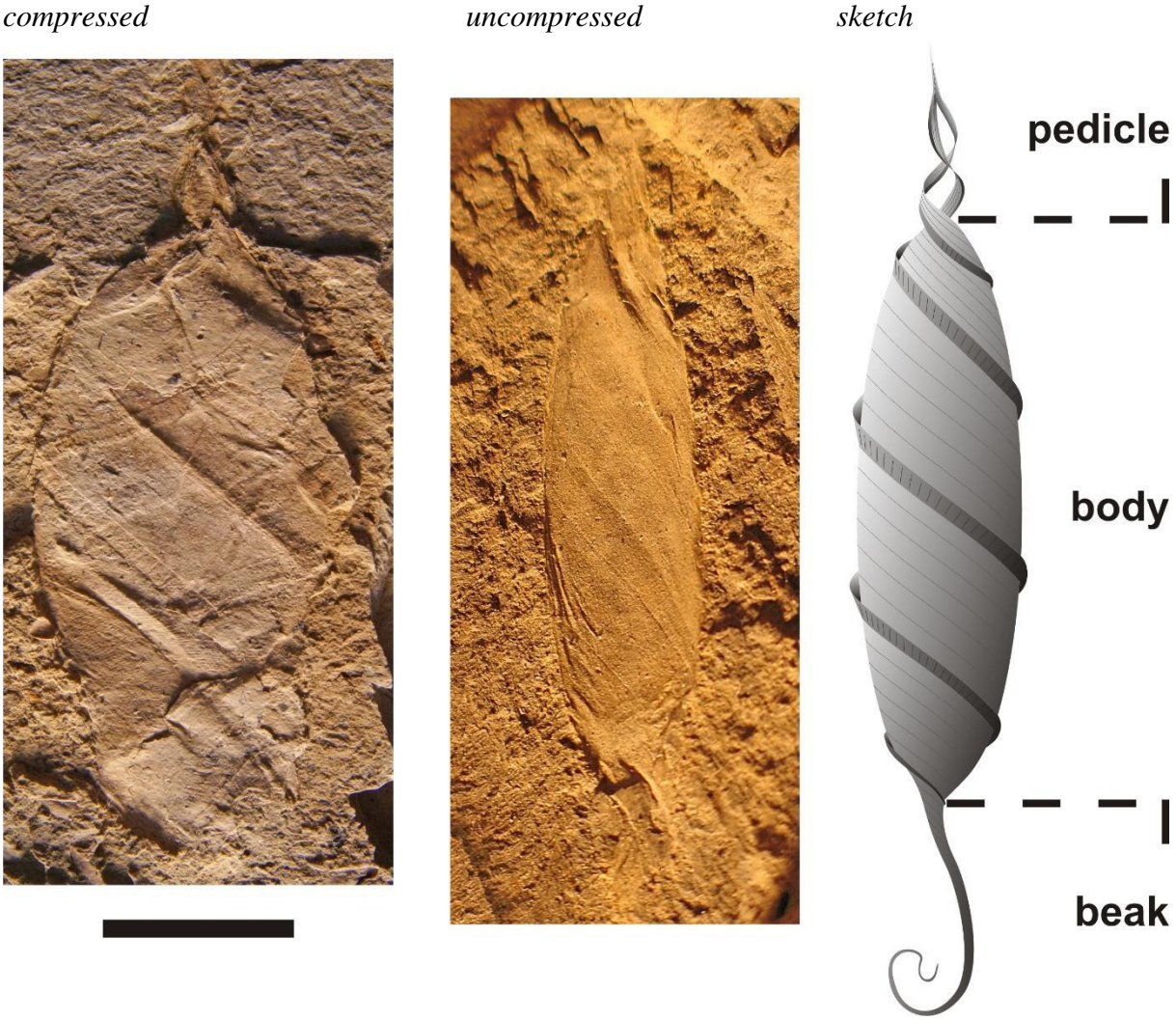

Fig. 1. *Fayolia sharovi*, sketch of the original shape of an uncompressed specimen, together with two remains from the Madygen Formation; scale bar = 1 cm.



Fig. 2. Specimen with two *Fayolia sharovi* capsules, agglutinated by their pointed beaks.

Fayolia sharovi is the youngest of the 16 *Fayolia* species formally described so far. *Fayolia* is interpreted as the egg capslues of xenacanth sharks, which disappear at the end of the Triassic. In Madygen, body evidence of xenacanths is still to be found!

Hybodontiformes

Genus *Palaeoxyris* Brongniart, 1828 (Fig. 3)

Palaeoxyris alterna

The body is broadly fusiform, 30 mm long and 13 mm wide, and gradually tapers towards each end. The pedicle is minimum 30 mm long, and invariably traversed by parallel arranged ribbing structures. The beak is 20 mm long, and traversed by roughly parallel arranged ribs. The body is sectioned by six spiral bands averaging 3 mm in width, show a rhythmic variation in breadth: b-b-n-b-b-n (b-broad, n-narrow), and also showing a double fissure line between them. The surface shows a secondary, characteristic transverse rhomboidal pattern resulted from compression during fossilization. Uncompressed specimens show the original spiral ribbing structure.

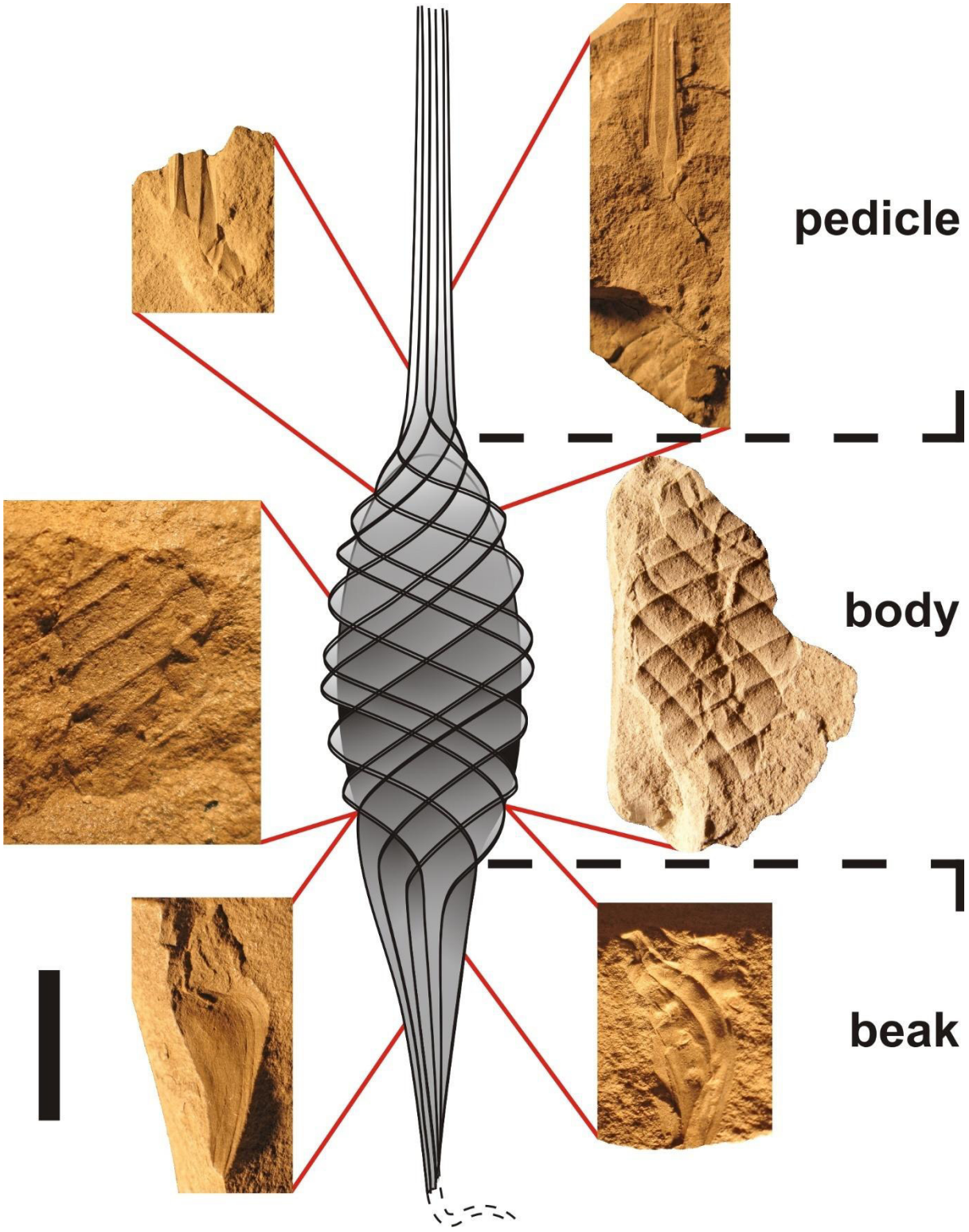

Fig. 3. *Palaeoxyris alterna*, sketch of the original shape of a flattened specimen, correlated with fossil fragments (compressed and uncompressed) from the Madygen Formation; scale bar = 1 cm.

Genus *Lonchidion* Estes, 1964 (Fig. 4)

Lonchidion ferganensis

Dozens of hybodont teeth recovered from the Madygen Formation derive from small sharks that hatched from the *Palaeoxyris* capsules and fed on bivalves in the shallow nearshore lake parts. Only one larger tooth found so far points to the larger individuals laying the eggs.



Fig. 4. Tooth of *Lonchidion ferganensis* (left); life reconstruction of a hybodont shark (F. Spindler, right).

6.2.6 Osteichthyes

Seven taxa of bony fishes, both ray-fins and lobe-fins, have been described from the Madygen Formation. Ichthyoliths and hitherto undescribed skeletons suggest a much higher original diversity.

Actinopterygii

Ferganiscus osteolepis (Fig. 5) is a 10-20 cm long fish with a rather elongate body. The snout is elongated, with small, conspicuous teeth. The dorsal fin is equally removed from snout and tail; beginning of pelvic fin in front of dorsal, anterior margin of anal fin behind posterior margin of dorsal fin. The scales are medium-sized and sculptured by flat longitudinal ridges separated by narrow furrows.



Fig. 5. Holotype of the palaeoniscid *Ferganiscus osteolepis* (left) and a reconstruction thereof (Sytchevskaya 1999, right).

The known specimens of *Sixtelia asiatica* (Fig. 6) do not exceed 9.5 cm in length. The body only 3 to 3.5 times longer than deep, head short, jaws with medium-sized, conspicuous teeth. Beginning of dorsal fin in front of pelvic, anal fin close to the base of the caudal fin.

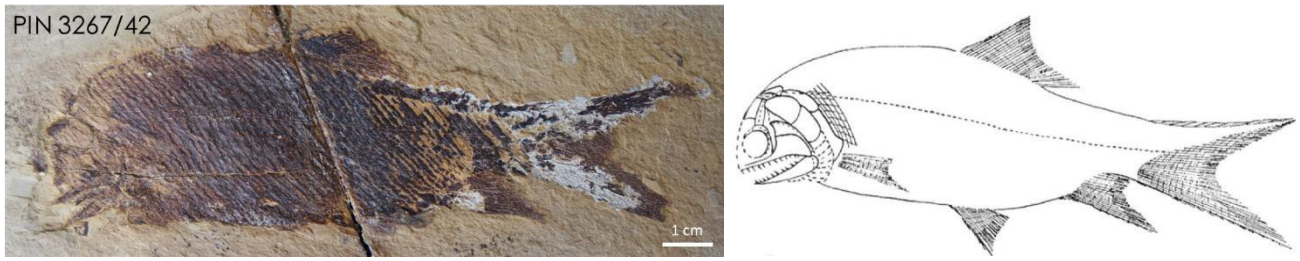

Fig. 6. Holotype of the palaeoniscid *Sixtelia asiatica* (left) and a reconstruction thereof (Sytchevskaya 1999, right).

Alvinia serrata (Fig. 7) resembles *Sixtelia asiatica* in the general body form, differing from it in smaller scales, whose posterior margin is serrated, and the position of fins (pelvic beginning in front of dorsal fin, the latter being closer to the snout than to the tail; anal beginning in line with posterior third of dorsal). The body itself less deep.

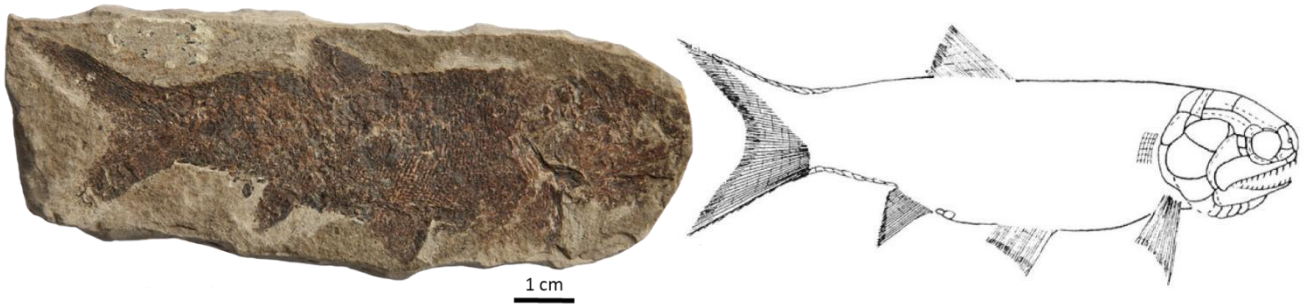

Fig. 7. Holotype of the 'perleidid' *Alvinia serrata* (left) and a reconstruction thereof (Sytchevskaya 1999, right).

Megaperleidus lissolepis (Fig. 8) is a relatively large (over 20 cm) fish with large, smooth scales and small teeth. Complete skeletons are not known yet.



The evenkiid *Oshia ferganica* (Fig. 9) was a large (up to 45 cm) predatory fish. Its squamation consisted of large, thick ganoid scales bearing pores and a faint striation. Fin rays were composed of short segments with numerous longitudinal ridges. The dorsal fin encompassed about 80 fin rays and extended over most of the back of the fish. *Oshia* belongs to scanilepiforms, a Permian–Triassic group of freshwater actinopterygians closely related to the recent bichir *Polypterus*.

Fig. 8. Holotype of the 'perleidid' *Megaperleidus lissolepis*.

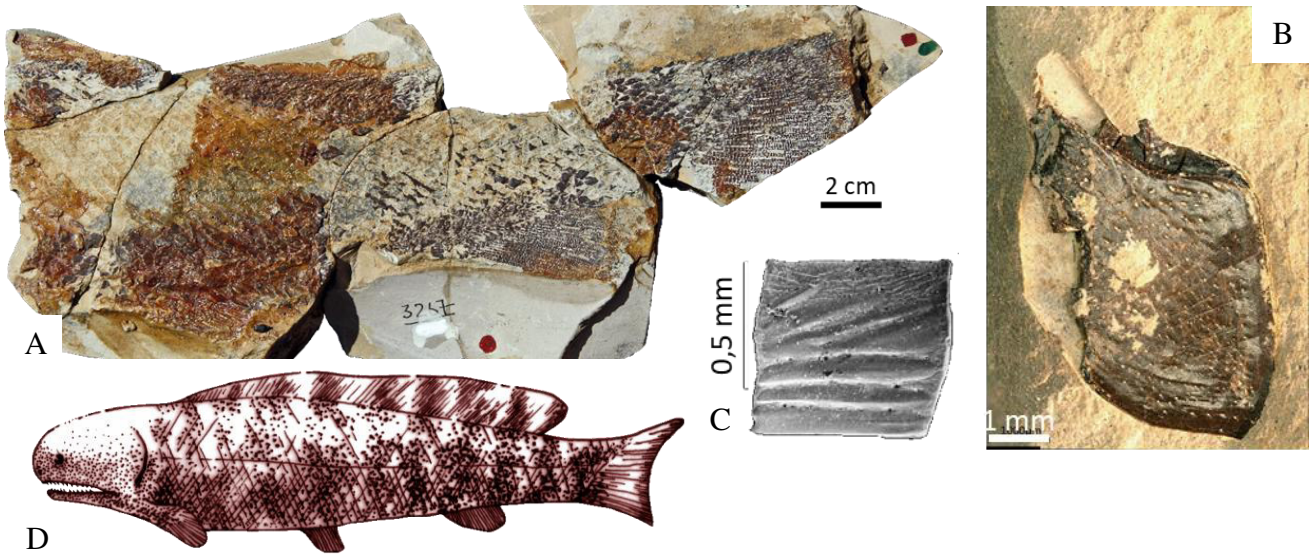

Fig. 9. *Oshia ferganica*. A, Holotype specimen; B, isolated flank scale (anterior to the left); C, isolated fin ray segment; D, reconstruction (F. Spindler).

Saurichthys orientalis (Fig. 10) is a representative of the cosmopolitan Triassic genus *Saurichthys*, known with more than 50 species from both marine and freshwater environments. *Saurichthys* was a fast-starting predator, whose extremely elongated body and head along with large, posteriorly placed fins enabled it to attack prey by quick, sudden darts, without being perceived by the lateral line sensory organ of the prey animal in order to escape. *S. orientalis* had a length of up to 45 cm. Its body was covered by scales or scutes arranged in longitudinal rows, with a specific interlocking mechanism in mid-dorsal and mid-ventral scutes in the caudal peduncle serving as a stiffening structure of the tail. The dentition consisted of characteristic large, conical teeth with a smooth cap and a striated base, alternating with series of smaller teeth.

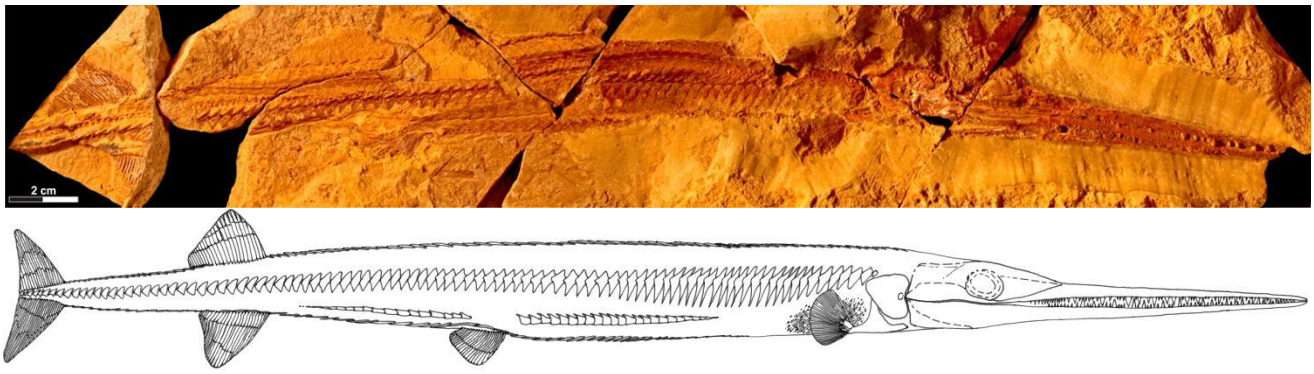

Fig. 10. The most complete specimen of *Saurichthys orientalis* (above), and a reconstruction (F. Spindler, below).

Sarcopterygii

The lungfish *Asiatoceratodus sharovi* (Fig. 11), described by VOROBIEVA (1967), is known from at least six skeletons and a wealth of disarticulated material including skulls, skull bones, tooth plates and scales. These finds make Madygen one of only four Triassic localities yielding complete skeletons of lungfish. *A. sharovi* reached up to 30 cm in length and probably lived in the vegetated lake front. Juvenile individuals fed on insect larvae and snails, while adults were omnivorous, adding algae and shrimps to their diet. Additionally, isolated scales and bones suggest the presence of a coelacanth in the ecosystem.

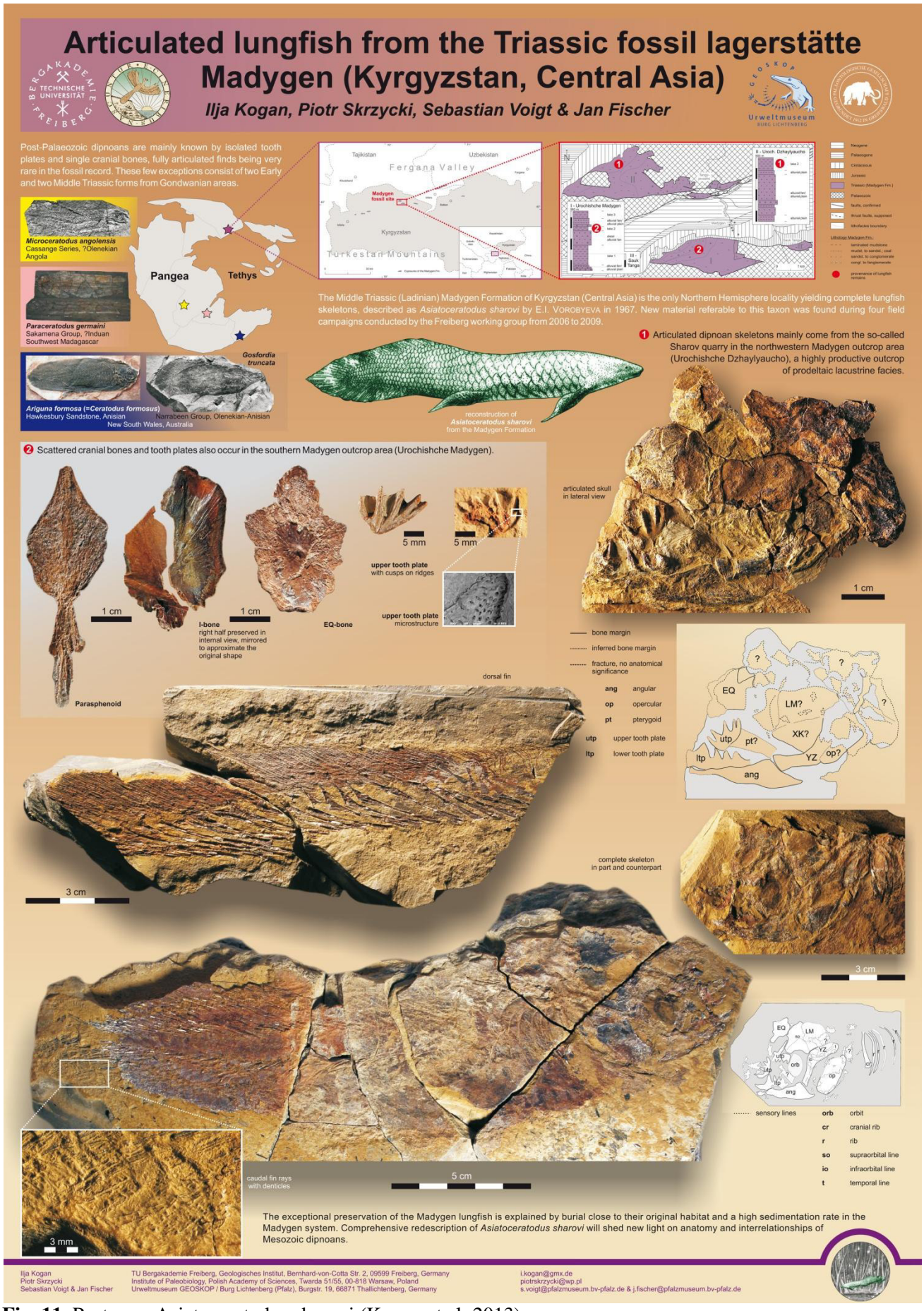

Fig. 11. Poster on Asiatoceratodus sharovi (Kogan et al. 2013).

6.2.7 Tetrapods

Tetrapod remains have been recovered from two localities within the Madygen Formation: (I) the lacustrine shales of "Sharov Quarry" in the north-western Madygen outcrop area (Urochishche Dzhaylyaucho) and (II) fluvial deposits within sediments of a wet alluvial plain in the south-western outcrop area (Urochishche Madygen). Preservation of skin impressions has only been recorded from the silt- to claystones of Sharov Quarry (**Plate 2**) – skeletal findings from there are often complete and articulated (**Plate 2** A, B, H; 3A, F, G): the diapsid reptiles *Longisquama insignis* (SHAROV 1970), and *Sharovipteryx mirabilis* (SHAROV 1971), the urodelan amphibian *Triassurus madygensis* (IVAKHNENKO 1978), the basal cynodont *Madysaurus sharovi* (TATARINOV 2005) and a not yet described reptile with squamate-like skin. The chroniosuchid locality has yielded numerous isolated and partially articulated bones of a reptiliomorph tetrapod *Madygenerpeton* (**Plate 1**), furthermore the articulated hindlimb and pectoral girdle of an archosaur, a lower jaw and thecodont teeth of unknown affinity, perhaps referable to the same taxon as the hindlimb, and up to 7 cm long vertebra fragments of a large reptile (**Plate 3** B-E). Most of the tetrapods are clearly terrestrial dwellers – this can also not be excluded for the only sparsely known group of chroniosuchians.

Plate 1. *Madygenerpeton pustulatum*. A, Rostral fragment of the skull, before preparation. **B,** Skull prepared, note the large preorbital foramina. **C- E,** Series of 21 articulated dorsal dermal plates; mostly the imprint of the inner (ventral side) is seen and only at the cranial end (right) the sculptured outside of the osteoderms has been uncovered (in C). In E the actual ventral side displays the characteristic curved trails on the articulation surfaces of two individual plates. **F,** Single osteoderm in ventral view – note the ventral process in the centre and the structure of the wings. **G**, The anteriormost osteoderm has a convex anterior margin (it articulates with only one neighbouring dermal plate). **H,** Series of five dermal plates (four seen) from ventrolateral view. Note how the anterior and posterior process of the plates overlap and also the deep V-shaped encarvement of the ventral processes. Scale bars: in A one unit equals 1 mm; C- F, 2 cm; G, H, 2.5 cm.

Plate 2. Diapsids with skin preservation. A, Holotype of the glider *Sharovipteryx mirabilis*, (PIN 2584/8) note the large uropatagium. **B**, The only skeletal specimen of *Longisquama insignis* (PIN 2584/4). It bears a series of seven elongated dorsal skin appendages. **C-D**, Moscow specimens (PIN 2584/6, 7) of isolated *Longisquama* appendages: C – proximal fragments, D, distal fragment. **E-G,** Freiberg specimens: E – distal fragment; F – the largest yet known appendage fragment covers both the expanded bipartite distal section and the narrow tripartite proximal section, which is also displayed in G (counter slab). **H**, holotype of *Kyrgyzsaurus bukhanchenkoi*, an ?archosauromorph reptile with a complex pattern of scales and osteoderms preserving traces of pigmentation. Scale bars: B, 10 cm; C-E, the displayed sections are 4.3, 8.2, and 4 cm long; F, G, see mm mesh.

Plate 3. Other tetrapod finds. A, Skeletal drawing of the urodelan *Triassurus sixtelae* (PIN 2584/10), currently interpreted as the oldest known salamander. **B,** Large vertebra in dorsal view, the spinal process in the midst is broken off and not preserved. **C, D,** V-shaped lower jaw associated with teeth (green arrow) and individual tooth of an undescribed amniote. Note the cusps and long root of the thecodont teeth. **E,** Hind leg of an archosaur. Note the constriction and expanded ends of pubis and ischium, the roundish head of the S-shaped femur, the narrow fibula, and the shape of tarsal bones calcaneus and astragalus. **F, G,** Postcranium and skull of the cynodont *Madysaurus sharovi* (PIN 2584/11), which has been regarded as being related to the Late Permian Procynosuchidae, the earliest group of cynodont therapsids. Scale bars: B, 5 mm; D, E, 2.5 mm.

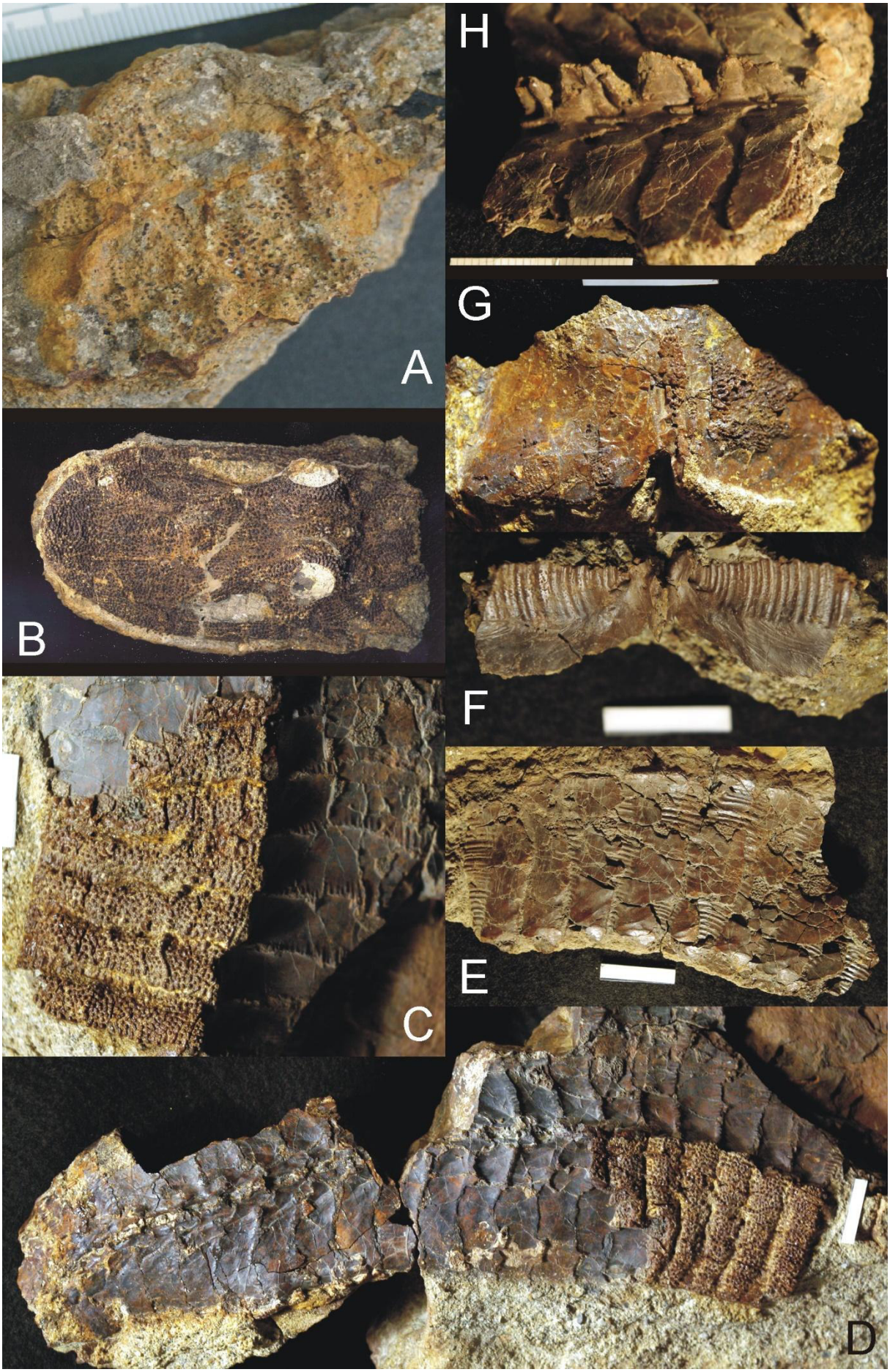

Plate 1

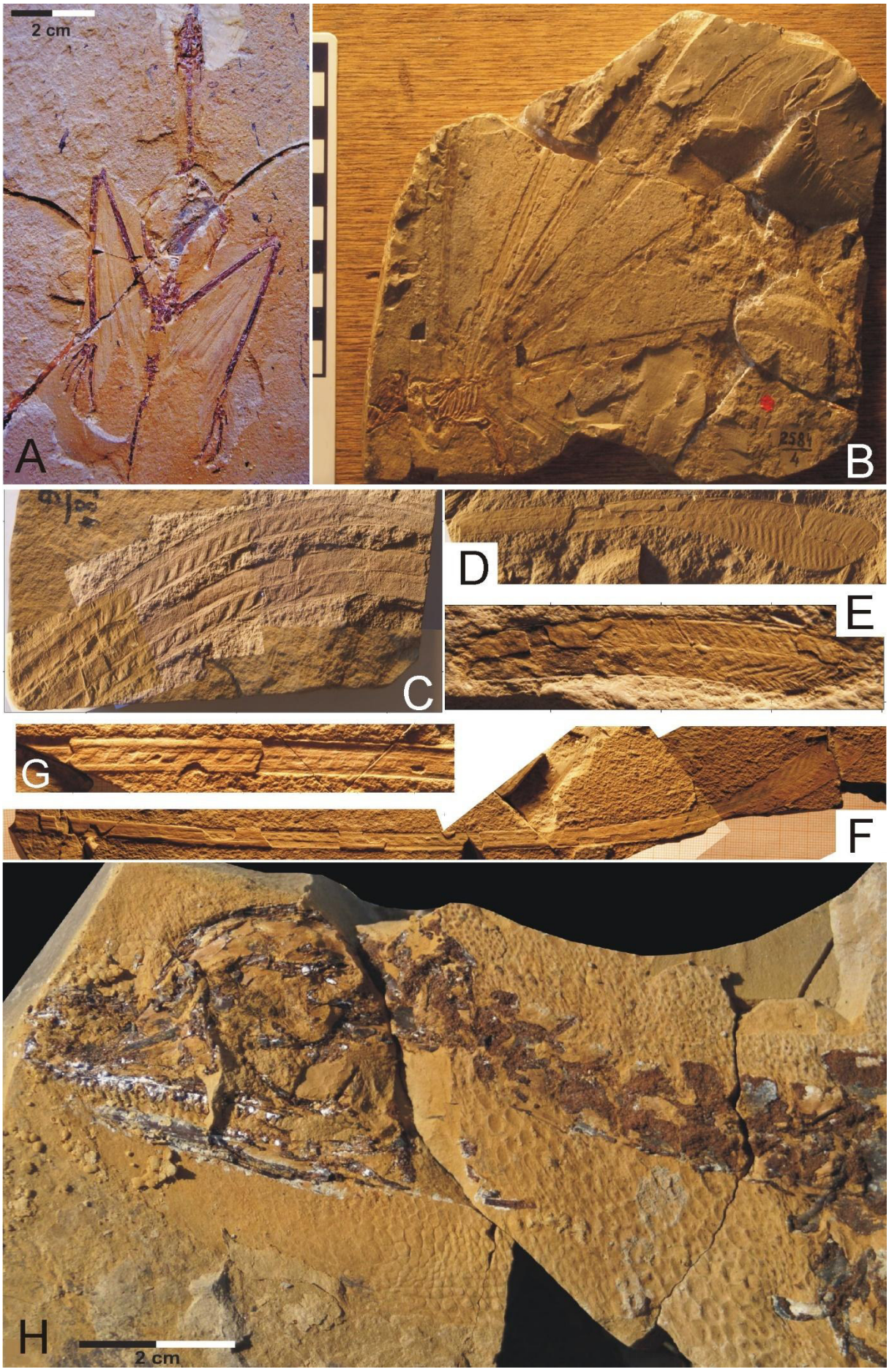

Plate 2

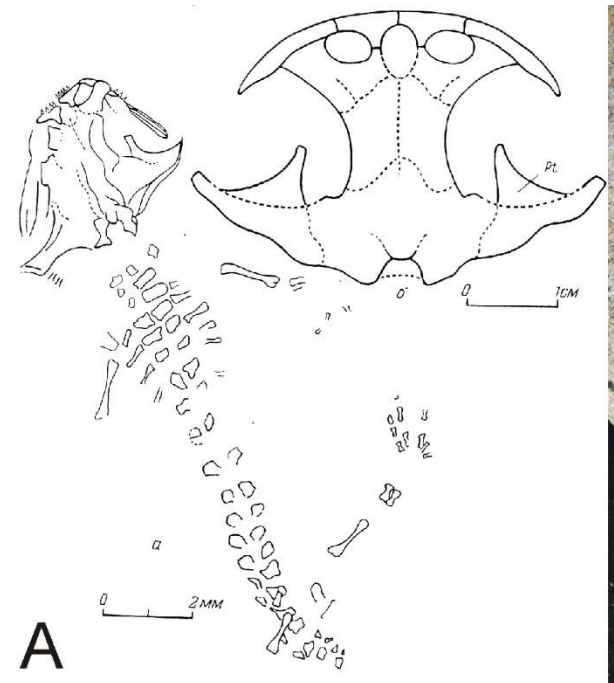
Pt
0
1CM
0
2MM
A


E


B

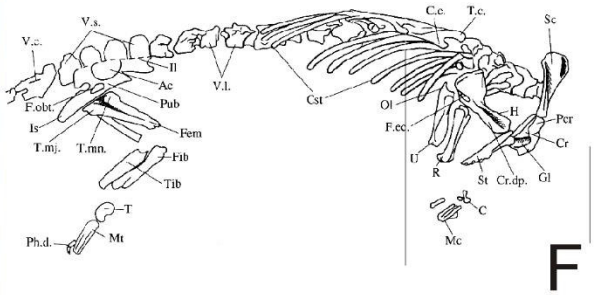
V.s.
V.c.
Il
Ac
V.l.
Cst
C.c.
T.c.
Sc
F.obt.
Pub
Is
Fem
T.mj.
T.mn.
Fib
Tib
T
Ph.d.
Mt
Ol
F.ec.
H
Per
Cr
U
R
St
Cr.dp.
Gl
C
Mc
F


C


D

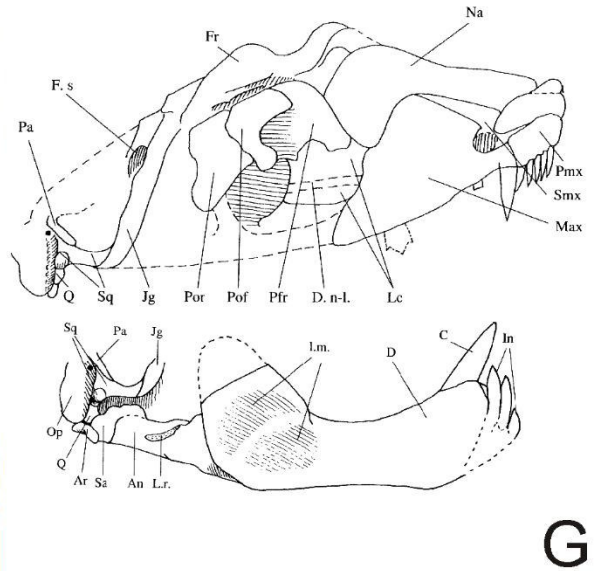
Na
Fr
F. s
Pa
Pmx
Smx
Max
Q
Sq
Jg
Por
Pof
Pfr
D. n-l.
Lc
Sq
Pa
Jg
l.m.
D
C
In
Op
Q
Ar
Sa
An
L.r.
G

Plate 3

6.2.8 Trace fossils

Penetrative trace fossil in the form of 1 to 2 mm wide branching and interweaved burrows are known from the lacustrine sediments of the Madygen Formation, but also from ephemeral ponds in the floodplains of the Kamysh-Bashi Formation. The burrows, resembling *Helmithoidichnites tenuis* (Fitch, 1850) can probably be assigned to insect larvae.

In another floodplain pond of the Kamysh-Bashi Formation in Sauk Tanga, a more diverse ichnofauna is preserved:

Heteropodichnus sauktangense isp. nov.
Complex trace with central furrow, sometimes replaced by paired bean-shaped imprints, lateral two complexly overprinted traces of two to four staggered leg imprints and slightly curved drag marks, likely trace of the branchiopod *Almatium gusevi*

Kouphichnium pterodactyli (Winkler) Malz 1964
Central furrow with two rows of distinct well separated three-toed imprints, traces of xiphosurans

Lithographus hieroglyphicus Hitchcock, 1858
Double rows of groups of three leg imprints, sometimes coalescing and difficult to separate

Diplichnites cf. *triassicus* Linck 1943
Double row of small singular leg imprints

Cochlichnus anguineus Hitchcock, 1858
Simple sinusoidal traces 1 – 2 mm wide, with no discernible internal structure

Undichna unisulcata Gibert 1999
Long sinuous traces, several centimetres wide, impressed more deeply in the straight central parts, fish swimming trace

Lunichnium rotterodium Walter 1983
Straight central furrow, sometimes discontinuous with little sediment pile-ups, two lateral sets of slightly curving drag marks, occasional claw imprints, swimming trace of small tetrapod

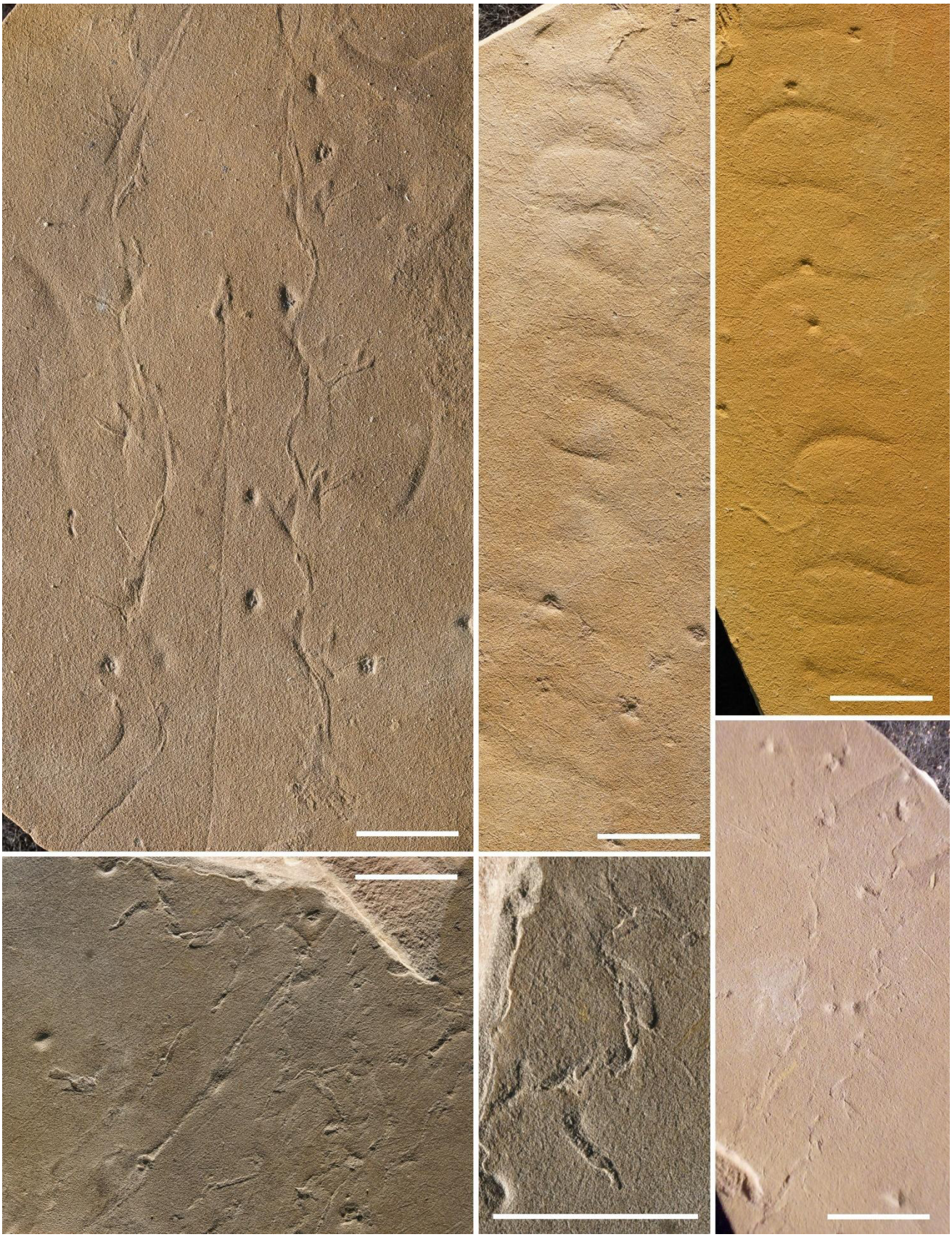

Fig. 1: Ichnofossils from the Kamysh-Bashi trace fossil site: (top left) *Lunichnium rotterodium*, with claw marks at regular intervals, pointing upward, (top middle and right) *Undichna unisulcata,* (bottom left) *Lunichnium rotterodium*, (bottom middle) *Cochlichnus anguineus*, (bottom right) *Lithographus hieroglyphicus*; all scale bars = 1 cm.

Fig. 2 (next page): Drawing of the largest slab with *Heteropodichnus sauktangense* isp. nov. traces. Eleven individual traces show the degree of along-track morphological changes in this ichnospecies

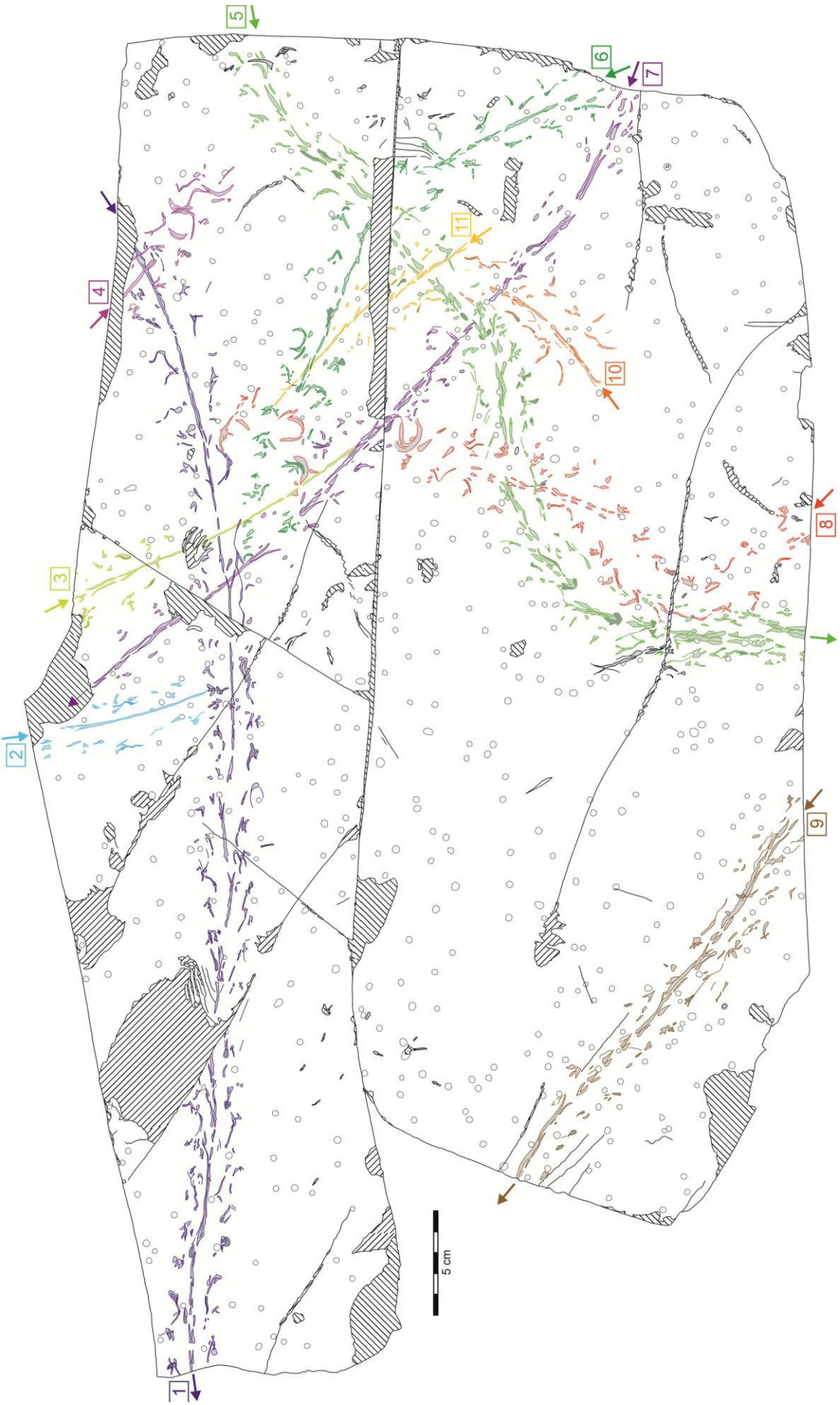
5
6
7
11
4
10
8
3
2
9
1
5 cm

6.3 Cretaceous

In all three known outcrops, the ichnofossils occur homogeneously in large and dense clusters, and are exposed above the ground in one stratigraphic horizon. The assemblages can reach total heights of 3 m and can extend laterally over several tens of meters. The burrows' architectural morphology is uniform and regular, although preservation status, sediment type and assemblage sizes and shapes may vary (fig). The top of the burrowed sediment layers has been eroded and none of the burrows' openings or potential chimney structures are preserved.

All burrows consist of sub-vertical to vertical, slightly bending or turning, lined shafts of various lengths. On average, one burrow can be traced down vertically for over a meter until disruptive structures do not allow any further distinguishing from co-occurring tube-like structures. The burrows are ellipsoid to subcircular in cross section, with a constant diameter along the entire burrow. The smallest diameter observed, including the wall, was about 9 cm, while the vast majority range between 20 and 25 cm in size.

The burrows do not show horizontal connections such as tunnels or galleries, nor do they exhibit turnarounds, chambers or similar structures that could have been used by the inhabitant. Although being clustered densely, the burrows generally don't intersect each other or bifurcate. Scratch or scrape marks, fecal pellets, fossil body remains or imprints in the burrows or in near proximity are yet absent.

The surface of the burrows is irregularly bulbous but smooth. The burrows are filled with carbonaceous mud (often dolomitic) with the exception of a central cavity that is about one fifth of the burrows external diameter in width. The cavity is originally subcircular, but in some burrows collapsed into narrow and elliptical or star-shaped forms. Burrows with collapsed cavities tend to be more elliptical in cross-section, indicating deformation of the entire burrow.



Fig. 1: The ichnofossil cluster close to the field camp, likely decapod (crayfish) burrows in the uppermost Kyzylpilyal Formation.

6.4 Paleogene

Shark Teeth

Odontaspis

- narrow, sharp primary cusps with multiple slender cusplets
- broadly splayed, U-shaped, narrow (when viewed labially) deep (when viewed laterally) root lobes

Carcharias

- anterior teeth: long and slender cusps (sigmoid in profile) with lateral cusplets, lingual face strongly convex, high root
- lateral teeth: shorter, broader (particularly at base), flatter (blade-like), cutting-edge reaches lateral cusplets

Striatolamia

- anterior teeth: elongated crown, sigmoid in shape when viewed laterally, striations on the lingual face. Lateral cusplets are greatly reduced or absent.
- lateral teeth: lower and broader, striations and cusplets reduced or lacking entirely

Mennerotodus (glueckmani)

- anterior teeth: tall and narrow triangular main cusp (sinuous in profile view), single pair of small and conical lateral cusplets, thin root lobes with rounded extremities
- lateral teeth: similar but shorter and more broadly triangular main cusp, one pair or (very rarely) two pairs of large lateral cusplets

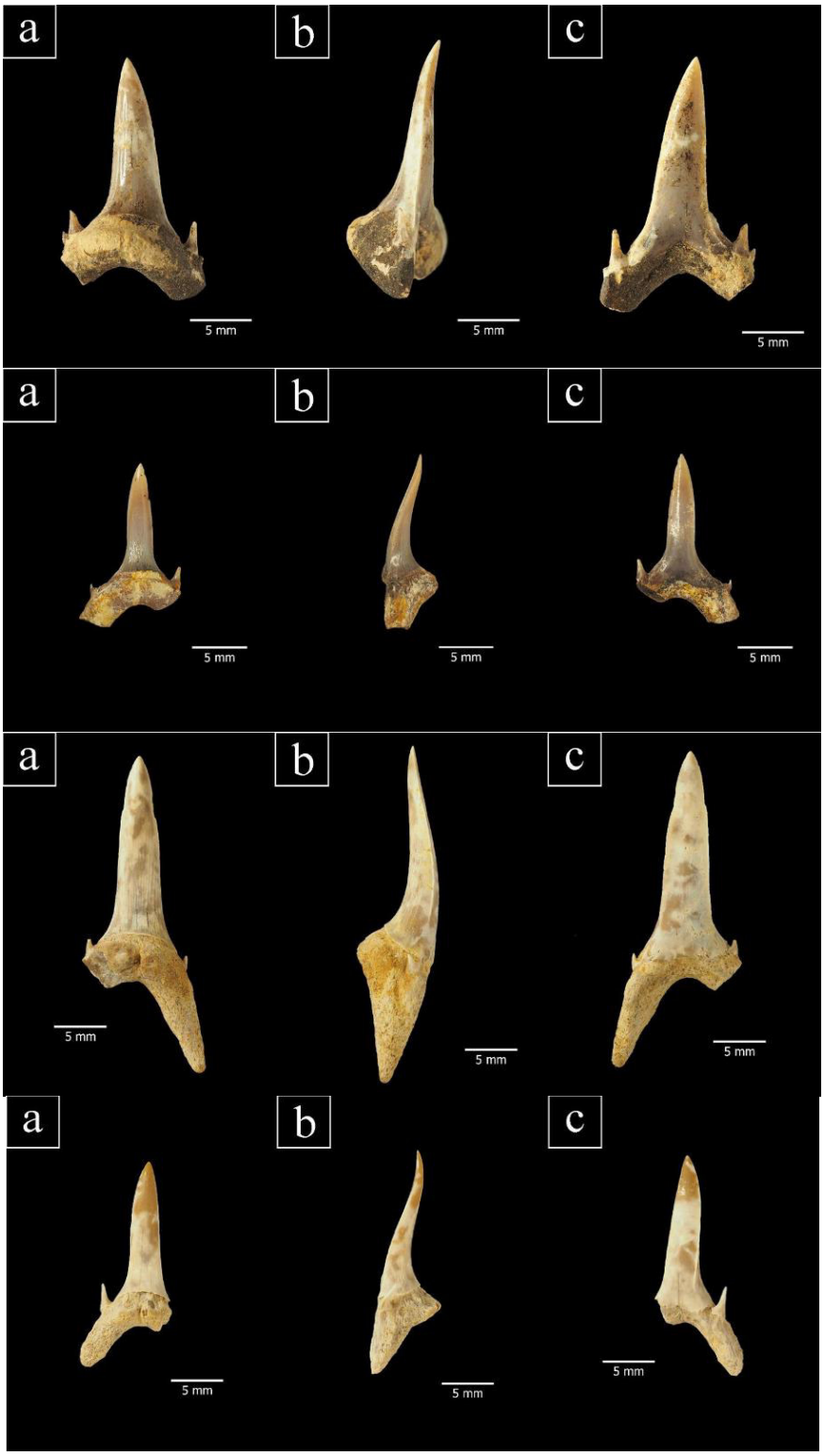

Jaekelotodus

- stout teeth with massive roots, strong lingual protuberance, clear nutrient groove and flat labial side
- rather short, but broad (sometimes triangular), completely smooth crown,
- flat labial cusp face, medio-basally depressed, and a non-sigmoidal profile
- one or two pairs of sharp and rather high cusplets.

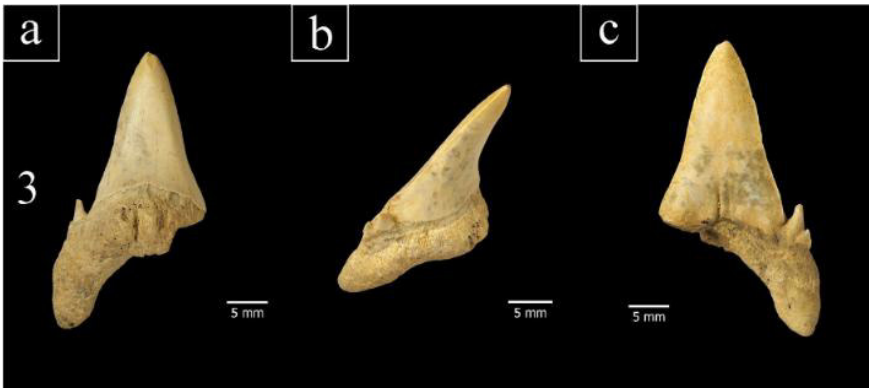

Skate teeth

Aetobatus

- large teeth, crowns lack hexagonal shape, lateral margins are smoothly curved and directed rearward, all teeth are elongated.
- upper and lower teeth have distinctly different shapes
- roots with the strong, lingual displacement of the laminae and strongly sloped labial face

Mylobatis

- laterally elongated medial tooth (6.5:1 ratio) and multiple lateral files
- hexagonal, lateral teeth and lateral angle is centered.
- weakly sutured teeth, labial and lingual crown faces are vertical and bear baso-apical ridges, lingual shelf is short but prominent.



? Rhinoptera

- teeth are numerous, varying degrees of elongation that can be seen, hexagonal shape

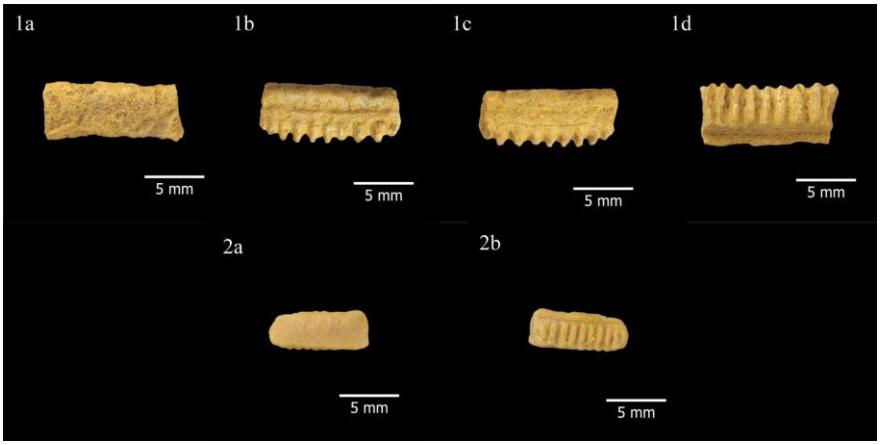

Mollusca

Cardita

- small (1,2 cm), robust and thick shell
- valves virtually identical, with ornamentation
- umbo positioned medially

scale bar 1 cm



Meretrix

- small shell (0.5 – 3cm), almost triangular in shape
- valves anteriorly almost rounded and posteriorly slightly pointed
- umbo positioned rather anteriorly
- slight ornamentation, particularly visible at valve margins

scale bar 1 cm



Turritella

- cone-shaped and tightly coiled shell, sharply pointed apex
- numerous whorls with spiral risged and grooves
- small aperture
- 1 – 3 cm long

scale bar 1 cm

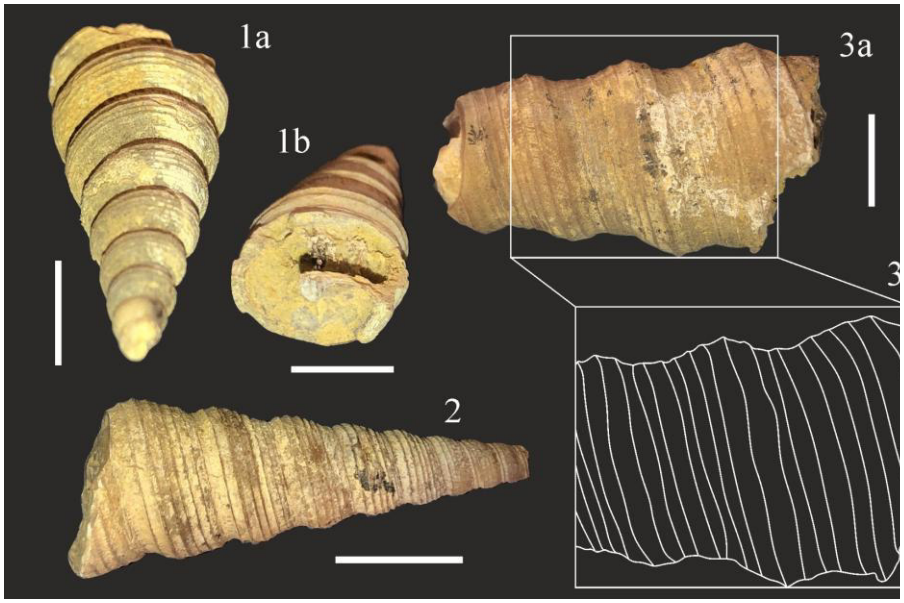

Epitonium

- high-spired shell
- typical, blade-like vertical rips (costae)

scale bar 1 cm



? Natica

- low-spired shell of subglobose, and slightly depressed shape
- smooth shell surface

scale bar 1 cm



7 Mineralization

The Madygen Geopark contains several ore occurrences that haven been the target of mineral exploration in the 20th century and in one case (Kon-i-gut cave mine) also were the object of historic mining. Although no one of the occurrences are of economic interest under current conditions, they are of great interest to study the effects of consecutive phases of mineralization in Late Paleozoic fold-thrust belt. Types of ore mineralization include Ag-Pb-Zn thermokarst deposits, Pb-Zn epithermal veins along structural contacts, low-temperature impregnative U mineralisation in Lower Paleozoic black shales, roll-front type U mineralisation in Paleogene marine sediments, bauxitic ores in Triassic-Jurassic sediments and associated weathering crusts on Paleozoic rocks proximal to the old land surface and late-stage hematitization along reactivated faults. The genetic classification of some mineralisations and the age relationships between the different mineralisations are in some cases poorly known and require further research.

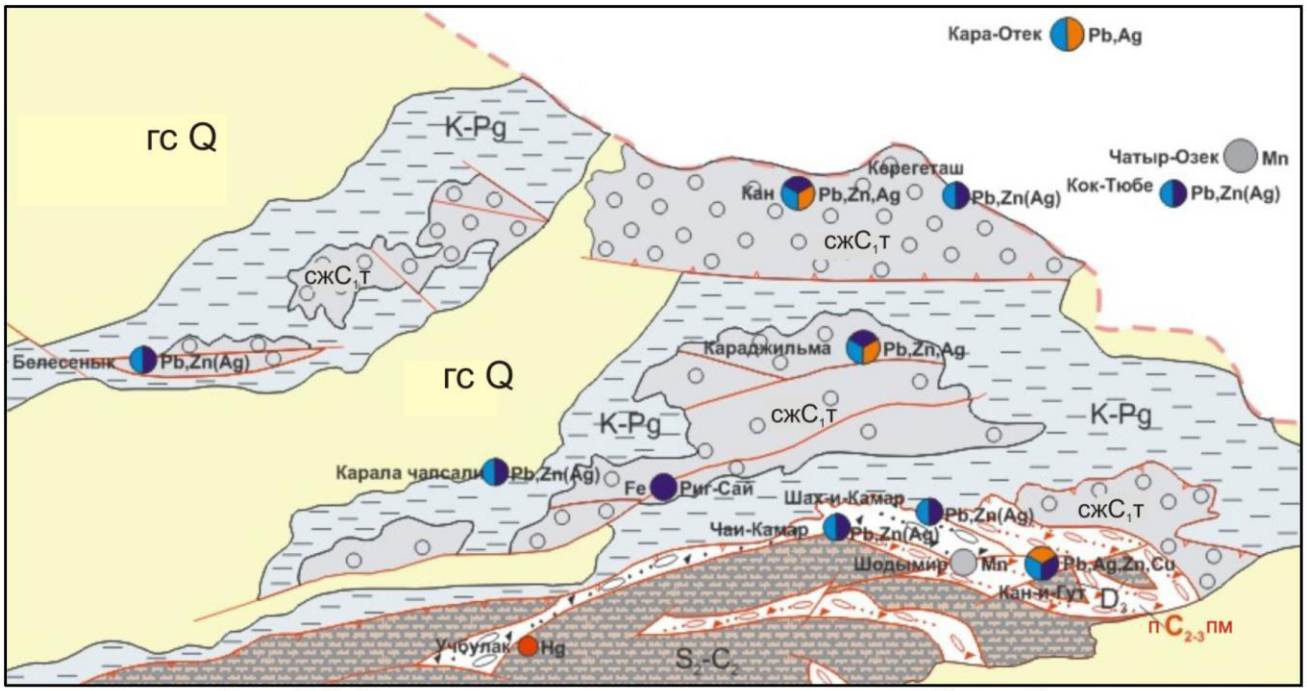

Рис. 5.2. Геодинамическая карта рудного поля Кан-и-Гут

Fig. 1: The individual mineral occurrences in the Kon-i-gut ore field and their metal content according to Vaulin, 2017.

7.1 Pb-Zn-Ag

The Kon-i-Gut ore field exhibits a "block-like" structure, here the mineralized blocks occur within a polymictic terrigenous mélange (C2–3). The ore field comprises more than a dozen polymetallic occurrences. At the Kon-i-Gut deposit, stratiform galena-sphalerite mineralization is concentrated in six tabular ore bodies (30–70 x 0.5–10 m) situated between D3 limestones and dolomites. Ag content ranges from 185 to 372.3 g/t, Pb from 1.75% to 3.74%, and Zn from 0.9% to 1.76%. As of January 1, 1992, resources stood at: Pb – 34.1 thousand tonnes, Zn – 17.1 thousand tonnes, and Ag – 357.36 tonnes. The potentially economic as of January 1, 1999 (categories C1 + C2) was: Pb – 7.4 thousand tonnes @ 3.6%, Zn – 3.4 thousand tonnes @ 1.6%, and Ag – 76.6 t @ 375 g/t.

At the Chai-i-Kamar polymetallic deposit, a pronounced oxidation zone has developed along faults within blocks of Devonian dolomite. There are four steeply dipping bodies composed of pigmented limonite and ferruginous limestones (75–400 x 12–25 m).

The lead isotope composition indicates a deep-seated source for the ore-forming metals. Sulfur isotope composition is determined by processes occurring in the vicinity of the ore deposit; it is typically sedimentary-diagenetic for sulfides, whereas for barite it resembles seawater sulfur, aligning the ores more closely with hydrothermal-sedimentary types. Homogenization and decrepitation data, along with sulfide isotope pairs, indicate that the ores formed at an early stage at temperatures below 100°C and were subsequently altered at temperatures between 120°C and 220°C. The involvement of diverse material sources in ore formation (mantle-crust for metals; marine and biogenic sources for sulfur), deposition in a near-surface environment, and widespread regeneration processes point to a polygenetic origin, a characteristic feature of stratiform-type deposits.

The Kon-I-Gut deposit was known as early as antiquity. Archaeological findings indicate that the deposit was already being exploited by ancient miners in the 10th century. Legends, stories, and various Arabic records concerning the Kon-I-Gut deposit—which was referred to as a "cave" in ancient times—have survived to the present day, indicating that the site was widely known even beyond Asia. The primary target of extraction was silver. Preliminary estimates place the total volume of rock excavated from these ancient sites at between 300,000 and 500,000 tonnes.

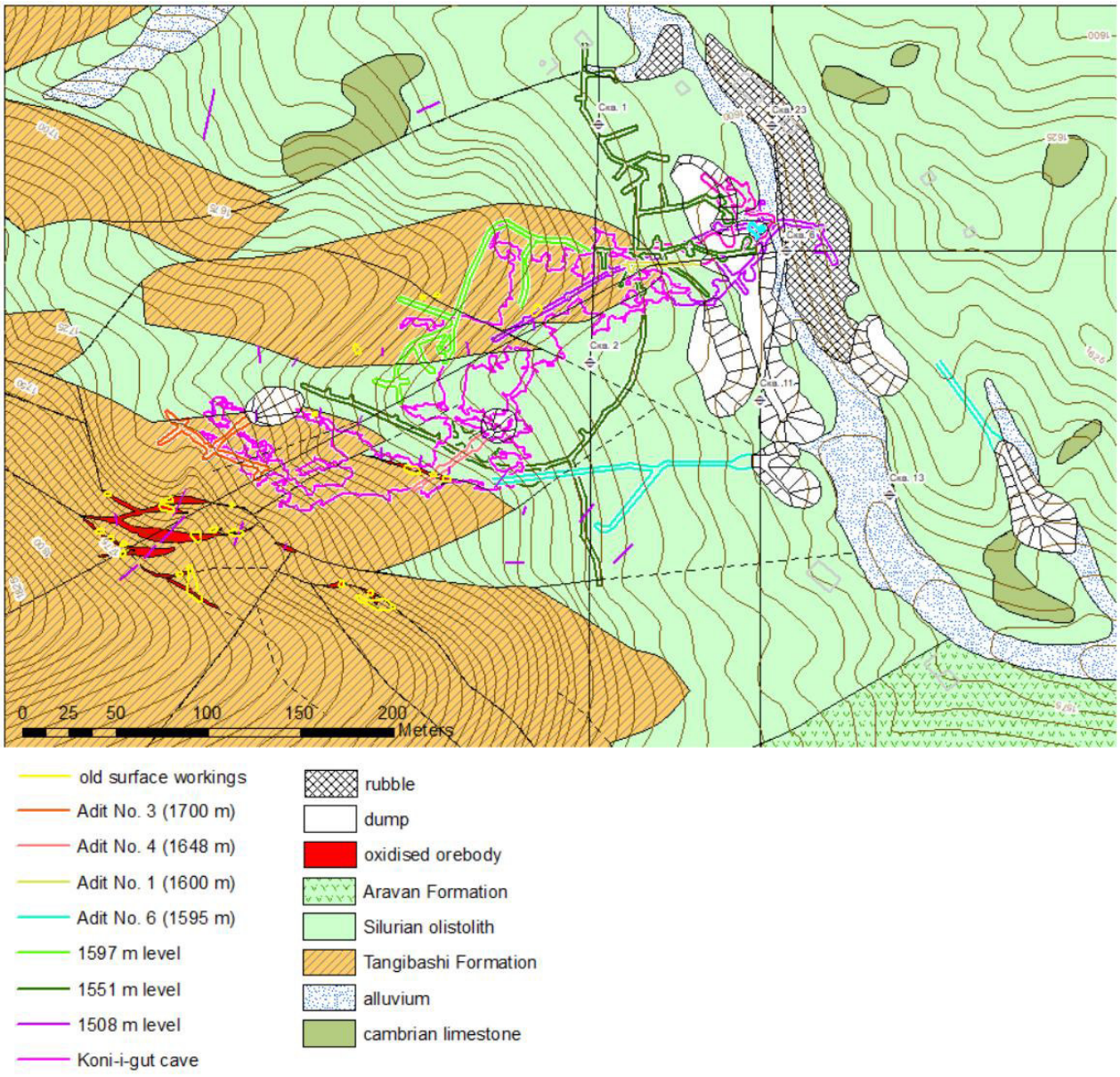

Fig. 2: Geologic map of Kon-i-gut with underground cavities projected on the surface

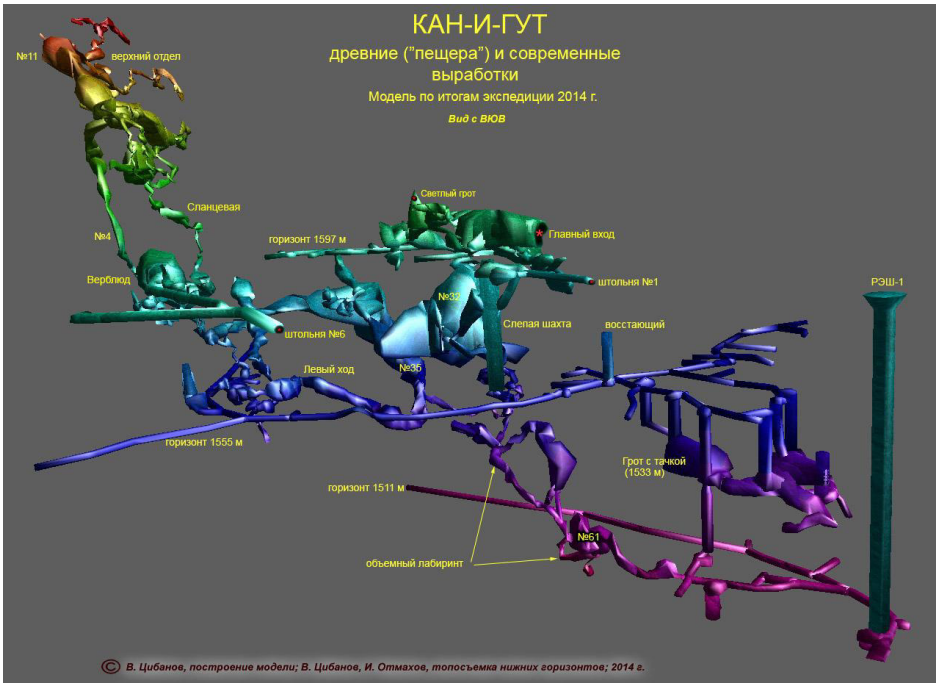

Fig. 3: 3D view of the cave and mine works from the Southwest

7.2 Uranium

The known uranium mineralisation is associated with organic-rich Cambro-Ordovician siliceous slates and Mesozoic pro-deltaic black shale units which typically contain pitchblende and uranyl-vanadate-phosphates. A number of prospects have been recorded and assayed in the past – either at surface, by drilling or within old mine workings. Average recorded grades from these prospects vary between 0.06% U_3O_8 to 0.13% U_3O_8. Anomalous amounts of molybdenum, vanadium, yttrium and gold have also been recorded. However, the most significant mineralisation identified to date is the Sai Sogul Prospect.

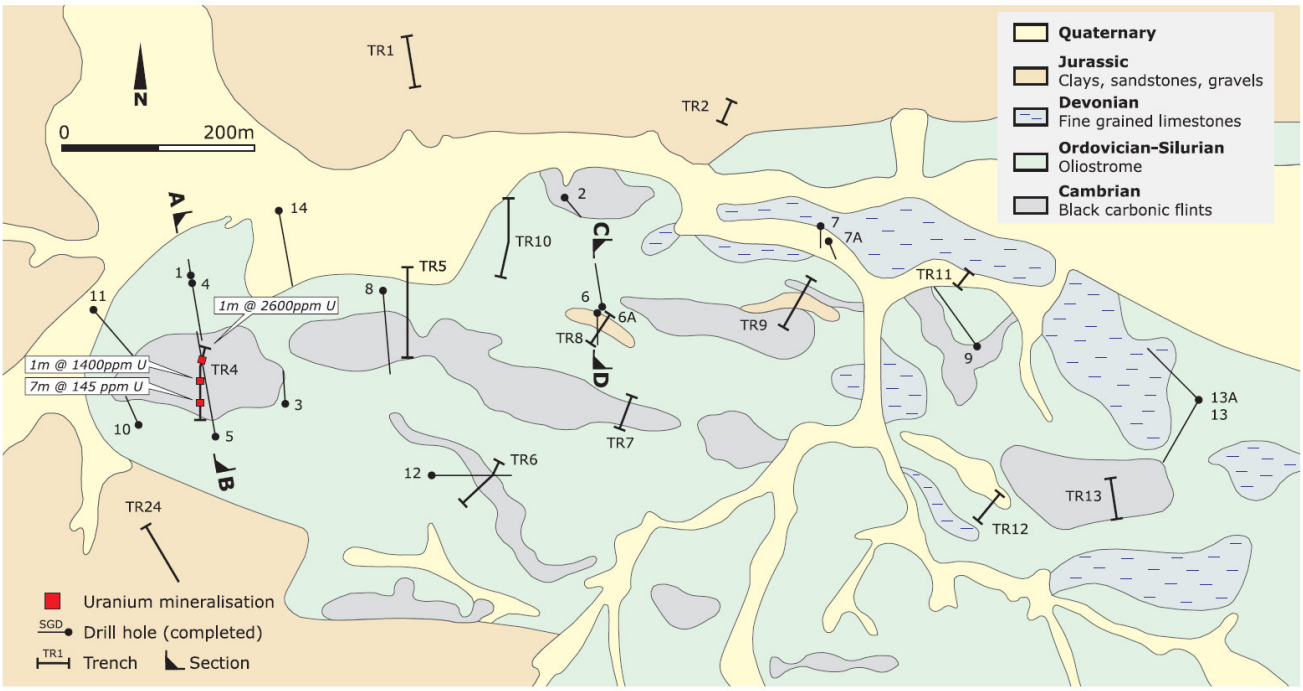

Fig. 3: Geologic map of the Sai Sogul uranium prospect (Monaro Mining, 2007)

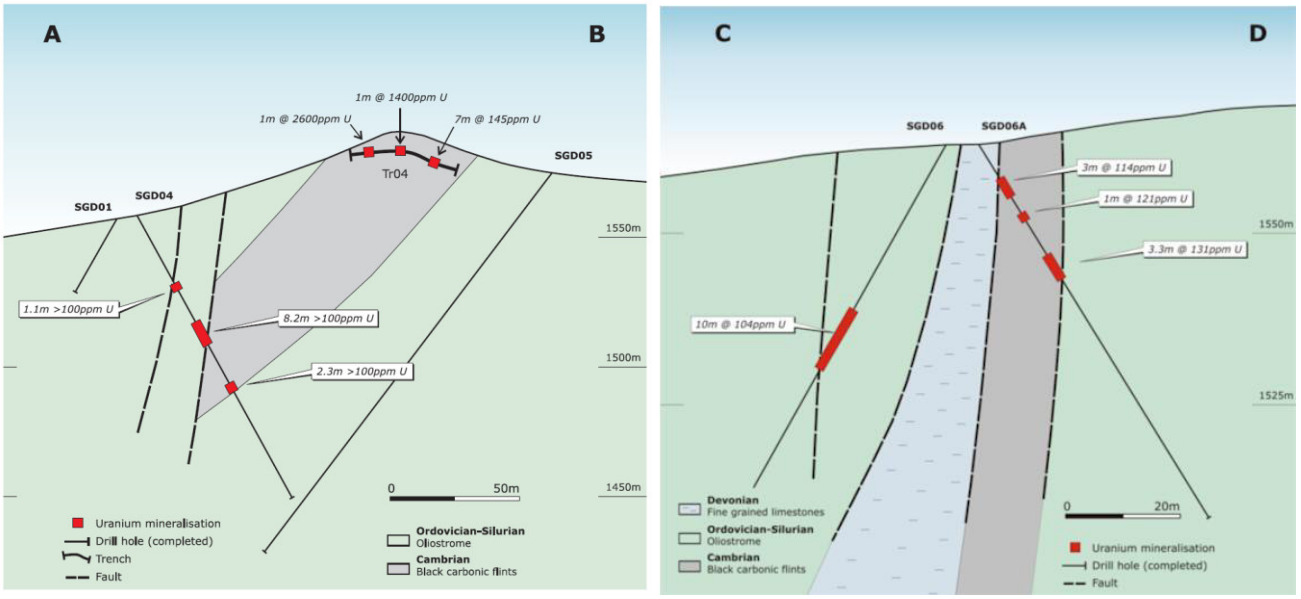

Fig. 4: Mineralized intercepts in drill holes and trenches. Low-grade uranium mineralisation is confined to fault zones and the contacts of carbonaceous shales with limestone or silicic rocks (Monaro Mining, 2007).

The mineralisation is confined to zones of alteration at the contact between resistant strata (silica lenses and limestone) and ductile graphitic shales. Based on the drilling results, it was concluded that the observed mineralisation is related to the movement of uranium from a localised repository in marine sediments. Uranium mineralisation is then transported by low temperature, oxidized meteoric waters into zones of low strain around the siliceous lenses and at limestone contacts during a phase of orogenic deformation. Precipitation of uranium then occurred at sites where chemical conditions were reduced, notably at graphitic shale contacts.

8 Selected References

BURTMAN, V. 2008: Nappes of the southern Tien Shan. Russian Journal of Earth Sciences. 10. 10.2205/2007ES000223

BYKADOROV, V.A., BUSH, V.A., FEDORENKO, O.A., FILIPPOVA I. B., MILETENKO, N.V., PUCHKOV, V.N., SMIRNOV, A.V., UZHKENOV, B.S., VOLOZH, Y.A. 2003: Ordovician – Permian paleogeography of Central Eurasia: Development of Paleozoic petroleum-bearing basins. Journal of Petroleum Geology 26: 325–350

DE GRAVE, J., BUSLOV, M.M., VAN DEN HAUTE, P. 2007: Distant effects of India–Eurasia convergence and Mesozoic intracontinental deformation in Central Asia: Constraints from apatite fission-track thermochronology. Journal of Asian Earth Sciences 29: 188–204

FISCHER, J., VOIGT, S., FRANZ, M., SCHNEIDER, J.W., JOACHIMSKI, M.M., TICHOMIROWA, M., GÖTZE, J., FURRER, H. 2012: Palaeoenvironments of the late Triassic Rhaetian Sea: Implications from oxygen and strontium isotopes of hybodont shark teeth. Palaeogeography, Palaeoclimatology, Palaeoecology 353–3: 60–72

FISCHER, J., VOIGT, S., SCHNEIDER, J.W., BUCHWITZ, M., VOIGT, S. 2011: A selachian freshwater fauna from the Triassic of Kyrgyzstan and its implication for Mesozoic shark nurseries, Journal of Vertebrate Paleontology, 31(5): 937–953

DOBRUSKINA, I. A. 1995: Keuper (Triassic) Flora from Middle Asia (Madygen, Southern Fergana). New Mexico Museum of Natural History & Science Bulletin, 5: 1-49

FEDORENKO, O., MILITENKO, K. (EDS.) 2002: Atlas of the lithology-paleogeographical, structural, palinspastical and geo-environmental maps of Central Eurasia. Scientific Research Institute of Natural Resources (YUGGEO), Almaty

GEYER, G., PEEL, J. S., STRENG, M., VOIGT, S., FISCHER, J., PREUßE, M. 2014: A remarkable Amgan (Middle Cambrian, Stage 5) fauna from the Sauk Tanga, Madygen region, Kyrgyzstan. Bulletin of Geosciences (89): 2

HECKER, R.T., OSSIPOVA, A.I., BELSKAYA, T.N. 1963: Fergana Gulf of Paleogene Sea of Central Asia, its History, Sediments, Fauna and Flora, their Environment and Evolution. Bulletin of the American Association of Petroleum Geologists, 47: 617-631

KOGAN, I., SCHÖNBERGER, K., FISCHER, J., VOIGT, S. 2009: A nearly complete skeleton of Saurichthys orientalis (Pisces, Actinopterygii) from the Madygen Formation (Middle to Late Triassic, Kyrgyzstan, Central Asia) – preliminary results. Freiberger Forschungshefte, C 532 - psf (17): 139-152

MOISAN, P., VOIGT, S., POTT, C., BUCHWITZ, M., SCHNEIDER, J.W., KERP, H. 2011: Cycadalean and bennettitalean foliage from the Triassic Madygen Lagerstätte (SW Kyrgyzstan, Central Asia). Review of Palaeobotany and Palynology 164 (1-2): 93–108

SCHOCH, R.R., VOIGT, S., BUCHWITZ, M. 2010: A chroniosuchid from the Triassic of Kyrgyzstan and analysis of chroniosuchian relationships. Zoological Journal of the Linnean Society 160, 515–530.

SHCHERBAKHOV, D.E. 2008: Madygen, Triassic Lagerstätte number one, before and after Sharov. Alavesia 2: 113-124

TRUBIN, Y. S., WINKLER, A., KOGAN, I., BROSIG, A., ZHANG, J., YASUHARA, M., TIAN, S. Y., MARINOV, V. A., LANGER, M. R. 2025: New insights into the middle Eocene environmental conditions and biostratigraphic setting of the Fergana Basin (Central Asia): Micropaleontological approaches. Journal of Asian Earth Sciences (288): 106613

VOIGT, S., BUCHWITZ, M., FISCHER, J., KOGAN, I., MOISAN, P., SCHNEIDER, J.W., SPINDLER, F., BROSIG, A., PREUßE, M., SCHOLZE, F., LINNEMANN, U. 2017: Triassic life in an inland lake basin of the warm-temperate biome – the Madygen Lagerstätte (southwest Kyrgyzstan, Central Asia). In: Fraser, N.C., Suess, H.-D. (Eds.) Conservation Lagerstätten – Windows into the Evolution of Life on Land. Dunedin, Edinburgh, 65-104

VOIGT, S., HOPPE, D. 2010: Mass Occurrence of Penetrative Trace Fossils in Triassic Lake Deposits (Kyrgyzstan, Central Asia). Ichnos, 17(1): 1-11

VOIGT, S., HAUBOLD, H., MENG, S., KRAUSE, D., BUCHANTSCHENKO, J., RUCKWIED, K., GÖTZ, A.E. 2006: Die Fossil-Lagerstätte Madygen: Ein Beitrag zur Geologie und Paläontologie der Madygen-Formation (Mittel- bis Ober-Trias, SW-Kirgisistan, Zentralasien). Hallesches Jahrb. Geowiss., Beiheft 22, pp 85-119